


2017

Molecular Mechanisms Of Mrna Transport By A Class V Myosin And Cytoplasmic Dynein

Thomas Edward Sladewski
University of Vermont

Follow this and additional works at: <https://scholarworks.uvm.edu/graddis>

 Part of the [Biochemistry Commons](#), and the [Molecular Biology Commons](#)

Recommended Citation

Sladewski, Thomas Edward, "Molecular Mechanisms Of Mrna Transport By A Class V Myosin And Cytoplasmic Dynein" (2017).
Graduate College Dissertations and Theses. 689.
<https://scholarworks.uvm.edu/graddis/689>

This Dissertation is brought to you for free and open access by the Dissertations and Theses at ScholarWorks @ UVM. It has been accepted for inclusion in Graduate College Dissertations and Theses by an authorized administrator of ScholarWorks @ UVM. For more information, please contact donna.omalley@uvm.edu.

MOLECULAR MECHANISMS OF mRNA TRANSPORT BY A CLASS V MYOSIN
AND CYTOPLASMIC DYNEIN

A Dissertation Presented

by

Thomas Edward Sladewski Jr.

to

The Faculty of the Graduate College

of

The University of Vermont

In Partial Fulfilment of the Requirements
For the Degree of Doctor of Philosophy
Specializing in Physiology and Biophysics

May, 2017

Defense Date: November 30, 2016
Dissertation Examination Committee:

Kathleen Trybus, Ph.D., Advisor
Gary Ward, Ph.D., Chairperson
David Warshaw, Ph.D.
Christopher Berger, Ph.D.
Jason Stumpff, Ph.D.

Cynthia J. Forehand, Ph.D., Dean of the Graduate College

ABSTRACT

mRNA localization ensures correct spatial and temporal control of protein synthesis in the cell. Using a single molecule *in vitro* approach, we provide insight into the mechanisms by which localizing mRNAs are carried by molecular motors on cytoskeletal tracks to their destination.

Budding yeast serves as a model system for studying the mechanisms of mRNA transport because localizing mRNAs are moved on actin tracks in the cell by a single class V myosin motor, Myo4p. Molecular motors that specialize in cargo transport are generally double-headed so that they can ‘walk’ for many microns without dissociating, a feature known as processivity. Thus, it was surprising when Myo4p purified from yeast was shown by *in vitro* assays to be non-processive. The reason for its inability to move processively is that the Myo4p heavy chain does not dimerize with itself, but instead binds tightly to the adapter protein She3p to form a single-headed motor complex. The mRNA-binding adapter protein She2p links Myo4p to mRNA cargo by binding She3p. To understand the molecular mechanisms of mRNA transport in budding yeast, we fully reconstituted a messenger ribonucleoprotein (mRNP) complex from purified proteins and a localizing mRNA (*ASH1*) found in budding yeast. Using single molecule *in vitro* assays, we find that She2p recruits two Myo4p-She3p complexes, forming a processive double-headed motor complex that is stabilized by mRNA at physiological ionic strength. Thus, only in the presence of mRNA is Myo4p capable of continuous mRNA transport, an elegant mechanism that ensures that only cargo bound motors are motile.

We next wished to understand if the principles of mRNA transport in budding yeast are conserved in higher eukaryotes. In *Drosophila*, mRNA is transported on microtubule tracks by cytoplasmic dynein, and the adapters that link the motor to localizing transcripts are well-defined. The adapter protein bicaudal D (BicD) coordinates dynein motor activity with mRNA cargo binding. The N-terminus of BicD binds dynein, and the C-terminus interacts with the mRNA-binding protein Egalitarian. Unlike mammalian dynein alone, it was recently shown that an N-terminal fragment of BicD (BicD2^{CC1}), in combination with a large 1.2MDa multi-subunit accessory complex called dynactin, forms a complex (DDB^{CC1}) that is activated for long processive runs. But unlike the constitutively activated BicD2^{CC1} fragment, the full-length BicD molecule fails to recruit dynein-dynactin because it is auto-inhibited by interactions between the N-terminal dynein binding domain and the C-terminal cargo binding domain. To understand how dynein is activated by native cargo and full-length adapters, we fully reconstituted a mRNP complex *in vitro* from tissue-purified dynein and dynactin, expressed full-length adapters BicD and Egalitarian, and a synthesized localizing mRNA found in *Drosophila*. We find that only mRNA-bound Egalitarian is capable of relieving BicD auto-inhibition for the recruitment of dynein-dynactin, and activation of mRNA transport *in vitro*. Thus, the presence of an mRNA cargo for activation of motor complexes is a conserved mechanism in both budding yeast and higher eukaryotes to ensure that motor activity is tightly coupled to cargo selection.

CITATION

Material from this dissertation has been published in the following form:

Krementsova, E.B., Hodges, A.R., Bookwalter, C.S., Sladewski, T.E., Travaglia, M., Sweeney, H.L., Trybus, K.M.. (2011). Two single-headed myosin V motors bound to a tetrameric adapter protein form a processive complex. *Journal of Cell Biology*. 14;195(4):631-41.

Hodges, A.R., Krementsova, E.B., Bookwalter, C.S., Fagnant, P.M., Sladewski, T.E., Trybus, K.M.. (2012). Tropomyosin is essential for processive movement of a class V myosin from budding yeast. *Current Biology*. 7;22(15):1410-6.

Sladewski, T.E., Bookwalter, C.S., Hong, M.S., Trybus, K.M.. (2013). Single-molecule reconstitution of mRNA transport by a class V myosin. *Nature Structural and Molecular Biology*. 8;20(8):952-7.

Sladewski, T.E., Trybus, K.M.. (2014). A single molecule approach to mRNA transport by a class V myosin. *RNA Biology*. 10;11(8):986-91.

Sladewski, T.E., Krementsova, E.B., Trybus, K.M.. (2016). Myosin Vc Is Specialized for Transport on a Secretory Superhighway. *Current Biology*. 22;26(16):2202-7.

DEDICATION

To my wife, Aoife Heaslip for her unconditional love and support. I couldn't have done this without your team work and understanding, and I look forward to a bright future together. To my daughters, Maeve and Orla; You can do anything you dream possible, and we will always be here to support your greatest ambitions in life. Finally, to my parents, Thomas and Debra Sladewski for their support and encouragement over the years, and for showing us that we can accomplish anything we set our minds to with gumption, bold thinking and hard work.

ACKNOWLEDGMENTS

I am grateful to my advisor, Kathleen Trybus for her mentorship and guidance over the last six years. I will truly miss chatting for hours about data. Thanks for reminding me that I'm getting older but I don't need to grow up (Aoife knows I haven't). I would like to thank the members of my thesis committee, Gary Ward, David Warshaw, Christopher Berger and Jason Stumpff for their guidance and Teresa Ruiz for making this a truly exceptional graduate program. I would like to thank members of the Trybus lab, Carol Bookwalter for her brilliant work on the mRNA project and for dinners at Papa Franks. I wish you the happiest retirement. I would like to thank Elena Kremensova for her work on the MyoVc project and fearlessly leading the charge on cow brain preparations. I would also like to thank Patty Fagnant for putting up with graduate students, Hailong Lu for his deep insights, Yusuf Ali and Jim Robblee for their useful conversations, and Maria Sckolnick for her practical discussions on data analysis and parenting. I would like to thank Susan Lowey for her thoughtful conversations that allowed me to think about my findings in the context of the field. This work wouldn't be possible without you all. I would also like to thank Matthew Lord for hiring me as a technician and starting this journey. Finally, I would like to thank the members of the Department of Molecular Physiology and Biophysics. You have made me feel like part of the family over the past 10 years.

TABLE OF CONTENTS

	Page
CITATION.....	ii
DEDICATION.....	iii
ACKNOWLEDGMENTS	iv
LIST OF TABLES.....	ix
LIST OF FIGURES	x
LIST OF ABBREVIATIONS.....	xii
CHAPTER 1: INTRODUCTION.....	1
mRNA localization.....	1
Mechanisms of mRNA transport.....	6
<i>ASH1</i> mRNA	7
Pair-rule transcripts	8
Maternal transcripts	9
<i>ASH1</i> mRNA transport in budding yeast.....	10
Two motor heads are needed for processivity	13
<i>K10</i> mRNA transport in <i>Drosophila</i>	18
Cytoplasmic dynein	20
Dynactin	23
Bicaudal D	24
BicD is auto-inhibited.....	27
CHAPTER 2: SINGLE MOLECULE RECONSTITUTION OF mRNA TRANSPORT BY A CLASS V MYOSIN	30
ABSTRACT.....	31
INTRODUCTION	32
MATERIALS AND METHODS.....	33
Protein constructs	33
Protein expression and purification	34

Actin tracks	34
<i>ASH1</i> mRNA constructs	34
Total internal reflection fluorescence (TIRF) microscopy	35
Electron microscopy	38
RESULTS	39
<i>ASH1</i> mRNA triggers assembly of a processive complex	39
Multiple zip codes increases mRNP run frequency and length.....	41
Multiple motors support longer run lengths	44
Electron microscopy of mRNA complexes	46
mRNPs are optimized to walk on actin cables	48
Variable inter-motor spacing during mRNP movement.....	49
DISCUSSION	51
Implications for mRNA transport in higher organisms	54
ACKNOWLEDGEMENTS	55
REFERENCES.....	55
SUPPORTING MATERIAL	59
Movie legends	63
CHAPTER 3: SINGLE-MOLECULE RECONSTITUTION OF A MICROTUBULE-BASED mRNA TRANSPORT COMPLEX	64
ABSTRACT	65
INTRODUCTION	66
MATERIALS AND METHODS	69
<i>K10</i> mRNA constructs.....	69
Protein constructs	69
Protein expression and purification	70
RNA synthesis	74
Flow cell preparation.....	75
Single molecule total internal reflection fluorescence (TIRF) microscopy assays	75

FLAG immunoprecipitation	78
Imaging and analysis	79
Analytical ultracentrifugation.....	79
Negative stain electron microscopy.....	80
RESULTS	81
Full-length BicD is auto-inhibited for dynein-dynactin recruitment.....	81
BicD forms a folded looped conformation	83
BicD extends when bound to Egalitarian but not Rab6 ^{GTP}	83
mRNA cargo is needed for dynein-dynactin recruitment to BicD-Egalitarian in single molecule in vitro assays.....	86
<i>K10</i> mRNA activates mRNPs for processive movement and fast speeds	89
mRNPs contain multiple copies of Egalitarian and are dynamic	92
DISCUSSION	94
ACKNOWLEDGEMENTS	100
REFERENCES.....	100
CHAPTER 4: DISCUSSION.....	104
Mechanisms of mRNA transport in budding yeast	104
Mechanisms of mRNA transport in <i>Drosophila</i>	104
Comparison of yeast and <i>Drosophila</i> mRNA transport mechanisms	106
Molecular motors involved in cargo transport are auto-inhibited	107
Two adapters couple motor activation with cargo selection	110
Models of BicD activation by cargo binding adapters	113
The requirement of mRNA cargo for activation of motor processivity	118
Implications for other cargo systems.....	119
Mechanisms for speed enhancements with multiple dynein motors	121
Recruitment of multiple motors to localizing mRNA	125
Bidirectional mRNA transport	127
LITERATURE CITED	129

APPENDIX I: INVOLVMENT OF THE MYO4P GLOBULAR TAIL IN MEMBRANE ATTACHMENT AND TETHERING	151
mRNA anchoring.....	151
Cortical ER transport.....	152
METHODS	156
Vesicle preparation.....	156
Vesicle motility	158
REFERENCES.....	158
APPENDIX II: ALTERNATIVE DYNEIN CARGOS AND RECRUITMENT OF KINESIN-1 FOR BIDIRECTIONAL TRANSPORT	160
Rab6 is a vesicular cargo adapter protein.....	160
Rab6 ^{GTP} alone is not sufficient to activate BicD	162
FMRP is an mRNA cargo adapter protein	168
FMRP forms protein droplets.....	169
Dynein and kinesin motor coupling through a shared cargo	173
METHODS	177
mRNA constructs	177
Protein constructs	177
Protein expression and purification	178
Single molecule motility assays with Rab6 ^{GTP}	179
Motility assays for complexes containing kinesin-1 and dynein.....	179
FLAG immunoprecipitations.....	180
Lipid droplet formation	181
REFERENCES.....	182

LIST OF TABLES

Table	Page
Table 2-1. Characteristic motion of mRNPs containing various <i>ASH1</i> mRNA zip codes	42
Table 2-S1. Sequences constituting the four native <i>ASH1</i> mRNA zip codes	62
Table 2-S2. Nucleotide sequences present or base pair changes made to ablate zip code elements for each <i>ASH1</i> mRNA construct	62

LIST OF FIGURES

Figure	Page
Figure 1-1. Factors required for localizing budding yeast <i>ASH1</i> mRNA and <i>Drosophila K10</i> mRNA	3
Figure 1-2. <i>ASH1</i> mRNA localization in budding yeast and attributes of a processive myosin motor	11
Figure 1-3. Myo4p–She3p bound to She2p forms a double-headed complex.....	16
Figure 1-4. <i>K10</i> mRNA localization and domain organization of dynein and dynactin	22
Figure 1-5. Mechanisms of dynein/dynactin activation.....	26
Figure 1-6. Potential Mechanisms of BicD activation by Egalitarian	28
Figure 2-1. The frequency of mRNP processive runs increases with zip code number	40
Figure 2-2. The Myo4p globular tail stabilizes the mRNP, and the recruitment of multiple motors to <i>ASH1</i> is concentration dependent	45
Figure 2-3. Metal-shadowed images show variable recruitment of motors.....	47
Figure 2-4. Comparison of mRNP movement on single actin filaments versus bundles	49
Figure 2-5. The spacing between two moving motor complexes coupled by mRNA varies.....	50
Figure 2-S1. Gel electrophoresis showing the relative sizes of Alexa-488 labeled <i>ASH1</i> mRNA constructs following <i>in vitro</i> synthesis	59
Figure 2-S2. Characteristic run length and speed of Myo4p mRNPs containing <i>ASH1</i> mRNA with the indicated number of zip codes	60
Figure 2-S3. Characteristic run length and speed of labeled Myo4p mRNPs in the presence of excess unlabeled motor and <i>ASH1</i> mRNA to promote zip code occupancy	61

Figure 3-1. Truncated but not full-length BicD binds dynein and dynactin	82
Figure 3-2. Conformation of BicD alone and when bound to Rab6 ^{GTP} or Egalitarian.....	85
Figure 3-3. <i>K10</i> mRNA is needed for BicD-Egalitarian to recruit dynein-dynactin.....	88
Figure 3-4. Comparison of the motile properties of DDB ^{CC1} and <i>K10</i> mRNPs.....	91
Figure 3-5. Imaging of multiple Egalitarian proteins and dynamics of motile mRNPs	93
Figure 4-1. Mechanisms for mRNA transport in budding yeast and <i>Drosophila</i>	106
Figure 4-2. Models of BicD activation	115
Appendix I - Figure 1. Structural comparison between the Myo4p globular tail and exocyst subunit Sec6p.....	152
Appendix I - Figure 2. Myo4p–She3p directly binds lipid vesicles through the Myo4p globular tail domain	153
Appendix I - Figure 3. Extruder setup	157
Appendix II - Figure 1. Diagram showing interactions between BicD, dynein/dynactin and Rab6	160
Appendix II - Figure 2. FLAG BicD pull-downs with <i>Drosophila</i> kinesin-1 (no light chains) and Rab6 ^{GTP}	164
Appendix II - Figure 3. FLAG BicD pull-downs with <i>Drosophila</i> kinesin-1	165
Appendix II - Figure 4. FMRP domain structure.....	168
Appendix II – Figure 5. Formation of FMRP protein droplets and mRNA-dependent FMRP micro-domains	171
Appendix II – Figure 6. Bidirectional motility of reconstituted complexes containing dynein and <i>Drosophila</i> kinesin-1	174

LIST OF ABBREVIATIONS

AAA+.....	ATPases associated with various activities
AMP-PNP	Adenylyl-imidodiphosphate
Arp	Actin related protein
BicD	Bicaudal D
CaM.....	Calmodulin
CC	Coiled-coil
DDB	Dynein-dynactin-BicD
FMRP	Fragile X mental retardation protein
GDP.....	Guanosine diphosphate
GTP	Guanosine triphosphate
HC	Heavy chain
IC.....	Intermediate chain
LIC	Light intermediate chain
MgADP	Magnesium adenosine diphosphate
MgATP	Magnesium adenosine triphosphate
mRNP.....	Messenger ribonucleoprotein
OAc	Acetate
Qdot.....	Quantum dot
S	Svedberg
TIRF.....	Total internal reflection fluorescence
TLS	Transport and localization sequence
Tpm	Tropomyosin
YFP	Yellow fluorescent protein

CHAPTER 1: INTRODUCTION

mRNA localization

The discovery of protein-encoded signal peptides that direct transport and subcellular localization of secretory proteins led to the general idea that protein sorting occurs post-translationally (Blobel and Dobberstein, 1975). More recently, it was shown that protein localization can also be controlled by targeting mRNA transcripts that encode them. Similar to signal peptides that direct protein localization in the cell, localizing mRNAs contain mRNA-encoded localization elements called ‘zip codes’ that direct their transport. For many years, mRNA localization was thought to apply to only a few transcripts with specialized biological functions but only in the past few years has it been fully appreciated the extent by which cells utilize this mechanism for a diversity of cellular processes. Recently, a comprehensive high resolution fluorescence *in situ* hybridization screen of over 3000 genes in the *Drosophila* embryo showed that 71% of mRNA transcripts are localized (Lecuyer et al., 2007). Similarly, in mammalian neurons, hundreds of mRNA transcripts encoding proteins with diverse biological functions are localized to polyribosome-rich regions in dendritic spines (Eberwine et al., 2002; Martin and Zukin, 2006).

mRNA location is fundamentally distinct from other protein sorting mechanisms because it allows gene expression to become spatially restricted in the cytoplasm. This offers a number of key advantages. One of these is the ability to regulate gene expression ‘on site’ in response to local stimuli. This function of localizing mRNAs is best described in neurons. The discovery that dendritic spines contain mRNA, ribosomes and translation

factors first suggested that synapses can be modified individually through local gene regulation (Steward and Levy, 1982). More recently, studies have shown that active translation of a number of transcripts in spines is important for maintaining synaptic plasticity (Huber et al., 2000; Miller et al., 2002). One of the most well studied examples of this is the role of Arc in long term potentiation (LTP). The induction of LTP in cortical neurons induces the expression of a number of immediate early genes (Link et al., 1995; Lyford et al., 1995). One of these genes, Arc (activity-regulated cytoskeleton-associated protein) is rapidly delivered to a subset of activated dendritic segments (Steward et al., 1998). Once delivered, Arc couples gene expression with actin dynamics to remodel the synapse in response to local signals (Chen et al., 2007; Fukazawa et al., 2003; Kim and Lisman, 1999; Krucker et al., 2000; Matsuzaki et al., 2004; Rex et al., 2007; Steward et al., 1998; Steward and Worley, 2001).

A second advantage of spatially restricting gene expression is the strict requirement of some proteins to be expressed in defined cytoplasmic regions to determine cell fate. One classic example of this is the establishment of dorsalventral polarity in the *Drosophila* embryo (Johnstone and Lasko, 2001). Ectopic localization of mRNA transcripts that establish polarity of the developing oocyte lead to severe developmental defects and this process is essential for survival to adulthood (Mohler and Wieschaus, 1986). In stage 9 of *Drosophila* embryogenesis, the egg chamber contains a single oocyte, 15 nurse cells that are connected to the oocyte by cytoplasmic bridges, and a surrounding epithelium of somatic follicle cells (**Fig. 1-1, B**). The selective differentiation of follicle cells in relation to the oocyte nucleus defines the dorsal and ventral axis of the *Drosophila* embryo. This

A Mother Bud
ASH1 mRNA

B Nurse cells K10 mRNA oocyte
Anterior Stage 8 Stage 2 Posterior

C Budding yeast
Actin
Myo4p She3p
She2p
ASH1 E3

D Drosophila
Microtubule
Dynein/dynactin BicD
Egalitarian
K10 TLS

3

to the anterior margin relies on its transport by dynein (purple) on microtubules (grey/cyan) and the adapter proteins BicD (cyan) and Egalitarian (yellow). BicD binds directly to dynein/dynactin and Egalitarian binds BicD and *K10* mRNA through a single zip code called *K10* TLS (minimal sequence shown).

Early in oogenesis, *K10* mRNA is produced in nurse cells and immediately transported into the oocyte. This is a highly selective process as most mRNAs produced in the nurse cells are retained until later stages of development (Mahowald and Strassheim, 1970). In stage 9, *K10* mRNA localizes to the anterior margin of the oocyte and its nucleus migrates to the dorso-anterior corner (**Fig. 1-1, B**). Beginning at this stage and continuing until stage 12, *K10* protein becomes sequestered in the nucleus creating a morphogen gradient where somatic follicle cells nearest the oocyte nucleus are stimulated for dorsal-like cell differentiation and those furthest from the nucleus are repressed (Cheung et al., 1992). Thus, the strict spatial localization of *K10* mRNA in relation to the nucleus is needed to define somatic cell fates in the early embryo.

A second cell fate determinate is *ASH1* mRNA in the budding yeast, *Saccharomyces cerevisiae*. *ASH1* encodes the protein Ash1p, a suppressor of HO endonuclease and mating-type switching (Bobola et al., 1996). This requirement ensures that Ash1 protein is produced only in the emerging bud. The resulting asymmetric distribution of Ash1 protein determines that the mother and daughter have distinct mating types (Long et al., 2001; Long et al., 1997; Sil and Herskowitz, 1996). A mutagenic screen identified five genes that are required for *ASH1* mRNA localization to the bud tip: *SHE1-SHE5* (short for Swi5p-dependent HO expression) (Jansen et al., 1996). *SHE1* encodes a class V myosin motor, Myo4p that specializes in the transport of mRNA and

cortical ER on actin cables. *SHE2* encodes the mRNA binding protein She2p that binds specifically to zip code sequences in *ASH1* mRNA and *SHE3* encodes an adapter protein that links She2p to the motor (**Fig. 1-1, C**). Little is known about the function of *SHE5* in mRNA transport. It encodes for the protein Bni1 which is shown to involve maintaining of actin cytoskeleton polarity which is likely important for targeting of Myo4p-mRNA complexes to the bud tip (Munchow et al., 1999).

In these examples, mRNA localization is required to establish well defined protein gradients and this special requirement is undoubtedly the most extensively studied function of localizing mRNAs.

Another function of mRNA localization is co-translational assembly of large cytoskeletal structures. A number of cytoskeletal proteins have been shown to assemble with large molecular complexes during translation. These include the incorporation of vimentin, myosin heavy chain, titin, and tropomyosin into the contractile apparatus of muscle (Cripe et al., 1993; Isaacs and Fulton, 1987; Isaacs et al., 1989; L'Ecuyer et al., 1998). The major advantage of co-translational protein assembly is that organizational information is provided during translation. mRNA localization is likely critical for this retaining this information. In support of this, some mRNAs such as vimentin co-localize with their protein product in the sarcomere (Cripe et al., 1993). Surprisingly, this mechanism appears conserved in protozoa. *Naegleria gruberi* amebas differentiate to a motile flagellated form which requires the assembly of two basal bodies, two flagella, and cytoskeletal microtubules (Baron and Salisbury, 1988). These structures appear to be nucleated by localizing mRNAs raising the intriguing possibility that the maturing basal

body may template the incorporation of nascent proteins during assembly (Han et al., 1997).

Mechanisms of mRNA transport

Localizing mRNAs encode localization elements that bind specifically to RNA-binding proteins linking the mRNA to transport machinery. The first demonstration of mRNA localization was shown with the β -actin mRNA in mammalian fibroblasts. Using *in situ* hybridization, Lawrence and Singer found that a 54 base-pair element encoded in the 3'UTR of the β -actin gene was both necessary and sufficient for its localization at the leading edge (Lawrence and Singer, 1986; Ross et al., 1997). This element was called a 'zip code' because it encodes the information needed for its delivery in the cell.

Zip codes vary dramatically in terms of sequence, structure and organization, which likely reflects the diversity of mRNA binding proteins that target transcripts through a number of localization mechanisms. Some localizing mRNA transcripts are targeted through selective stabilization. One of the best studied example of this is the localization of heat shock protein 83 (hsp83) mRNA in the posterior pole plasm of *Drosophila* embryos. *hsp83* mRNA encodes a degradation element in the 3'UTR that binds the mRNA binding protein, Smaug which signals the destruction of the transcript through the CCR4/Not deadenylase pathway. Interestingly, the *hsp83* transcript also contains a separate 'protection' element in the 3' UTR which protects the transcript from degradation at the posterior pole. Deletion of this element results in complete loss of transcript from the cell (Bashirullah et al., 2001; Tadros et al., 2007).

A second mechanism of targeting is through diffusion and entrapment. In the *Xenopus* oocyte, a subset of localizing mRNAs contains elements in their 3' UTR necessary for localizing to the vegetal pole. These mRNAs are linked to a densely packed mitochondrial network called the mitochondrial cloud through the mRNA-binding protein Vg1RBP/Vera. Targeting of these transcripts require the detachment of the mitochondrial cloud from the nucleus and migration to the vegetal cortex (Chang et al., 2004). Similar diffusion and entrapment mechanisms have been described in other systems (Forrest and Gavis, 2003).

The majority of targeted transcripts achieve their localization through mechanisms involving active, molecular motor-based transport on either actin or microtubule tracks (Gagnon and Mowry, 2011). There are three classes of molecular motors. Myosin is an actin-based cargo transporter and dynein and kinesin transport their cargoes on microtubules. Localizing mRNAs use all three classes of motors for their transport, sometimes working together.

ASH1 mRNA

Budding yeast *ASH1* mRNA is the most extensively studied localizing transcript because proteins involved in its transport and localization are not required for cell survival. *ASH1* mRNA uses actin cables as its method of transport in budding yeast. It contains four well defined stem loops, each sufficient for mRNA localization to the bud tip (**Fig. 1-1, C**). Three of these are located in the coding sequence (E1, E2A and E2B) and one is located in the 3'UTR (E3). Mutagenesis studies indicate that both the structure and primary sequence of these stem loops are necessary for associating with transport machinery (Chartrand et

al., 1999; Gonzalez et al., 1999; Olivier et al., 2005). Each of these zip codes is sufficient for its transport but all are necessary to restrict *ASH1* to the bud tip. Thus, multiple zip codes cooperate to promote attachment by enhancing transport or facilitating anchoring (Chartrand et al., 1999; Gonzalez et al., 1999).

Pair-rule transcripts

In higher eukaryotes, localizing mRNAs are often transported on microtubules by dynein and/or kinesin. One model system that has provided the most molecular insight into microtubule-based mRNA transport is the localization of pair-rule transcripts in the patterning of *Drosophila* embryos. Pair-rule transcripts encode transcription factors that localize to the apical side of peripheral nuclei in the *Drosophila* syncytial blastoderm embryo (stage 4). These proteins cooperate to establish segmental organization by overlapping their localization to sets of circumferential stripes (Bullock et al., 2004). Mis-localization of pair-rule mRNA results in mild segmentation defects and gene dose sensitivity (Bullock et al., 2004). One hypothesis for the observed defects is that localization to the apical end of the cell targets translation to the nucleus. Similar mechanisms which position mRNA near the nucleus to aid in nuclear import has also been observed in cultures mammalian cells and may serve as a general mechanism to aid in nuclear import of proteins expressed in low levels or with short half-lives (Edgar et al., 1987; Levadoux et al., 1999).

Pair-rule transcripts encode zip code sequences in their 3'UTR that are required for their localization (Davis and Ish-Horowicz, 1991). Extensive studies using injected labeled mRNA transcripts in *Drosophila* embryos showed that these mRNAs are linked to

cytoplasmic dynein by the mRNA binding protein Egalitarian and the dynein adapter protein BicD for transport on microtubule tracks (Bullock and Ish-Horowicz, 2001; Wilkie and Davis, 2001) (**Fig. 1-1, D**).

Maternal transcripts

This transport machinery is shared later in *Drosophila* development to establishment of dorsalventral polarity in the *Drosophila* embryo. (Johnstone and Lasko, 2001). *K10* mRNA is transported from nurse cells to the oocyte where it localizes to the anterior margin to establish dorsal polarity. *K10* mRNA contains a single localization element in its 3'UTR. This zip code forms a small, 44 base-pair stem loop that is necessary for localization at the anterior margin of the oocyte (Serano and Cohen, 1995) (**Fig. 1, D**). Interestingly, injected labeled *K10* mRNA transcripts in the syncytial blastoderm embryo are immediately transported apically and require Egalitarian and BicD for its localization (Bullock and Ish-Horowicz, 2001; Dienstbier et al., 2009). Thus, recruitment of the dynein-Egalitarian-BicD transport complex appears to be a general mechanism to control mRNA transport and localization throughout *Drosophila* development.

K10 mRNA has a relatively simple localization program because it remains at the anterior of the embryo from early to late oogenesis. This is because, in mid-oogenesis, microtubules nucleate from the anterior and grow to the posterior pole of the oocyte. Thus, by design, *K10* needs only to be trafficked towards the minus-end of the microtubule. Other maternal transcripts have a more complicated localization program. In early oogenesis, *oskar* mRNA is trafficked by the dynein-Egalitarian-BicD transport complex to the anterior of the oocyte. This trafficking requires the zip code sequence, OES (for oocyte entry signal)

(Jambor et al., 2014). From stage 9 onwards, *oskar* re-localizes to the posterior of the oocyte to establish proper posterior patterning of the embryo (Snee et al., 2007). This localization requires a separate zip code called SOLE (also located in the 3'UTR) that binds the mRNA adapter protein Staufen and links the mRNA to kinesin 1 for transport to the posterior pole (Brendza et al., 2000; Hachet and Ephrussi, 2004).

ASH1 mRNA transport in budding yeast

Budding yeast provides an attractive model organism to study the spatial and temporal control of mRNA localization, because yeast exclusively use one class V myosin motor for this process. The mRNA binding protein She2p links the myosin motor to its mRNA cargo. The simplicity of this system led to a large number of cell biological experiments in budding yeast, primarily aimed at understanding the features required for correct localization of mRNA transcripts to the bud tip (**Fig. 1-2, A**) (Bobola et al., 1996; Bohl et al., 2000; Chartrand et al., 1999; Jansen et al., 1996; Long et al., 1997; Takizawa et al., 1997; Takizawa and Vale, 2000). One of the most widely-studied localizing mRNAs is the budding yeast *ASH1* mRNA.

ASH1 encodes the protein Ash1p, a suppressor of HO endonuclease and mating-type switching (Bobola et al., 1996). Its localization ensures that Ash1 protein is produced only in the emerging bud. The resulting asymmetric distribution of Ash1 protein determines that the mother and daughter have distinct mating types (Long et al., 2001; Long et al., 1997; Sil and Herskowitz, 1996). The *ASH1* transcript contains four well defined stem loops, each sufficient for mRNA localization. Three of these are located in the coding sequence (E1, E2A and E2B) and one is located in the 3'UTR (E3). Mutational

studies indicate that both the structure and primary sequence of these stem loops are necessary for associating with transport machinery (Chartrand et al., 1999; Gonzalez et al., 1999; Olivier et al., 2005). Each of these zip codes is sufficient for mRNA transport but all are necessary to restrict *ASH1* mRNA to the bud tip. Thus, multiple zip codes cooperate to promote localization by enhancing transport and/or facilitating anchoring (Chartrand et al., 1999; Gonzalez et al., 1999).

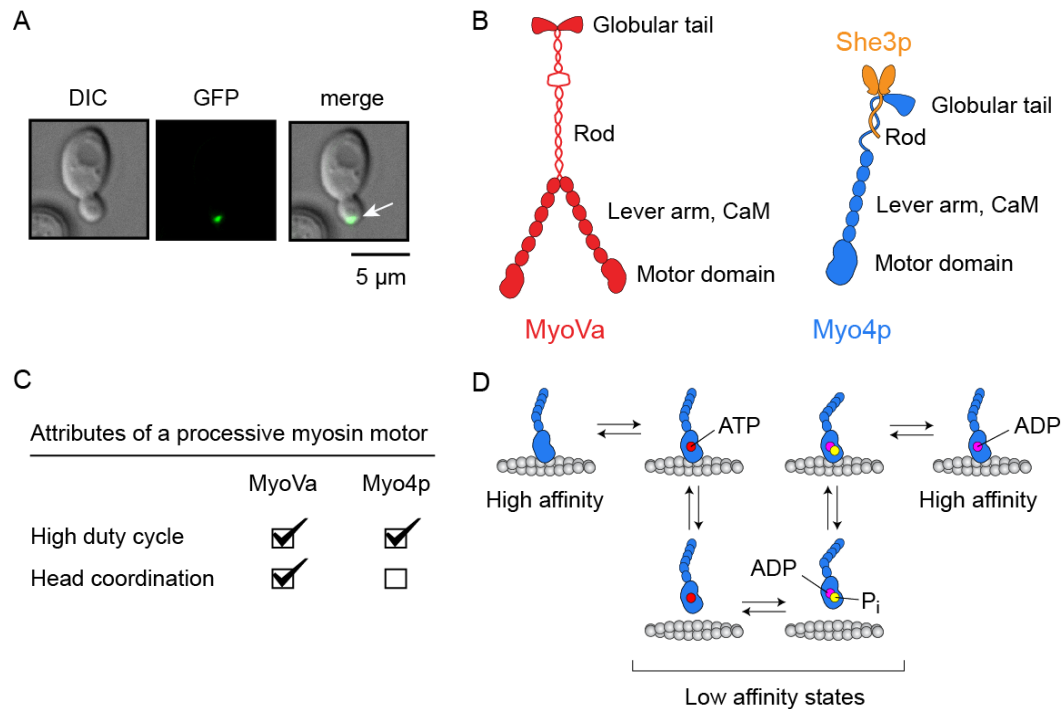


Figure 1-2. *ASH1* mRNA localization in budding yeast and attributes of a processive myosin motor. (A) Image of *ASH1* mRNA localization to the bud tip (green dot, white arrow) in budding yeast. *ASH1* mRNA was localized using a GFP *in vivo* reporter system (Bertrand et al., 1998). Differential interference contrast (DIC) microscopy shows the outline of the cell. (B) Diagram comparing structural features of mammalian myosin Va (MyoVa) (Red) and the class V myosin in budding yeast, Myo4p (Blue). Myo4p forms a complex with the adapter protein She3p (orange) (C) Comparison between MyoVa and Myo4p of features important for myosin processivity on actin. (D) Kinetic cycle of myosin Va showing that the motor transitions between states with a high affinity for actin when the motor is bound to ADP or no nucleotide, and states with a weak affinity for actin when the motor is bound to ATP or ADP and P_i .

Budding yeast contains two class V myosins, one of which is Myo4p. Myo4p is specialized in the transport of cortical ER, and over 20 different localizing mRNAs from the mother to the bud tip on actin cables, including *ASH1* mRNA (Bobola et al., 1996; Estrada et al., 2003; Jambhekar et al., 2005; Long et al., 1997; Shepard et al., 2003; Takizawa et al., 1997). Imaging of tagged mRNA in budding yeast showed its continuous transport over several microns at a rate of $\sim 0.3 \mu\text{m}/\text{sec}$, (Bertrand et al., 1998) as expected for a motor-driven process. Surprisingly, when Myo4p was purified from yeast cells (Reck-Peterson et al., 2001) and characterized by ensemble *in vitro* motility assays, it appeared to have a low duty cycle meaning that the myosin head stays attached to actin for only a small fraction of its ATPase cycle. A cargo transporter needs to have a high duty cycle, (i.e., the myosin head needs to stay attached to actin for a large fraction of its ATPase cycle), which enables the motor to move micron-long distances along actin tracks as a single molecule, a feature known as processivity.

The discrepancy between the *in vivo* and *in vitro* observations needed to be reconciled. One possibility is that mRNA transport is accomplished by teams of non-processive motors that act together to move cargo continuously. Alternatively, other factors such as the adaptor protein She2p or the mRNA cargo itself, which were not present in the simplified *in vitro* assays, could affect the properties of Myo4p. If true, cargo transport could be regulated in the cell by accessory factors that turn the motor “on” or “off” for processive transport.

Two motor heads are needed for processivity

Mammalian myosin Va (MyoVa) is a processive cargo transporter and serves as a model for a transporting myosin (**Fig. 1-2, B and C**) (Trybus, 2008). The N-terminal motor domain of MyoVa binds MgATP and actin, and their binding is mutually exclusive (Coureux et al., 2004; Coureux et al., 2003). Thus, myosin transitions between weakly-bound and strongly-bound actin states. The rate limiting step in its kinetic cycle is ADP dissociation from the strongly bound actomyosin-ADP complex. As a result, myosin V spends the majority of its kinetic cycle strongly bound to actin (De La Cruz et al., 1999) (**Fig. 1-2, D**). The ratio of time myosin spends in the strongly bound state over the total cycle time is called its ‘duty ratio’. MyoVa is also double-headed and the ATPase cycles of the two heads are coordinated (Veigel et al., 2002). Having both a high duty cycle and two coordinated heads allows cargo transporting myosins to take multiple steps on actin without dissociating (**Fig. 1-2, B and C**).

To determine if Myo4p has a high duty ratio, we expressed and purified a chimeric construct from the *Sf9*/baculovirus system containing the motor domain of Myo4p and the lever arm and rod domains of MyoVa. This chimera was capable of supporting processive motion as a single molecule on actin filaments (Krementsova et al., 2011), demonstrating that it must have a sufficiently high duty cycle (>50%) to support single molecule processivity.

The motor domain of MyoVa is followed by a long extended alpha helical lever arm that has six calmodulin-binding IQ motifs, defined by the consensus sequence IQxxxRGxxxR, where x denotes any amino acid. The length of the lever arm is important

as it determines the motor's step size which follows the 36 nm pseudo-repeat of an actin filament (Moore et al., 2001; Purcell et al., 2002; Sakamoto et al., 2005). The sequence of the Myo4p lever arm domain indicates that it has a full complement of IQ motifs for binding six calmodulins (Krementsova et al., 2011). In principle, Myo4p can walk with a 36 nm step size on actin, similar to MyoVa.

The MyoVa alpha-helical coiled-coil rod domain adjacent to the lever arm contains >20 heptads, a repeating sequence of seven amino acids (abcdefg) where “a” and “d” positions are typically hydrophobic. This domain is sufficient for dimerization (Lu et al., 2006). Thus, an essential function of the rod is to ensure that the motor is double-headed. This feature of class V myosin ensures that one of the two heads always remains attached to the filament for many kinetic cycles without dissociating (Churchman et al., 2005; Warshaw et al., 2005).

In contrast, the number of heptad repeats in the rod region of Myo4p is small (~5), making it unlikely to form an alpha-helical coiled-coil dimer. Sedimentation velocity experiments showed that myosin constructs containing the rod and globular tail domains of Myo4p had a strong tendency to aggregate (Hodges et al., 2008), suggesting that an additional binding partner might be needed to stabilize the myosin. One candidate is the adapter protein She3p. Once co-expressed with She3p, the motor complex became homogeneous, and sedimentation equilibrium showed that the molecular weight was consistent with a single-headed motor.

Myo4p isolated from yeast co-purifies with She3p, consistent with its role in *ASH1* mRNA transport (Dunn et al., 2007). The N-terminus of She3p forms a coiled-coil that

interacts with Myo4p, and the C-terminal domain binds the mRNA adapter protein She2p (Bohl et al., 2000; Shi et al., 2014). Myosin constructs containing the rod and globular tail domains of Myo4p, when co-expressed with She3p in the *Sf9*/baculovirus system, co-purifies as a homogenous complex (Hodges et al., 2008). The stoichiometry of Myo4p to She3p is 1:2 (one myosin heavy chain to one She3p dimer) (Heym et al., 2013; Shi et al., 2014). Negative stain electron microscopy confirmed that the Myo4p-She3p complex is single-headed (Dunn et al., 2007; Krementsova et al., 2011). Thus, the most unusual feature of Myo4p is that it forms a single-headed complex with She3p (Hodges et al., 2008). The simple reason why the Myo4p-She3p motor complex cannot “walk” processively on actin filaments like other class V myosins is because it is a single-headed motor that cannot step in a coordinated fashion actin (Dunn et al., 2007; Hodges et al., 2008).

Structural insights from X-ray crystallography showed that an interaction between Myo4p and a truncated dimeric fragment of She3p is mediated through a hydrophobic patch in the globular tail domain of Myo4p (Shi et al., 2014). But we also know that a truncated version of Myo4p lacking the globular tail still binds She3p tightly (Hodges et al., 2008; Sladewski et al., 2013), implying that there are likely to be additional interactions between the Myo4p rod and She3p that were not observed in the crystal structure. Future structural studies on additional domains of Myo4p-She3p will be needed to fully understand how the motor complex is stabilized.

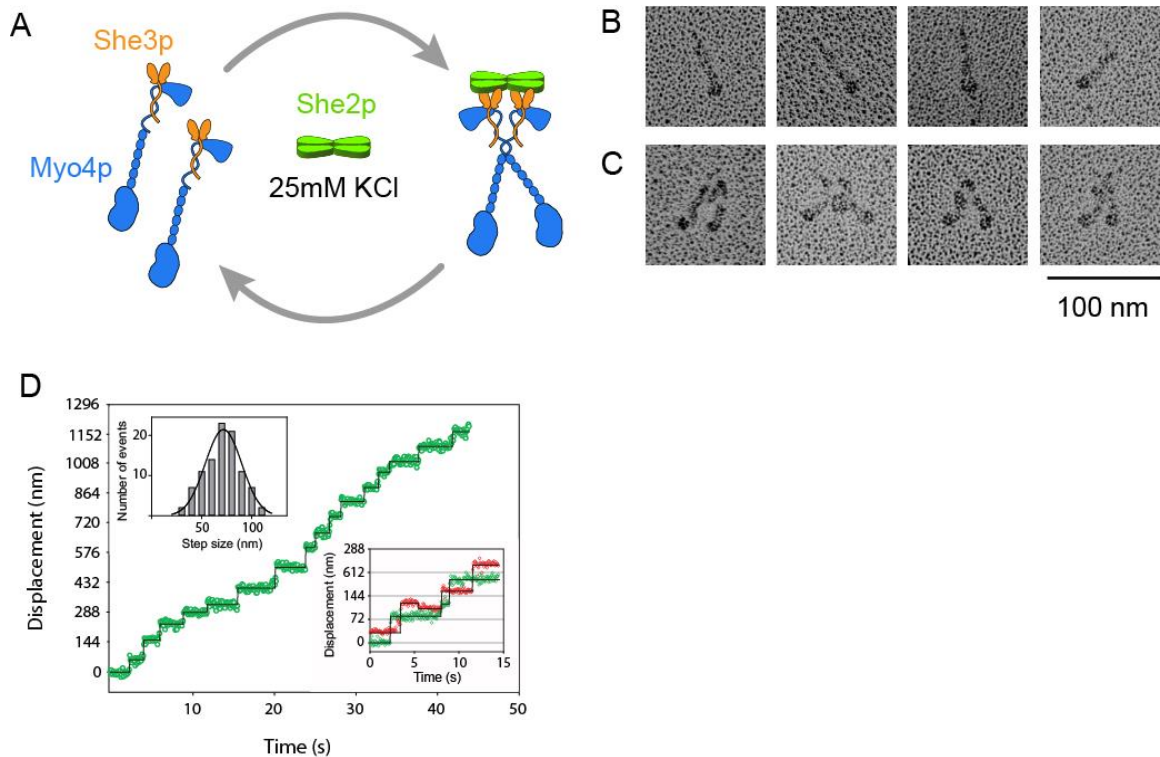


Figure 1-3. Myo4p-She3p bound to She2p forms a double-headed complex. (A) Diagram showing that She2p recruits two single-headed Myo4p-She3p complexes to form a processive double-headed motor complex at low ionic strength (<50mM KCl). She3p is shown as a dimer interacting with the Myo4p globular tail and rod. (B, C) Electron microscopy of metal-shadowed images showing (B) single-headed Myo4p-She3p complexes, and (C) double-headed Myo4p-She3p-She2p motor complexes at low ionic strength. (D) Trace showing the displacement versus time of the Myo4p-She3p-She2p motor complex on an actin filament at low ionic strength (50 mM KCl). The multiple steps without dissociation illustrate that the complex is processive. Myo4p-She3p is labeled with a Quantum dot on only one head of the two-headed motor complex. The top left inset shows the histogram of step sizes, that average 72 ± 18 nm. The bottom right inset shows a stepping trace of a two-headed complex in which each head is labeled with a different colored Quantum dot. These data illustrate the hand-over-hand stepping pattern of the two heads, which implies communication between the heads (Sladewski et al., 2013). Images were from (Sladewski and Trybus, 2014) reprinted with permission from Taylor & Francis.

The Myo4p-She3p complex is recruited to localizing transcripts through the mRNA-binding protein She2p (Krementsova et al., 2011; Muller et al., 2009). She2p is a tetramer (Chung and Takizawa, 2010; Krementsova et al., 2011; Muller et al., 2009), and

the four binding sites provide a potential mechanism to recruit multiple Myo4p-She3p motor complexes in close proximity (**Fig. 1-3, A**). Electron microscopy of metal-shadowed images showed that in the absence of She2p, the Myo4p-She3p complex is single-headed (**Fig. 1-3, B**). However, addition of She2p to this complex revealed V-shapes structures that closely resemble double-headed vertebrate myosin Va (**Fig. 1-3, C**). She2p is thus capable of recruiting two single-headed Myo4p-She3p motors, resulting in a stoichiometry of two Myo4p heavy chains: two She3p dimers: one She2p tetramer (Heym et al., 2013; Shi et al., 2014). Importantly, we showed that this two-headed motor complex, recruited via She2p, steps processively on actin filaments with a 36 nm step-size (Krementsova et al., 2011) and with a hand-over-hand stepping pattern identical to that observed with myosin Va (**Fig. 1-3, D**) (Warshaw et al., 2005).

Myo4p-She3p assembles into a processive dimer when bound to She2p at low ionic strength (50 mM KCl), but this complex dissociates when the ionic strength is raised to near physiological (140 mM KCl). Salt concentrations ~50 mM KCl are typically used in *in vitro* motility assays to enhance interactions, but these conditions may lead to conclusions that are not relevant in the cell. In this case, our observation that the complex dissociates at 140 mM KCl implies that to function as a cargo transporter in the cell, other cellular factors are required to stabilize the two-headed motor complex. An obvious candidate is the cargo itself.

We therefore reconstituted a messenger ribonucleoprotein (mRNP) by adding the budding yeast localizing mRNA transcript *ASH1*, to the Myo4p-She3p-She2p complex. The mRNA was synthesized with a fluorescently labeled UTP to visualize mRNPs moving

on actin filaments with high spatial (~10 nm) and temporal (70 ms) resolution. At ionic strength approximating physiologic (140 mM KCl), *ASH1* mRNA was required to stabilize the double-headed motor complex, which moved for long distances on actin (discussed in detail in **Chapter 2**). Cargo is usually thought to be a passive player during transport, but in this case, mRNA participates in the assembly of the mRNP by providing additional interactions that stabilize the complex.

K10 mRNA transport in Drosophila

We next wished to understand if the molecular mechanisms of mRNA transport in yeast are conserved in more complex biological systems. Higher eukaryotes utilize microtubule tracks for most mRNA transport. The *Drosophila* embryo contains a polarized microtubule cytoskeleton and provides a suitable model system for studying how microtubule-based motors, cytoplasmic dynein and kinesin moves mRNA cargo. The RNA-binding protein Egalitarian links dynein to a number of localizing transcripts. One of the most well studied of these is *K10* mRNA. *K10* mRNA is transported from nurse cells to the *Drosophila* oocyte where it localizes to the anterior margin to establish dorsal polarity (Cheung et al., 1992) (**Fig. 1-1, B**). *K10* mRNA contains a single 44 base-pair localization element in its 3'UTR that binds Egalitarian and is necessary for its localization (Dienstbier et al., 2009; Serano and Cohen, 1995).

mRNA transport in *Drosophila* is one of the few model systems where the adapters that link dynein to cargo are well defined. Imaging of labeled mRNA transcripts shows that dynein supports the movement of localizing mRNAs for many microns in the *Drosophila* embryo (Bullock et al., 2006). Although budding yeast dynein is processive (Reck-

Peterson et al., 2006), single molecule *in vitro* studies of vertebrate dynein showed that it is at best weakly processive (King and Schroer, 2000; McKenney et al., 2014; Miura et al., 2010; Ross et al., 2006; Schlager et al., 2014; Trokter et al., 2012; Wang et al., 1995). One possibility is that dynein works in teams to move cargo (Mallik et al., 2013). Alternatively, adapter proteins and/or cargo may be required to activate dynein for processive movement. This latter idea has recently gained a great deal of support because studies showed that mammalian dynein without activators exists in an auto-inhibited state (McKenney et al., 2014; Schlager et al., 2014; Torisawa et al., 2014). This finding implies that similar to budding yeast Myo4p, dynein may be activated for processivity by additional proteins.

One protein shown to be important for dynein activation, dynactin, is a large complex of 11 proteins that is required for most of dynein's cellular functions. Dynactin enhances dynein processivity (King and Schroer, 2000; Ross et al., 2006; Tripathy et al., 2014). Another regulatory protein Bicaudal-D2 (BicD2) was shown to enhance dynein function *in vivo*. Hoogenraad and colleagues showed that a fragment of BicD, when fused to mitochondria and peroxisome anchoring sequences, supports robust dynein-driven motility in HeLa cells (Hoogenraad et al., 2001; Hoogenraad et al., 2003). This was the first evidence that a cargo adapter not only links dynein to cargoes but also activates the motor for transport.

We now know have a much better molecular understanding of how dynactin and BicD promote dynein motility in the cell. Dynein, dynactin and a fragment of BicD form a complex that converts single molecules of dynein from a diffusive motor to one that is highly processive *in vitro* (McKenney et al., 2014; Schlager et al., 2014). Interestingly,

BicD interacts with the mRNA binding protein Egalitarian (Dienstbier et al., 2009), indicating that dynein activity may be linked to cargo selection. Here, we explore how dynein, full-length adapters and an mRNA cargo interact to promote activation of a dynein-based messenger ribonucleotide protein (mRNP) complex *in vitro*.

Cytoplasmic dynein

Cytoplasmic dynein is a molecular motor that moves towards the minus-end of microtubules. It transports a variety of cellular cargos including Golgi, endosomes, lysosomes, mitochondria, signaling endosomes, autophagosomes, nuclei, mRNA, viruses and aggregated proteins (Aniento et al., 1993; Boldogh and Pon, 2007; Dodding and Way, 2011; Wilson and Holzbaur, 2012). Coordination of these cargoes requires that the activity of dynein is highly regulated by cargo adapter proteins that bind to its extensive multi-subunit tail domain.

Dynein is a large ~1.5 MDa complex containing two heavy chains (HC) bound to two intermediate (IC) and light intermediate chains (LIC) (**Fig. 1-4, A**). The intermediate chains bind three pairs of light chains (LCs) to form a cargo-binding tail. The largest subunit of dynein is its 500 kDa heavy chain, a member of the AAA+ ATPase (ATPase associated with various cellular activities) superfamily of proteins. One reason the heavy chain is so large is because unlike other AAA+ ATPase proteins which self-assemble into hexameric rings, subunits that makeup the dynein AAA+ ATPase motor domain are covalently linked. The first four AAA+ domains bind MgATP. Studies in budding yeast and in *Dictyostelium* show that mutations that disrupt MgATP hydrolysis in AAA1 completely block dynein function *in vivo* and *in vitro*, while ATP hydrolysis in the domains

2-4 likely serves regulatory functions (Kon et al., 2004; Reck-Peterson and Vale, 2004). Three extensions emerge from the C-terminal AAA+ ATPase motor domain that couple MgATP hydrolysis to motility: a linker domain, a microtubule-binding stalk and a buttress (Schmidt and Carter, 2016). Similar to class V myosins, MgATP and microtubule binding are mutually exclusive. Thus, dynein transitions between weakly and strongly bound microtubule states during its kinetic cycle that require conformational movement of the ring, buttress, stalk and microtubule-binding domain (Carter, 2013; Roberts et al., 2013). These states are coordinated with nucleotide-dependent conformational changes in the linker domain which produces the force needed for cargo movement (Imamura et al., 2007; Mogami et al., 2007).

The N-terminal region of the dynein heavy chain serves two purposes. It contains a small dimerization domain to ensure that dynein is double-headed (Urnavicius et al., 2015) and it also associates with five subunits forming a structural scaffold for recruiting cargo. Two copies of the 71 kDa intermediate chain and 54 kDa light intermediate chain associate directly with the dynein. Three small ~10-12 kDa light chains, TCTex1, LC7 (roadblock) and LC8, bind as homodimers to the intermediate chain.

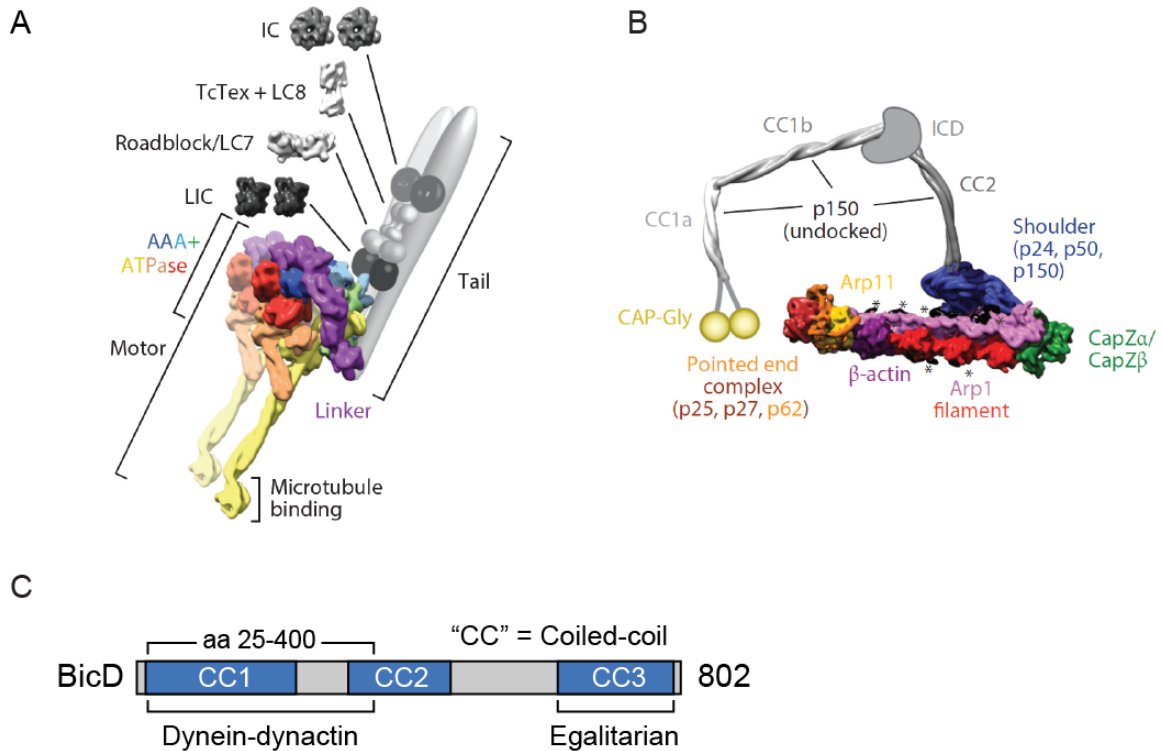


Figure 1-4. *K10* mRNA localization and domain organization of dynein and dynactin
(A) Structure of dynein showing that the dimeric dynein heavy chain contains a C-terminal microtubule-binding stalk (yellow) followed by a AAA+ (ATPase associated with various cellular activities) motor domain and a cargo-binding tail (grey) that associates with dimers of intermediate (IC) and light intermediate chains (LIC). Light chains, Roadblock/LC7, LC8 and TcTex associate with the intermediate chain. **(B)** Structure of dynactin showing that it is built from a ~40 nm-long Arp (Actin related protein) filament composed of Arp1, Arp11 and a β -actin monomer. The pointed end of the Arp filament contains a complex containing p25, p27 and p62. The filament is capped by the capping complex composed of CapZ α and CapZ β . The shoulder is composed of p24 and p50 subunits and is linked to the p150 arm, the largest subunit of dynactin and contains three coiled-coil domains (CC1a, CC1b and CC2), a linker (ICD) and microtubule-binding CAP-Gly domain. **(C)** Diagram showing that BicD contains three coiled-coil sequences (CC1, CC2 and CC3). N-terminal sequences (amino acids 25-400) are shown to interact with dynein and dynactin (Hoogenraad et al., 2003; Urnavicius et al., 2015). The cargo-binding CC3 domain interacts with cargo adapters including Egalitarian (Dienstbier et al., 2009). Images B-C were taken with permission from (Cianfrocco et al., 2015).

Dynactin

Cargo binding to dynein requires the 1.2 MDa accessory complex, dynactin. Dynactin contains 11 different subunits that self-assemble into distinct structural domains (Schroer, 2004) (**Fig. 1-4, B**). At the core of dynactin is a ~40 nm-long Arp (Actin related protein) filament composed of eight Arp1 monomers and a single β -actin subunit. The barbed end of the filament is capped with a CapZ $\alpha\beta$ heterodimer that probably functions to prevent elongation of the Arp filament. The β -actin-containing pointed end of the filament binds Arp11, p25, p27, and p62 to form the pointed-end complex. A shoulder domain projection from the barbed end of the filament contains p150^{Glued}, p50 (dynamitin), and p24 subunits. p150^{Glued} is the largest subunit of dynactin and contains three coiled-coil domains and an N-terminal Cap-Gly domain that binds microtubules. The C-terminus of p150^{Glued} is inserted into the shoulder domain and the coiled-coil regions (CC1A, CC1B and CC2) constitute the arm domain. A recent high resolution structure of dynactin showed that p150^{Glued} coiled-coils dock against the Arp filament in two locations. The CC2 coiled-coil which emerges from the shoulder docks against two Arp subunits near the barbed end and CC1 docks against the side of the pointed end complex (Urnavicius et al., 2015). The p50 subunit forms part of the shoulder complex and it determines the length of the Arp filament because it contains N-terminal extensions that run along a positively charged groove in the filament. These extensions stop where the β -actin monomer is inserted. Thus, p50 may be a molecular ruler that defines the number of Arp1 monomers in the dynactin rod (Urnavicius et al., 2015).

Bicaudal D

Bicaudal D (BicD) is a key adapter protein that links cargoes to dynein and dynactin. It forms a homodimer with a simple domain structure composed of three coiled-coil motifs (CC1, CC2 and CC3) (**Fig. 1-4, C**). A truncated fragment of BicD containing the CC1 and part of the CC2 domain (BicD2^{CC1}) interacts with dynein and dynactin (Hoogenraad et al., 2001). The C-terminal coiled-coil of BicD (CC3) interacts with cargo adapter proteins, linking dynein to a number of cellular cargoes (Bianco et al., 2010; Dienstbier et al., 2009; Januschke et al., 2007; Li et al., 2010; Matanis et al., 2002; Schlager et al., 2010; Splinter et al., 2010; Stuurman et al., 1999).

Recently it was shown that BicD2^{CC1} forms a complex with purified dynein and dynactin and activates single motors for long ultra-processive (>8 μ m) unidirectional motility *in vitro* that is consistent with the distances native cargoes move in cells (McKenney et al., 2014; Schlager et al., 2014) (**Fig. 1-5, A and B**).

Two recent structural studies have revealed how a truncated fragment of BicD (BicD2^{CC1}) activates dynein and dynactin processivity. BicD2^{CC1} makes up part of a functional interface that is needed to stabilize an interaction between the dynein tail domain and the Arp filament of dynactin (Schlager et al., 2014) (**Fig. 1-5, C**). This functional interface explains why all three components are required to form a stable dynein-dynactin-BicD (DDB^{CC1}) complex.

In the absence of cargo adapters, the auto-inhibited state of dynein is associated with a structural conformation known as the phi particle in which the two heads are stacked

together (**Fig. 1-5, D and E**). A truncated construct of dynein where the two heads are physically separated gives unidirectional motility indicating that dynein activation is associated with disrupting this head-head stacking (Torisawa et al., 2014) (**Fig. 1-5, F**). Multiple mechanisms have been proposed to disrupt dynein auto-inhibition. Forces that develop in cargo assemblies driven by multiple dynein motors may be sufficient to disrupt head-head stacking and activate ensembles for transport. In support of this mechanism of activation, multiple dynein motors attached to a bead can support directed motility (King and Schroer, 2000; Mallik et al., 2005). Studies show that only two dynein motors are needed for activation (Torisawa et al., 2014).

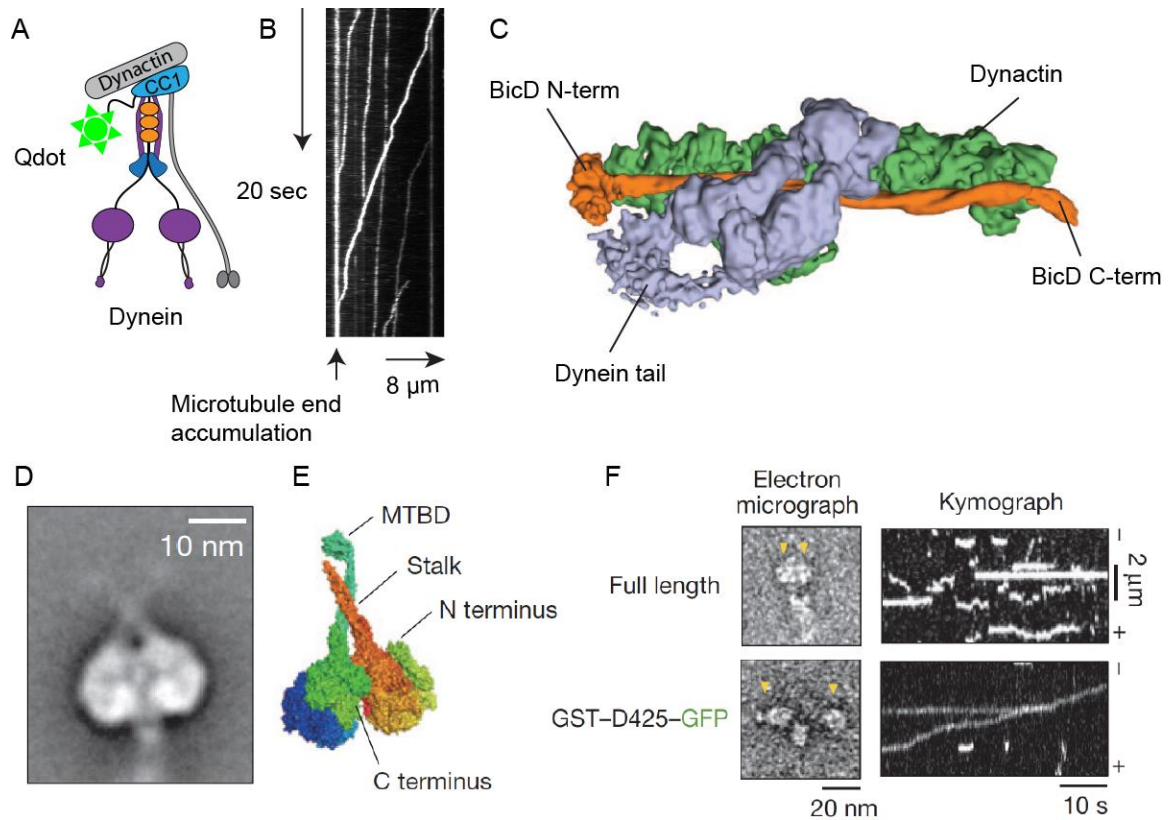


Figure 1-5. Mechanisms of dynein/dynactin activation. (A) Diagram showing that N-terminal sequences of BicD (amino acids 25-400) forms a complex with dynein and dynactin (DDB^{CC1}). (B) Kymograph (time vs distance) showing that the DDB^{CC1} complex labeled with a quantum dot on BicD, moves processively in a single molecule TIRF assay. Microtubule end accumulation is characteristic of DDB^{CC1} motility. (C) An 8.2 angstrom structure of the DDB^{CC1} complex (Urnavicius et al., 2015). BicD^{CC1} (orange) forms a functional interface between dynactin (green) and the dynein tail domain (blue). Dynactin is oriented with its pointed end on the right and barbed end on the left. The barbed end is adjacent to the N-terminus of BicD which is marked by globular YFP density in orange. The dynactin shoulder is mostly hidden by the dynein tail. (D) Class average of negatively stained EM images of dynein heads in an auto-inhibited stacked conformation (Torisawa et al., 2014). (E) Crystal structure of the dynein head domain, PDB 3VKH (Kon et al., 2011). (F) Left shows negative stained EM image of (top) full-length dynein (Full-length) and (bottom) a construct of dynein where the heads were separated by a rigid linker (GST-D425-GFP). Right shows kymographs (distance vs time) demonstrating that dynein in stacked conformations are diffusive while head-separated constructs are processive. Image C was from (Urnavicius et al., 2015), reprinted with permission from AAAS. Images D-F was reprinted by permission from Macmillan Publishers Ltd: [Nature Cell Biology] (Torisawa et al., 2014), copyright (2014) reprinted with permission from Nature Publishing Group.

The finding that only one chain of dynein in the DDB^{CC1} complex contacts the Arp filament suggests that head-head interactions may also be disrupted by this intrinsic asymmetry that may force the heads apart. This may explain in part why dynactin, a well-established dynein activator, is built from a long Arp filament (Schlager et al., 2014). Further support for this mechanisms of dynein activation comes from structural studies of the DDB^{CC1} complex bound to microtubules showing that the dynein heads are aligned to favor unidirectional transport (Chowdhury et al., 2015). Another finding from structural studies of the DDB^{CC1} complex is that the p150^{Glued} subunit of dynactin and BicD have overlapping binding sites near the pointed end complex. Undocking of p150^{Glued} by BicD binding is likely part of dynein's activation mechanism possibly by allowing p150^{Glued} subunit to bind microtubules (McKenney et al., 2014; Tripathy et al., 2014).

BicD is auto-inhibited

The DDB^{CC1} complex has been the focus of a number of studies because it is the minimal complex needed to activate dynein for transport. Unlike the truncated version, full-length BicD does not efficiently recruit dynein in the cell (Hoogenraad et al., 2003) because BicD is auto-inhibited in the absence of cargo binding. In the following sections, I use the term auto-inhibition to describe a state of myosin, dynein or BicD that renders the protein incapable of supporting cargo transport. For example, the auto-inhibited state of Myo4p is single-headed (Hodges et al., 2008), while the auto-inhibited state of dynein involves head-head stacking (Torisawa et al., 2014). The auto-inhibited state of BicD is a conformation that prevents dynein recruitment (Hoogenraad et al., 2003).

Yeast-2-hybrid results indicate that the CC1 domain of BicD interacts with the CC3 domain. Thus, one model is that BicD forms an N- to C-terminal auto-inhibitory interaction (Hoogenraad et al., 2001). However, metal shadowed images of purified *Drosophila* BicD show structures more consistent with a CC2-CC3 interaction (Stuurman et al., 1999) (**Fig. 1-6, A**). How is BicD auto-inhibition relieved? One hypothesis is that cargo adapter proteins that bind the CC3 of BicD may relieve its auto-inhibition.

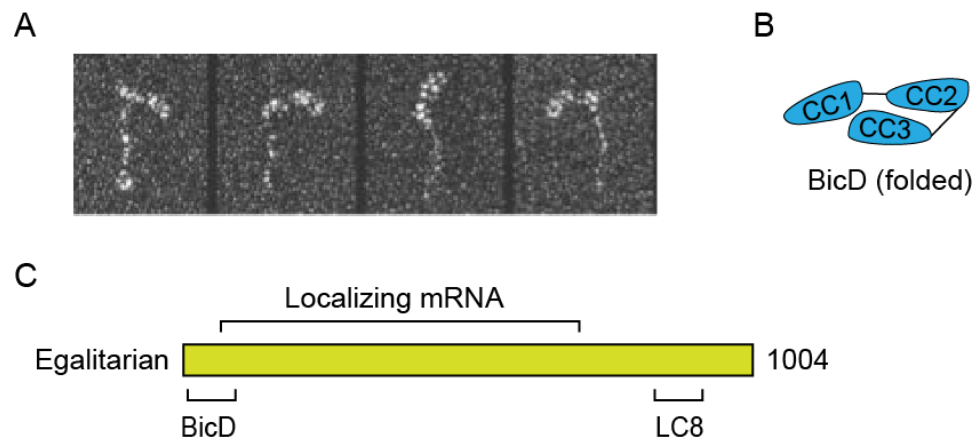


Figure 1-6. Auto-inhibited conformation of BicD and domain structure of Egalitarian. (A) Gallery of metal shadowed image of *Drosophila* BicD showing that it makes auto-inhibitory interactions. The thin segment at the bottom of the structures is the CC1 domain and the thicker segment corresponds to CC2 and CC3 sequences (Stuurman et al., 1999). (B) A cartoon depiction of this intramolecular folding. (C) Diagram showing Egalitarian interacts with BicD through N-terminal sequences (1-79) (Dienstbier et al., 2009). A large number of amino acids (1-812) are needed to interact with localizing mRNA (Dienstbier et al., 2009). Egalitarian has a C-terminal LC8 interacting domain (Navarro et al., 2004). Metal shadowed images were reprinted from: Interactions between coiled-coil proteins: *Drosophila* lamin Dm0 binds to the Bicaudal-D protein, 78(4), Stuurman N, Häner M, Sasse B, Hübner W, Suter B, Aebersold U, Pages No. 278-87, Copyright (1999), with permission from Elsevier. Reprinted from The Lancet, *Drosophila* lamin Dm0 binds to the Bicaudal-D protein, 78(4), Stuurman N, Häner M, Sasse B, Hübner W, Suter B, Aebersold U, Pages No. 278-87, Copyright (1999) with permission from Elsevier (Stuurman et al., 1999).

One of the best-studied mRNA adapter proteins that bind the BicD cargo binding domain is Egalitarian. Egalitarian is a model cargo adapter protein that links dynein to localizing mRNAs in *Drosophila* by associating with the CC3 of BicD (Dienstbier et al., 2009) (**Fig. 1-6, B and C**). The N-terminal 79 amino acids of Egalitarian associate with BicD and the most minimal sequences of Egalitarian that bind to localizing mRNA transcripts in cell extracts are amino acids 1-814. There is no obvious mRNA binding motifs in this region, however amino acids 557 to 726 share some homology with an RNaseD exonuclease domain (Mach and Lehmann, 1997). At its C-terminus, Egalitarian also associates with the dynein light chain, LC8 through a conserved motif (Navarro et al., 2004).

Here, we use mRNA as a model cargo understand how molecular motors are activated for transport in the cell. In **Chapter 2**, we explore how the class V myosin motor, Myo4p is activated for processive movement on actin filaments by adapters and the model mRNA cargo *ASH1*. In **Chapter 3**, we apply the principals of cargo activation in budding yeast to understand how cytoplasmic dynein is activated for processive movement on microtubules by the model mRNA cargo, *K10*. Results from these studies reveal general molecular mechanisms of motor activation by native cargoes. In addition, this research provides a molecular understanding of how mRNA is trafficked in the cell to achieve localization. These mechanisms will likely apply more broadly to other cargo systems.

CHAPTER 2: SINGLE MOLECULE RECONSTITUTION OF mRNA TRANSPORT BY A CLASS V MYOSIN

Thomas E. Sladewski¹, Carol S. Bookwalter¹, Myoung-Soon Hong² & Kathleen M. Trybus^{1,3}

¹Department of Molecular Physiology and Biophysics, University of Vermont, Burlington, Vermont, USA. ²Laboratory of Cell Biology, National Heart, Lung and Blood Institute, National Institutes of Health, Bethesda, MD, USA. ³Correspondence should be addressed to K.M.T.

Correspondence:
Kathleen M. Trybus
Health Science Research Facility 130
149 Beaumont Avenue
Department of Molecular Physiology & Biophysics
University of Vermont
Burlington VT 05405
phone: 802-656-8750
kathleen.trybus@uvm.edu
<http://physiology.med.uvm.edu/trybus>

This work was supported by funds from the US National Institutes of Health (GM078097 to K.M.T.).

Subject terms: Motor proteins, RNA transport, Single-molecule biophysics

ABSTRACT

Molecular motors are instrumental in mRNA localization, which provides spatial and temporal control of protein expression and function. To obtain mechanistic insight into how a class V myosin transports mRNA, we performed single-molecule *in vitro* assays on messenger ribonucleoprotein (mRNP) complexes that were reconstituted from purified proteins and a localizing mRNA found in budding yeast. mRNA is required to obtain a stable processive transport complex on actin, an elegant mechanism to ensure that only cargo-bound motors are motile. Increasing the number of localizing elements ('zip codes') on the mRNA, or configuring the track to resemble actin cables, enhanced run length and event frequency. In multi-zip-code mRNPs, motor separation distance varied during a run, showing the dynamic nature of the transport complex. Building the complexity of single-molecule *in vitro* assays is necessary to understand how these complexes function within cells.

INTRODUCTION

ASH1, the most well-studied localizing mRNA in budding yeast, serves as a paradigm for mRNA transport (Bobola et al., 1996; Long et al., 1997; Sil and Herskowitz, 1996; Takizawa et al., 1997). The *ASH1* transcript codes for a cell-fate determinant, and is transported and localized to the bud tip by the class V myosin motor Myo4p. The motor associates, via adapter proteins, with mRNA localization elements called ‘zip codes’. Class V myosins are uniquely suited to move cellular cargo because they can walk micron long distances on actin filaments without disassociating, a feature called processivity. Type V myosins are generally double-headed to ensure that at least one head remains bound to the track at all times during transport. Myo4p is unique among class V myosins in that it is single-headed and tightly bound to its sole adapter protein She3p, likely forming a hetero-coiled coil that prevents the myosin coiled-coil from self-dimerizing (Hodges et al., 2008). In essence, She3p is a subunit of Myo4p. The tetrameric mRNA binding protein She2p in turn recruits two single-headed Myo4p–She3p motors, hereafter referred to as the “motor complex” (**Fig. 2-1**). Surprisingly, the two myosin motors coupled via She2p walk processively in a hand-over-hand motion, similar to dimeric mammalian myosin Va (Krementsova et al., 2011). We showed that the motor complex was processive at low salt (50 mM KCl) (Krementsova et al., 2011), but no movement was observed near physiologic ionic strength, implying that the complex had dissociated. This led us to hypothesize that we had not assembled all the components necessary for efficient cargo transport, and that mRNA may be required for full motor activity.

To understand the molecular basis of mRNA transport, we fully reconstituted an mRNP *in vitro*. Using single molecule techniques, we showed that mRNA is not a passive cargo, but is instrumental for the stability of the motor complex at physiological salt. Any variation to our *in vitro* assay that more closely recapitulated conditions found in budding yeast led to more efficient movement of the mRNA transcript. The increased run frequency and run length observed *in vitro* are features that likely optimize mRNA localization in a cellular context.

MATERIALS AND METHODS

Protein constructs

DNA encoding full-length budding yeast *MYO4* (1471 amino acids), in pAcSG2, was followed by an eight amino acid FLAG-tag to facilitate purification by affinity chromatography. For experiments tracking motor domain position on actin, an N-terminal biotin tag was added for streptavidin conjugated Qdot (Invitrogen) attachment (Krementsova et al., 2011). For experiments quantifying YFP intensity of motile mRNPs, YFP was fused to the N-terminus of *MYO4*. Myosin constructs without the globular tail (Myo4pΔGT) were truncated at Leu 1024, followed by a FLAG tag. Constructs used to express budding yeast calmodulin (yCaM), Mlc1p, She3p, She2p, Tpm1p and yeast actin were previously described (Krementsova et al., 2011). She2p contained four point mutations (C14S, C68S, C106S, and C180S) to prevent aggregation. This construct was functional in a *ΔSHE2* background (Krementsova et al., 2011). Bacterially expressed Tpm1p constructs included an Ala-Ser before the start codon to mimic acetylation (Maytum et al., 2000). Constructs used for fascin expression were described

previously (Hodges et al., 2009).

Protein expression and purification

Myosin constructs were co-expressed with yeast CaM, Mlc1p, and She3p in Sf9 cells using the baculovirus system, and purified by FLAG affinity chromatography as described previously (Krementsova et al., 2011). Budding yeast proteins calmodulin (yCaM), Mlc1p, She2p and Tpm1p were expressed and purified as described previously (Krementsova et al., 2011). Human fascin purification was described previously (Hodges et al., 2009). Chicken skeletal actin used for myosin Va motility was purified from acetone powder (Pardee and Spudich, 1982) and labeled with rhodamine phalloidin (Invitrogen). *S. cerevisiae* actin was expressed and purified as described previously (Hodges et al., 2012) and labeled with Alexa Fluor 594 phalloidin.

Actin tracks

All actin tracks have Tpm1p bound (4:1 molar ratio). Yeast actin–tropomyosin bundles were prepared by mixing 0.8 μ M Alexa Fluor 594 phalloidin-labeled yeast actin, 2 μ M Tpm1 and 0.7 μ M fascin in motility buffer (25 mM imidazole, pH 7.4, 25 mM KCl, 1 mM EGTA and 4 mM MgCl₂) and incubated overnight at 4° C.

ASH1 mRNA Constructs

Sequences encoding the *ASH1* transcript were amplified from yeast genomic DNA and placed behind the SP6 promoter in the pSP72 vector (Promega). This sequence was followed by a polyA₁₁ tail for transcript stability. DNA sequences of *ASH1* zip codes and *ASH1* constructs used in this study are summarized in Supplementary Table 1 and S2. The

ASH1 transcript containing two zip codes designated 2-zip(E1,E3), used for determining the distance between the two motor domains, was made by mutating specific localization elements in the native *ASH1* sequence by site directed mutagenesis of a conserved CGA triplet motif necessary for She2p recognition thereby maintaining native zip code spacing (Olivier et al., 2005). mRNA was synthesized by linearizing the DNA template with blunt ends at an EcoRV site situated directly after the polyA₁₆ tail and transcribed using a phage SP6 RNA polymerase (RiboMAX system from Promega). *ASH1* RNA was labeled by adding a mixture of Alexa488 labeled dUTP (Molecular Probes - Invitrogen) in a 1:10 ratio to unlabeled nucleotides to allow fluorophore incorporation during RNA synthesis.

Total internal reflection fluorescence (TIRF) microscopy

She2p was diluted to 0.6 mg/mL and clarified at 386,000 x g for 15 min. She2p and Myo4p–She3p were premixed at concentrations of 2.8 μ M and 5.6 μ M respectively in buffer A (25 mM imidazole, pH 7.4, 140 mM KCl, 1 mM EGTA, 4 mM MgCl₂ and 1 mM DTT) containing 0.1 mg/mL yCaM and Mlc1p. To this, 20 units of RNasin Plus RNase Inhibitor (Promega) and 0.035 μ M of the indicated *ASH1* mRNA construct were added and incubated on ice for 30 min.

For experiments in which the distance between two motor pairs was measured, biotin-tagged and untagged full-length Myo4p heterodimers were formed by mixing 0.04 μ M tagged Myo4p and 0.04 μ M untagged Myo4p in buffer A. Half of this mixture was incubated with 0.2 μ M red (655-nm emission) streptavidin Qdots, and the other half with 0.2 μ M green (565-nm emission) streptavidin Qdots for 15 min on ice. To both mixtures, clarified She2p was added at 0.1 μ M and incubated for 15 min on ice. This results in two

populations of dimers: one that has only one head labeled with a red Qdot, and one that has only one head labeled with a green Qdot. Finally, the mixtures were combined 1:1 and unlabeled *ASH1* 2-zip(E1,E3) mRNA was added to 0.004 μ M, giving a myosin dimer:*ASH1* zip code ratio of 2:1. Only motile complexes containing two bound dimeric motors, one with a green head and another with a red head were analyzed.

For experiments measuring YFP intensity of motile partials, She2p-YFP, She2p, and mouse myosin Va (Mercer et al., 1991) HMM-YFP was clarified at 386,000 x g for 15 min. Where indicated, Myo4p-YFP or She2p-YFP was mixed with either She2p or Myo4p in a 1:1 mixing ratio (0.5:1 μ M respectively). Unlabeled native *ASH1* mRNA was then added to the Myo4p mixture at a 1:4, or 4:1 mixing ratio in buffer D (25 mM imidazole, pH 7.4, 140 mM potassium acetate, 1 mM EGTA, 4 mM MgCl₂ and 1 mM DTT). Myosin Va HMM-YFP was also prepared in buffer D.

Flow cells containing Alexa Fluor 594 phalloidin-labeled yeast actin–tropomyosin were prepared similar to that described previously (Krementsova et al., 2011). The Myo4p–*ASH1* mRNA mixture was diluted to obtain final Myo4p concentrations of 14–56 nM and *ASH1* mRNA concentrations of 0.2–0.7 nM in buffer A containing 0.1 mg/mL yCaM and Mlc1p, 2 μ M Tmp1, 1 mM MgATP and ATP regeneration and oxygen scavenging systems as described previously (Krementsova et al., 2011). For experiments measuring the distance between two motor pairs, the Myo4p–*ASH1*–Qdot mixture was diluted to obtain a final Myo4p concentration of 7 nM and an *ASH1* mRNA concentration of 0.3 nM. For experiments that included excess Myo4p–She3p and *ASH1* mRNA, 250 nM unlabeled motor and 10 nM unlabeled mRNA were added to the mixture. For experiments measuring

the YFP intensity of Myo4p-*ASH1* and mouse mMyosin Va HMM-YFP, mixtures were diluted in buffer D containing 0.1 mg/mL yCaM and Mlc1p, 2 μ M Tmp1, 1 mM MgATP and ATP regeneration and oxygen scavaging systems and added to flow cells containing Alexa Fluor 594 phalloidin-labeled yeast actin or rhodamine-phalloidin-labeled chicken skeletal actin respectively.

Data were collected as described previously (Krementsova et al., 2011). For experiments measuring mRNA motility, Alexa Fluors 594, 488 and Qdots were excited with a 488 nm argon laser. For YFP intensity measurements, Alexa Fluor 594 labeled actin and YFP was excited with a 532 and 488 nm laser line, respectively. Data were collected at four frames/sec with seven frame averaging. For experiments using labeled mRNA, movement of Alexa Fluor 488-labeled mRNA on actin was measured using ImageJ and the particle tracking plugin, MTrackJ (Meijering et al., 2012). For all processivity assays, frequencies were generated by counting the total number of runs in movies acquired no more than 7 min after dilution of the mRNP mixture. Total number of runs was divided by the total actin length, time and final myosin concentration to generate a run frequency.

For YFP fluorescence intensity measurements, fluorescence intensities of motile mRNPs were measured in ImageJ using the particle tracking plugin, SpotTracker (Sage et al., 2005). Fluorescence intensities over a 3 x 3 pixel window were recorded and averaged over the entire run and corrected for background intensity. For measuring distances between motor pairs on mRNA, the movement of particles containing red and green Qdots were tracked using SpotTracker and color aligned. The average motor separation distance

over an entire run was determined from instantaneous separation distances of runs where the separation distance did not vary significantly over the run.

Electron microscopy

Full-length Myo4p was diluted to 0.32 mg/mL in buffer B (10 mM MOPS, pH 7.0, 140 mM KCl, 1 mM MgCl₂, 1 mM EGTA, 2 mM DTT and 80 units RNasin Plus RNase Inhibitor) containing 0.04 mg/mL yCaM and Mlc1p. She2p was diluted to 0.6 mg/mL in buffer B. Both proteins were clarified at 350,000 x g for 15 min, and protein concentration after clarification was determined by a Bradford assay. For samples containing only mRNA, native *ASH1* mRNA was diluted to 0.042 μ M in buffer C (10 mM MOPS, 50 mM KCl, 1 mM MgCl₂, 1 mM EGTA, 2 mM DTT and 80 units RNasin Plus RNase Inhibitor), after which two volumes of the same buffer containing ~95% glycerol were added. For samples containing the Myo4p–She3p–She2p motor complex, 0.1 mg/mL Myo4p–She3p and 0.02 mg/mL She2p were mixed in buffer C. This equates to a 1:1.2 molar ratio of Myo4p–She3p dimer to She2p tetramer. The mixture was incubated on ice for 30 min and then mixed with two volumes of the same buffer containing ~95% glycerol. For samples containing the full mRNP, Myo4p–She3p and She2p was diluted in buffer B. To the myosin complex, 0.16 μ M, 0.16 μ M, 0.042 μ M and 0.02 μ M of *ASH1* constructs containing 0, 4 and 8 zip codes respectively were mixed such that the molar ratio of motors to zip codes was 2:1, followed by two volumes of the same buffer containing ~95% glycerol were added. 50 μ L of the mixture was sprayed onto a freshly split mica surface, metal shadowed with platinum at a stage angle of 7° and carbon-coated using an RMC RFD-9010 Freeze Fracture System. Replicas were imaged at a magnification of 50,000

with a JEOL JEM 1200EXII transmission electron microscope equipped with an AMT XR-60 digital camera.

RESULTS

ASH1 mRNA triggers assembly of a processive complex

An mRNP complex was reconstituted by adding *ASH1* mRNA, synthesized with Alexa Fluor 488 dUTP for visualization, to the motor complex (**Fig. 2-1, A and Fig. 2-S1**). Total internal reflection fluorescence (TIRF) microscopy was used to track mRNP movement on yeast actin–tropomyosin (Tpm1p) filaments. At low ionic strength (25 mM KCl), Myo4p–She3p supported robust motility of transcripts without localizing elements, independent of She2p. Only when the salt was raised to near physiological ionic strength (140 mM KCl) did a control mRNA without zip codes become non-motile (**Fig. 2-1, B-C and Table 2-1 and Movie 2-S1**), and thus this salt concentration was used for all processivity experiments. Strikingly, when the native four-zip code *ASH1* mRNA was added to the motor complex under these ionic conditions, the assembled mRNP showed long-range continuous motion (**Fig. 2-1, D and Table 2-1 and Movie 2-S2**). Importantly, this result suggests that mRNA triggers the assembly of a processive complex by enhancing the stability of the motor complex, independent of other proteins implicated in promoting correct mRNA localization (Long et al., 2001; Shen et al., 2009).

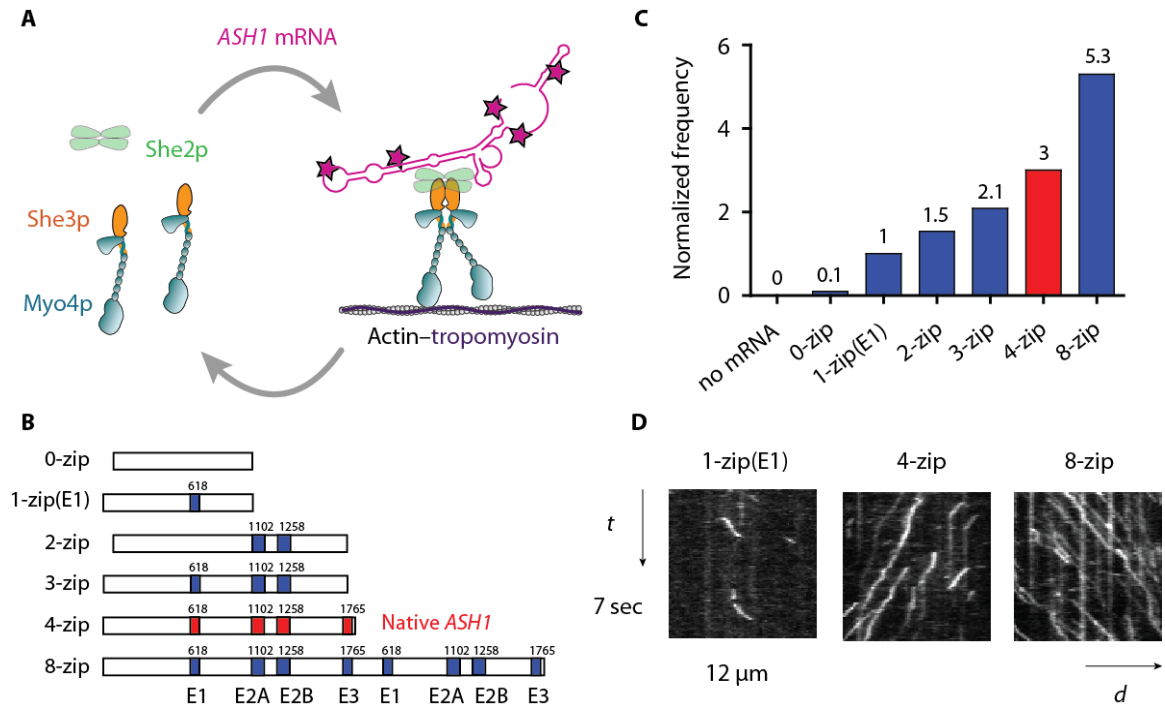


Figure 2-1. The frequency of mRNP processive runs increases with zip code number. (A) Diagram showing the She2p and mRNA dependent dimerization of Myo4p-She3p at 140 mM KCl. Motion of the motor-mRNA complex is visualized by incorporating Alexa Fluor 488-5-dUTP (indicated by red stars) into the *ASH1* mRNA transcript. (B) Schematic of *ASH1* mRNA constructs containing the indicated number of zip codes. The four zip code elements in native *ASH1* mRNA (E1, E2A, E2B, E3) are indicated in red. The initial base position of each element in the native *ASH1* sequence is indicated. The 0-zip construct has no zip codes. The 1-zip(E1) construct contains only the E1 motif, 2-zip both the E2A and E2B zip codes, and 3-zip the E1, E2A, and E2B zip codes, all in their native positions. The 8-zip construct is formed from two concatenated 4-zip sequences. (C) Run frequencies of Myo4p mRNP motility from a representative experiment comparing *ASH1* mRNA sequences containing varying numbers of zip codes. The run frequency (number of runs per μM Myo4p per μm actin per sec) with 1-zip(E1) is normalized to one. The actin track has Tpm1p bound. Motion of the Myo4p motor complex without mRNA is visualized with She2p-YFP. The native *ASH1* mRNA run frequency is indicated with a red bar. For *ASH1* transcripts containing zip codes, $n \geq 198$, without zip codes, $n=13$. (D) Kymographs of Myo4p mRNPs containing *ASH1* mRNA with the indicated number of zip codes. The slope of the trace is the speed of the mRNP. The length of the trace is its run length. The number of traces is related to run frequency. Conditions: 140 mM KCl, pH 7.4, 1 mM MgATP.

A domain of Myo4p that has not yet been assigned a function is the C-terminal globular tail, and we tested if it also contributes to stabilizing the mRNP. We performed *in vitro* assays with mRNPs assembled from Myo4p lacking the globular tail, and the single zip code (E3) mRNA. These mRNPs had significantly reduced run length, and a lower run frequency compared to mRNPs formed with wild type Myo4p (**Fig. 2-2, A**). Moreover, processive runs were only observed for a short period of time after diluting the mRNP mixture, implying a less stable mRNP.

Multiple zip codes increases mRNP run frequency and length

A feature of localizing mRNAs is the presence of multiple zip codes, and we wished to determine what advantage this confers. We used *ASH1* mRNA, which contains four zip codes, each capable of recruiting a motor complex for transport and supporting mRNA localization in the cell (Chartrand et al., 2002; Chartrand et al., 1999). Three zip codes (E1, E2A and E2B) are located in the coding region of the transcript, while the fourth element (E3) is located in the 3' UTR (**Fig. 2-1, B**) (Chartrand et al., 2002; Chartrand et al., 1999; Gonzalez et al., 1999). Each zip code has a highly conserved CGA triplet in one loop and a single conserved cytosine in a nearby loop (Jambhekar et al., 2005; Olivier et al., 2005). We first tested if each zip code element of the native *ASH1* transcript is equally effective for mRNP transport. mRNPs containing only the E1, E2A or E2B zip codes were indistinguishable from each other in terms of run length, frequency and speed (**Table 2-1 and Movie 2-S3**). In contrast, mRNPs with the E3 zip code supported longer run lengths and almost twice the run frequency compared to the other single zip code transcripts (**Table 2-1**). Because Myo4p switches between a monomer and a dimer depending on whether it

is in complex with She2p and mRNA, the characteristic run length of Myo4p is not only a function of the intrinsic properties of the motor (“duty cycle”, or fraction of the ATPase cycle spent attached to actin, and strain-dependent coordination between the heads), but also the stability of the motor complex. Assuming that modification of the mRNA cargo does not affect the motor properties of Myo4p, we interpreted the enhanced run lengths and frequencies of the E3 containing mRNP as promoting a more stable mRNP complex than either E1, E2A or E2B.

Table 2-1. Characteristic motion of mRNPs containing various *ASH1* mRNA zip codes

<i>ASH1</i> mRNA construct	Normalized Frequency	Run length (μm)	Speed ($\mu\text{m}/\text{sec}$)	N
Low concentration (25nM myosin, 0.035nM mRNA)				
0-zip	0.05	-	-	13
4-zip (native sequence)	3	1.1 ± 0.07	2.3 ± 0.06	211
8-zip	5.3	$1.5 \pm 0.11^*$	2.2 ± 0.05	197
1-zip(E1)	1	0.93 ± 0.03	1.9 ± 0.06	302
1-zip(E2A)	1.04	1.04 ± 0.04	1.7 ± 0.05	353
1-zip(E2B)	1.04	1.03 ± 0.02	1.9 ± 0.06	357
1-zip(E3)	1.85	$1.3 \pm 0.04^*$	1.6 ± 0.04	380
High concentration (250nM myosin, 10nM mRNA)				
1-zip(E1)	1	1.4 ± 0.1	1.6 ± 0.04	189
4-zip (native sequence)	2.2	$2.2 \pm 0.15^*$	1.4 ± 0.04	183
8-zip	2.3	$2.75 \pm 0.19^*$	1.5 ± 0.04	145

Speed is calculated from a mean \pm s.e.m. The total number of runs analyzed is ‘N’. Run frequency (number of runs per μM Myo4p per μm actin per sec) with 1-zip(E1) is normalized to one. Asterisk (*) indicates $P < 0.001$, using the Kolmogorov-Smirnov Test.

Because the E1, E2A, and E2B zip codes showed similar interactions with the motor complex, these elements were used in combination to gain mechanistic insight into how multiple redundant zip codes promote efficient mRNP transport. The run frequency of mRNPs with one zip code (E1) was compared to transcripts containing two (E2A and E2B) or three zip codes (E1, E2A, and E2B) (**Fig. 2-1, B**). We observed a linear relationship between run frequency and zip code number (**Fig. 2-1, C**). This result suggests that *ASH1* zip codes function independently with no long range interactions, and that mRNA transcripts with multiple zip codes recruit a motor complex more effectively to initiate transport. The lengths of the 2-zip and 3-zip mRNA constructs are comparable (1527 versus 1610 bases), and thus the higher recruitment rate correlates with zip code number and not mRNA transcript length.

Based on the data described above, the E3 zip code may be preferentially populated in multi-zip code mRNAs, at the low nanomolar motor concentrations of the standard single molecule assay. Consistent with this idea, the run frequency with E3 alone was only slightly lower than with the native *ASH1* sequence (**Table 2-1**). The relationship between zip code number and run frequency was further tested with an eight zip code transcript, formed by concatenating two native *ASH1* mRNAs (**Fig. 2-1, B**). mRNPs containing the eight zip code transcript had approximately twice the run frequency of the four zip code construct (**Fig. 2-1, C-D and Movie 2-S4**), and a small but significant increase in run length, but no change in speed (**Table 2-1 and Figure 2-2**). Recruitment of multiple motors typically increases run length (Beeg et al., 2008), and thus the eight zip code construct on

average has a higher occupancy of bound motors than native *ASH1* at low nanomolar protein concentration.

Multiple motors support longer processive runs

To directly quantify the number of She2p tetramers and Myo4p motors associated with the native *ASH1* transcript, mRNPs were assembled with a YFP tag on either Myo4p or She2p. The YFP intensity of motile particles was quantified by TIRF microscopy. A dimeric mouse myosin Va-HMM-YFP construct provided a 2-YFP intensity standard. When *ASH1* zip codes were in molar excess to Myo4p motor complexes, two Myo4p–She3p motors and one She2p tetramer were recruited to the transcript. When motor complexes were in excess of *ASH1* zip codes, a second higher intensity peak emerged, indicating binding of an additional motor complex and an additional She2p tetramer (**Fig. 2-2, B**). Additional zip code elements thus become populated as motor concentration increases.

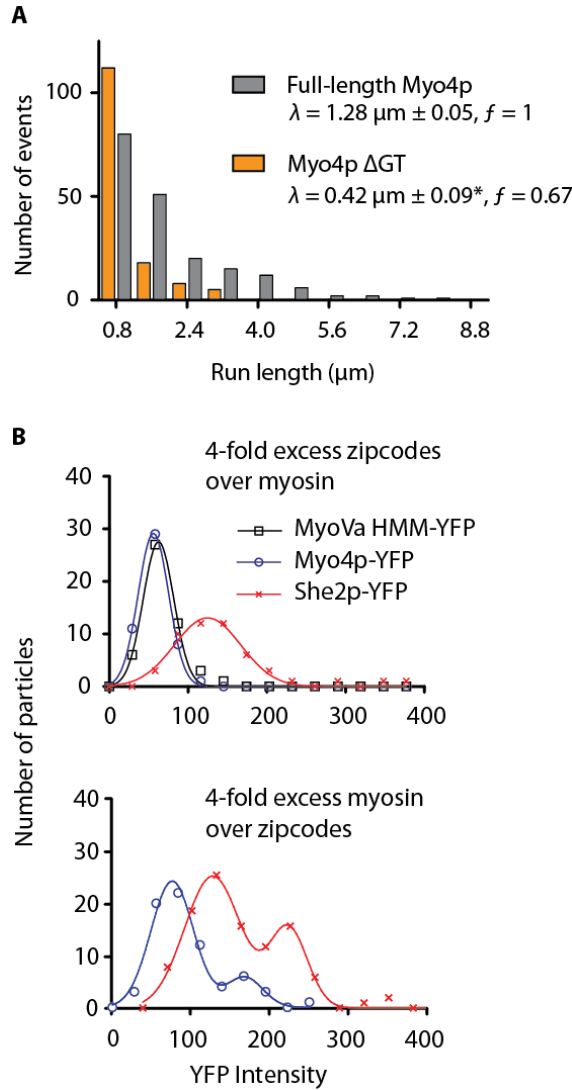


Figure 2-2. The Myo4p globular tail stabilizes the mRNP, and the recruitment of multiple motors to *ASH1* is concentration dependent. (A) Characteristic run length (λ) of mRNPs containing the E3 zip code and either wild type Myo4p (grey) or Myo4p lacking the globular tail (orange). Run length data is binned identically but displaced for presentation purposes. The asterisk (*) indicates that the run length is significantly reduced relative to wild type Myo4p ($P < 0.001$, using the Kolmogorov-Smirnov Test; $n \geq 199$). The run frequency (f) (number of runs per μM Myo4p per μm actin per sec) with wild type Myo4p is normalized to one. (B) Histograms of motile mRNP intensities with native *ASH1* mRNA. The upper panel shows recruitment of one dimeric Myo4p-YFP (blue) and one tetrameric She2p-YFP (red) at a 1 Myo4p dimer: 4 zip code mixing ratio. In a given experiment only one protein contained a YFP label. The lower panel shows multiple motor complex recruitment at a 4 Myo4p dimer: 1 zip code mixing ratio. MyoVa-HMM-YFP (black) serves as a 2-YFP intensity control.

To further populate additional zip codes with motor complexes, excess unlabeled Myo4p motor complex (250 nM) and unlabeled *ASH1* mRNA (10 nM) were added to the standard TIRF assay. Under these conditions, run lengths were significantly longer for transcripts with four and eight zip codes (2.2 μ m and 2.75 μ m, respectively) compared to *ASH1* transcripts containing only the E1 zip code (1.4 μ m), consistent with multiple motor recruitment (**Table 2-1, Fig. 2-S3**). The run length enhancement was less apparent in the standard TIRF assay (**Table 2-1**) because low motor (25 nM) and mRNA (0.35 nM) concentrations failed to promote full occupancy of four or eight zip code mRNAs with motor complexes.

Electron microscopy of mRNP complexes

Electron microscopy of metal-shadowed complexes provided structural information about the mRNP. The higher protein concentrations which favor zip code occupancy were used. As a control, the motor complex was visualized in the absence of mRNA at 25 mM KCl. Similar to our previous study (Krementsova et al., 2011), V-shaped structures were observed, consistent with She2p recruiting two single-headed Myo4p motors (**Fig. 2-3, A**). The images shown are representative of the four types of structures that were observed for the motor complex. Metal-shadowed images of *ASH1* mRNA alone showed structures distinctive from Myo4p. At 140 mM KCl, *ASH1* mRNA transcripts lacking zip codes did not bind the motor complex, consistent with the specificity seen at the single molecule level (**Fig. 2-3, A and B**). When the native four zip code *ASH1* transcript was mixed with the motor complex, the components assembled into mRNPs

containing anywhere from zero to eight motor heads, or as many as one motor pair per zip code (Fig. 2-3, C). mRNPs with eight zip codes recruited even more motors.

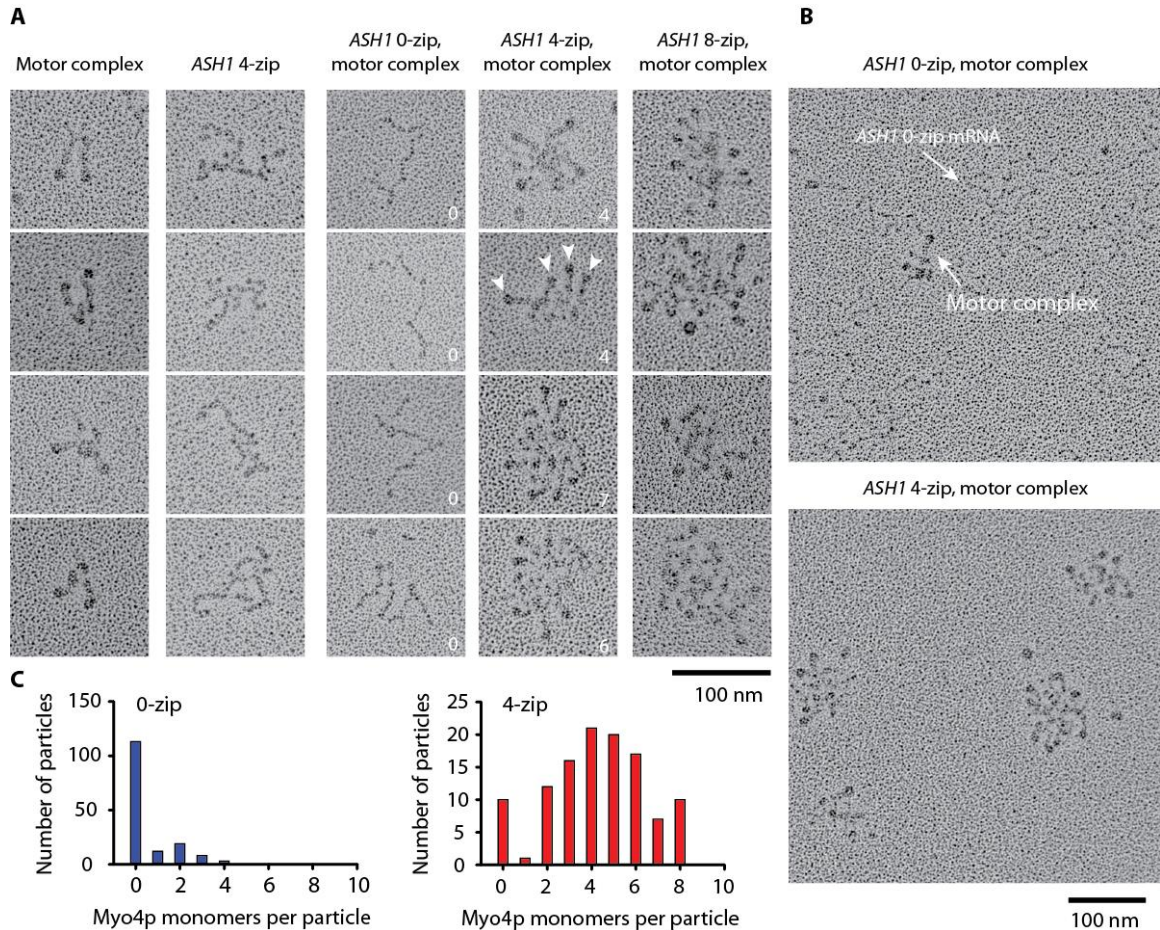


Figure 2-3. Metal-shadowed images show variable recruitment of motors. (A) Galleries of images showing (left to right) the recruitment of two Myo4p motors by She2p, the native 4-zip *ASH1* transcript alone, and *ASH1* transcripts containing 0, 4 or 8 zip codes in the presence of the Myo4p motor complex (Myo4p–She3p–She2p). Arrowheads indicate Myo4p motors, and the numbers indicate bound heads. (B) Fields of the Myo4p motor complex in the presence of 0-zip or 4-zip *ASH1*. (C) Histograms showing the number of Myo4p monomers associated with 0-zip or 4-zip *ASH1* mRNA.

mRNPs are optimized to walk on actin cables

The electron microscopy images highlight the dissimilarity in structure of the Myo4p motor complex in isolation, and the fully assembled mRNP. These images suggest that mRNPs are likely optimized to walk on actin cables, rather than single actin filaments, so that multiple motors do not interfere with each other. We mimicked the actin cables found *in vitro* with actin–fascin–tropomyosin bundles, composed of parallel actin filaments (Hodges et al., 2009). Motility of mRNPs carrying either the native *ASH1* transcript, or the E1 zip code only, was compared on single yeast actin–tropomyosin filaments versus bundles (**Fig. 2-4, A and B**). Strikingly, run lengths for mRNPs with the native *ASH1* transcript increased from 1 μm to 3 μm . Even the one zip code mRNP doubled its run length on bundles. Compared to single actin filaments, frequencies on actin bundles were 5-fold higher with the native *ASH1* mRNP, and nine-fold higher for the one zip code mRNPs (**Fig. 2-4, C**). No significant changes in speed were observed (**Fig. 2-4, D**).

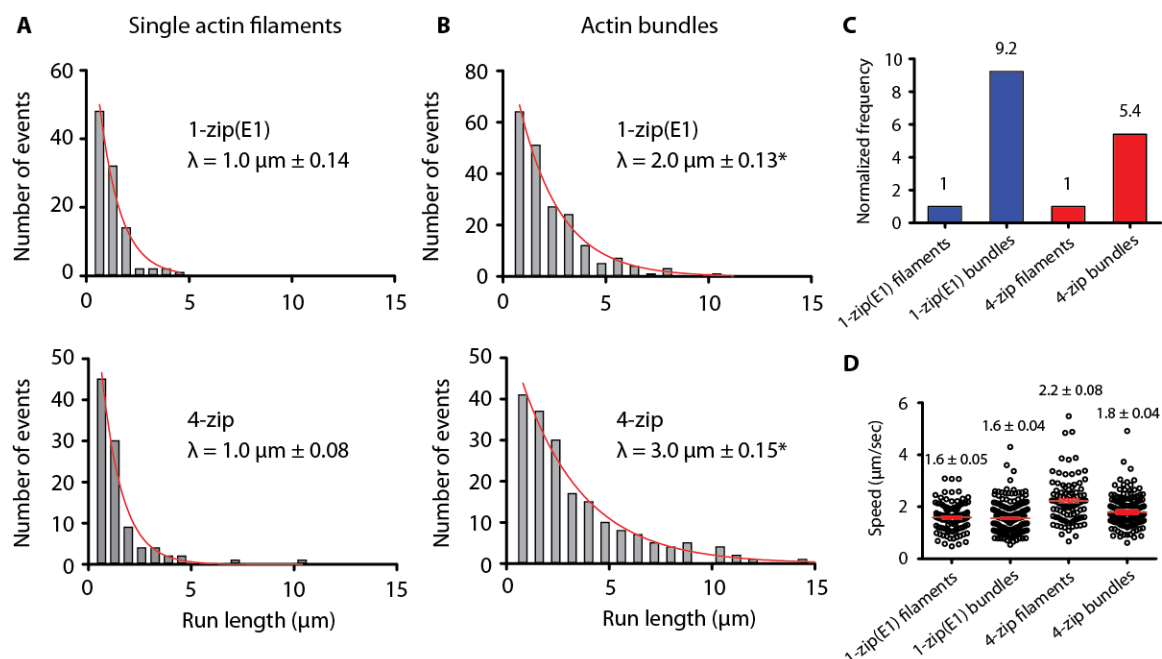


Figure 2-4. Comparison of mRNP movement on single actin filaments versus bundles. Representative run length histograms of Myo4p mRNPs containing 1 zip code (E1) or 4 zip codes on (A) single actin filaments or (B) actin bundles. Both tracks have Tpm1p bound. Asterisk (*) indicates run lengths that are significantly different between filaments and bundles with $P < 0.001$ (Kolmogorov-Smirnov Test; $n \geq 103$). (C) Run frequencies of Myo4p mRNP motility containing 1 (E1) or 4 zip codes on single actin filaments or bundles. The run frequency (number of runs per μM Myo4p per μm actin per sec) with single actin filaments is normalized to one. (D) Speed distributions of Myo4p mRNPs on single actin filaments and bundles. The mean speed is indicated with a red line. Error is in s.e.m; $n \geq 103$. Conditions: 140 mM KCl, pH 7.4, 1 mM MgATP.

Variable inter-motor spacing during mRNP movement

To obtain more detailed and dynamic information on how multiple motor complexes move on actin filaments, we followed the separation distance between two motor domains on different motor complexes as the mRNP is processively transported on single actin filaments. To simplify the analysis, a two zip code *ASH1* transcript containing

only the E1 and E3 zip codes was used (**Fig. 2-5, A**). Only one head of each motor complex was labeled with either a red or a green quantum dot (Qdot). The labeled-motor complexes were then assembled into mRNPs with unlabeled transcript. Only motile mRNPs containing a red and a green Qdot, i.e. two motor complexes, were analyzed by TIRF microscopy. Qdot position was tracked with ~6 nm accuracy (Warshaw et al., 2005).

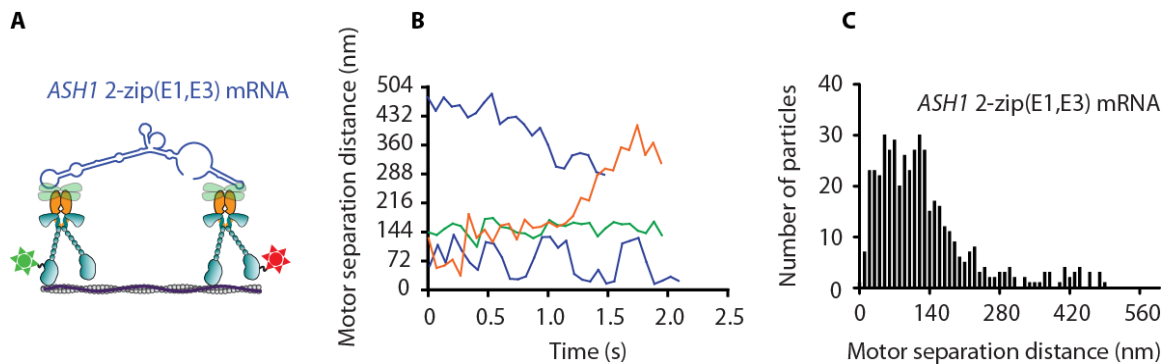


Figure 2-5. The spacing between two moving motor complexes coupled by mRNA varies. (A) Diagram of the experimental setup for quantifying the distance between two Myo4p motor complexes coupled by a 2-zip *ASH1* mRNA construct containing E1 and E3 zip codes. One head of one motor complex was labeled with a red Q-dot, and one head of a second motor complex was labeled with a green Q-dot. (B) Motor separation distances of four representative mRNP run trajectories as a function of time. (C) Distribution of instantaneous head separation distances for 25 mRNP run trajectories.

The spacing between the coupled motors varied greatly during a run. **Fig. 2-5, B** shows that motors coupled by a naturally compliant ~140 nm mRNA cargo can get closer together, further apart, remain constant, or oscillate between shorter and longer inter-motor distances as a function of time. Combining measurements from multiple processive runs

shows a range of inter-motor separation distances, with 90% of the observed spacings falling in the range of 10 to 250 nm (**Fig. 2-5, C**).

DISCUSSION

Here we fully reconstituted an mRNP composed of a localizing *ASH1* mRNA transcript and the budding yeast class V myosin motor complex (Myo4p–She3p–She2p). Using single molecule techniques, we demonstrated that mRNA is essential to form a processive complex near physiologic strength. Consistent with our direct demonstration of processive movement, *in vitro* binding assays showed that the She2p–She3p complex had an ~60-fold higher affinity for localizing mRNAs than for control mRNAs (Muller et al., 2011). In budding yeast, She2p interacts with *ASH1* mRNA in the nucleus and then shuttles the complex into the cytoplasm (Du et al., 2008; Shen et al., 2009). Our observations suggest that at this point each zip code-bound She2p would recruit a pair of Myo4p–She3p monomers that is capable of initiating processive motion. The requirement for mRNA to stabilize the motor complex provides a regulatory checkpoint such that unbound Myo4p monomers are not motile, and only cargo-bound Myo4p dimers can move processively along actin cables to localize the transcript to the bud tip.

Each of the four zip code elements in *ASH1* is sufficient for supporting transport and localization of a reporter mRNA in budding yeast, but the presence of all four zip codes increased the quality of cellular localization in the bud (Chartrand et al., 1999; Gonzalez et al., 1999). By modifying the number of localizing elements in *ASH1*, we showed that two clear advantages of multiple zip codes are an enhanced ability to initiate processive movement, and an increased run length. Both of these parameters become optimal when

all zip codes are fully occupied by motors. The single molecule and electron microscopy data indicate that motor recruitment to mRNPs is probabilistic, and multiple zip codes function to bias the average number of motors associated with the mRNP.

The approximate cellular concentration of Myo4p, based on cell volume ($30\ \mu\text{m}^3$ (ref. (Jorgensen et al., 2007))) and Myo4p copy number (2210 (ref. (Ghaemmaghami et al., 2003))), is $\sim 100\ \text{nM}$. When motor concentrations similar to this were used, we obtained the highest run frequency and run length *in vitro*. Electron microscopy showed that the native *ASH1* transcript can bind as many as eight Myo4p monomers, implying that *ASH1* transcripts in yeast are likely transported by multiple motor complexes. Increased run frequency and length are features that likely promote cellular localization, providing a rationale for why localizing mRNAs tend to have multiple zip codes (Jambhekar and Derisi, 2007).

We also showed that a novel function of the Myo4p globular tail is to stabilize the mRNP by providing additional weak interactions with She2p and/or mRNA. In typical dimeric class V myosins, the globular tail interacts with various adapter proteins to specify different cargos, or it interacts with the myosin motor domain to form an auto-inhibited complex. Biochemical studies with Myo4p indicate that the globular tail is not required for interaction with its adapter protein She3p (Hodges et al., 2008), nor does it contain the conserved residues required for auto-inhibition of the motor (Heuck et al., 2010). *In vivo* studies, however, demonstrated the importance of the tail for correct mRNA localization (Bookwalter et al., 2009; Heuck et al., 2010). Our *in vitro* results showing reduced run length and frequency, and lower stability of the mRNP formed with Myo4p lacking the

globular tail, provides a mechanistic reason for impaired mRNA localization. It has been suggested that the stability of mRNA transport complexes result from a large number of weak interactions, none of which is essential for transport (Arn et al., 2003). Here we showed potential interactions between all proteins in the motor complex and the mRNA, which leads to the synergistic assembly of the mRNP.

Electron microscopy of an *ASH1* transcript with multiple bound motors gave the visual impression that motors would interfere with each other if they walked on single actin filaments. Our results indicated that mRNPs are indeed optimized to walk on yeast actin cables, which provide additional lateral actin binding sites for multi-motor complexes. It should also be noted that all the actin tracks we used had the major tropomyosin isoform Tpm1p bound, to mimic the composition of the actin cables *in vivo*. Tropomyosin enhanced run frequency compared to bare actin, but was not essential to obtain processive movement. This differs from what we observed for Myo2p, the other class V myosin in budding yeast, where tropomyosin was the switch that was necessary to convert Myo2p into a processive motor (Hodges et al., 2012).

In contrast to the static electron micrographs of the mRNPs, which were fairly uniform in diameter with head spacings no greater than ~100 nm, high resolution single molecule tracking of the separation distance between two motor complexes coupled by *ASH1* revealed a highly dynamic view of mRNPs moving on actin. This variable and sometimes long inter-motor spacing is consistent with what we observed for mouse myosin Va motors coupled through a 50 nm DNA scaffold, which supported inter-motor spacings in the range of ~10-225 nm (Lu et al., 2012). Spacings that exceed the length of the scaffold

are likely due to the reach of the motors. Visualizing two motor complexes moving on actin provides the first dynamic view of mRNP transport at the single molecule level.

Implications for mRNA transport in higher organisms

Our results from budding yeast have implications for mRNA transport in higher organisms. Mammalian myoVa, best-known for transport of membranous organelles, has recently been shown to have both mRNA and RNA binding proteins as another class of cargo (reviewed in (McCaffrey and Lindsay, 2012)). The similar processive behavior of the yeast motor complex and myosin Va imply that our observations likely apply to both motors. In eukaryotes, microtubule-based motors perform much of the long-range mRNA transport. There, the situation is complicated by having motors that move in opposing directions bound to the mRNA: dynein moving cargo toward the microtubule minus-end, and kinesin driving plus-end directed motion. During *Drosophila* embryogenesis, both non-localizing and localizing mRNAs undergo bidirectional transport on microtubules. Increasing zip code number increases the average motor number associated with a localizing transcript in a probabilistic way, which in turn regulates the speed, frequency and duration of minus-end directed runs (Amrute-Nayak and Bullock, 2012; Bullock et al., 2006). This variation in motor occupancy was proposed to account for the large variation in dynein driven mRNP motility in the cell. Our results also show variable motor recruitment to *ASH1* mRNPs, indicating that this is a widely conserved mechanism to achieve efficient transport.

In conclusion, our study highlights the idea that only by reconstituting biological function from multiple purified components, can one fully understand how molecules that are parts of cellular complexes *in vivo* work at a mechanistic level.

ACKNOWLEDGMENTS

The authors thank M. Daniels for EM support and the use of the National Heart, Lung, and Blood Institute Electron Microscopy Core Facility. We also thank G. Kennedy for technical assistance, D. Warshaw for use of the TIRF microscope, E. Krementsova for protein expression, M. Skolnick, A. Hodges, H. Lu and S. Lowey for helpful discussions. This work was supported by funds from the US National Institutes of Health (GM078097 to K.M.T.).

REFERENCES

- Amrute-Nayak, M., and S.L. Bullock. 2012. Single-molecule assays reveal that RNA localization signals regulate dynein-dynactin copy number on individual transcript cargoes. *Nat Cell Biol.*
- Arn, E.A., B.J. Cha, W.E. Theurkauf, and P.M. Macdonald. 2003. Recognition of a bicoid mRNA localization signal by a protein complex containing Swallow, Nod, and RNA binding proteins. *Dev Cell.* 4:41-51.
- Beeg, J., S. Klumpp, R. Dimova, R.S. Gracia, E. Unger, and R. Lipowsky. 2008. Transport of beads by several kinesin motors. *Biophys J.* 94:532-541.
- Bobola, N., R.P. Jansen, T.H. Shin, and K. Nasmyth. 1996. Asymmetric accumulation of Ash1p in postanaphase nuclei depends on a myosin and restricts yeast mating-type switching to mother cells. *Cell.* 84:699-709.
- Bookwalter, C.S., M. Lord, and K.M. Trybus. 2009. Essential features of the class V myosin from budding yeast for ASH1 mRNA transport. *Mol Biol Cell.* 20:3414-3421.

- Bullock, S.L., A. Nicol, S.P. Gross, and D. Zicha. 2006. Guidance of bidirectional motor complexes by mRNA cargoes through control of dynein number and activity. *Curr Biol.* 16:1447-1452.
- Chartrand, P., X.H. Meng, S. Huttelmaier, D. Donato, and R.H. Singer. 2002. Asymmetric sorting of ash1p in yeast results from inhibition of translation by localization elements in the mRNA. *Mol Cell.* 10:1319-1330.
- Chartrand, P., X.H. Meng, R.H. Singer, and R.M. Long. 1999. Structural elements required for the localization of ASH1 mRNA and of a green fluorescent protein reporter particle in vivo. *Curr Biol.* 9:333-336.
- Du, T.G., S. Jellbauer, M. Muller, M. Schmid, D. Niessing, and R.P. Jansen. 2008. Nuclear transit of the RNA-binding protein She2 is required for translational control of localized ASH1 mRNA. *EMBO Rep.* 9:781-787.
- Ghaemmaghami, S., W.K. Huh, K. Bower, R.W. Howson, A. Belle, N. Dephoure, E.K. O'Shea, and J.S. Weissman. 2003. Global analysis of protein expression in yeast. *Nature.* 425:737-741.
- Gonzalez, I., S.B. Buonomo, K. Nasmyth, and U. von Ahsen. 1999. ASH1 mRNA localization in yeast involves multiple secondary structural elements and Ash1 protein translation. *Curr Biol.* 9:337-340.
- Heuck, A., I. Fetka, D.N. Brewer, D. Huls, M. Munson, R.P. Jansen, and D. Niessing. 2010. The structure of the Myo4p globular tail and its function in ASH1 mRNA localization. *J Cell Biol.* 189:497-510.
- Hodges, A.R., C.S. Bookwalter, E.B. Krementsova, and K.M. Trybus. 2009. A nonprocessive class V myosin drives cargo processively when a kinesin- related protein is a passenger. *Curr Biol.* 19:2121-2125.
- Hodges, A.R., E.B. Krementsova, C.S. Bookwalter, P.M. Fagnant, T.E. Sladewski, and K.M. Trybus. 2012. Tropomyosin is essential for processive movement of a class v Myosin from budding yeast. *Curr Biol.* 22:1410-1416.
- Hodges, A.R., E.B. Krementsova, and K.M. Trybus. 2008. She3p binds to the rod of yeast myosin V and prevents it from dimerizing, forming a single-headed motor complex. *J Biol Chem.* 283:6906-6914.
- Jambhekar, A., and J.L. Derisi. 2007. Cis-acting determinants of asymmetric, cytoplasmic RNA transport. *RNA.* 13:625-642.
- Jambhekar, A., K. McDermott, K. Sorber, K.A. Shepard, R.D. Vale, P.A. Takizawa, and J.L. DeRisi. 2005. Unbiased selection of localization elements reveals cis-acting

- determinants of mRNA bud localization in *Saccharomyces cerevisiae*. *Proc Natl Acad Sci U S A*. 102:18005-18010.
- Jorgensen, P., N.P. Edgington, B.L. Schneider, I. Rupes, M. Tyers, and B. Futcher. 2007. The size of the nucleus increases as yeast cells grow. *Mol Biol Cell*. 18:3523-3532.
- Krementsova, E.B., A.R. Hodges, C.S. Bookwalter, T.E. Sladewski, M. Travaglia, H.L. Sweeney, and K.M. Trybus. 2011. Two single-headed myosin V motors bound to a tetrameric adapter protein form a processive complex. *J Cell Biol*. 195:631-641.
- Long, R.M., W. Gu, X. Meng, G. Gonsalvez, R.H. Singer, and P. Chartrand. 2001. An exclusively nuclear RNA-binding protein affects asymmetric localization of ASH1 mRNA and Ash1p in yeast. *J Cell Biol*. 153:307-318.
- Long, R.M., R.H. Singer, X. Meng, I. Gonzalez, K. Nasmyth, and R.P. Jansen. 1997. Mating type switching in yeast controlled by asymmetric localization of ASH1 mRNA. *Science*. 277:383-387.
- Lu, H., A.K. Efremov, C.S. Bookwalter, E.B. Krementsova, J.W. Driver, K.M. Trybus, and M.R. Diehl. 2012. Collective dynamics of elastically-coupled myosinV motors. *J Biol Chem*.
- Maytum, R., M.A. Geeves, and M. Konrad. 2000. Actomyosin regulatory properties of yeast tropomyosin are dependent upon N-terminal modification. *Biochemistry*. 39:11913-11920.
- McCaffrey, M.W., and A.J. Lindsay. 2012. Roles for myosin Va in RNA transport and turnover. *Biochem Soc Trans*. 40:1416-1420.
- Meijering, E., O. Dzyubachyk, and I. Smal. 2012. Methods for cell and particle tracking. *Methods Enzymol*. 504:183-200.
- Mercer, J.A., P.K. Seperack, M.C. Strobel, N.G. Copeland, and N.A. Jenkins. 1991. Novel myosin heavy chain encoded by murine dilute coat colour locus. *Nature*. 349:709-713.
- Muller, M., R.G. Heym, A. Mayer, K. Kramer, M. Schmid, P. Cramer, H. Urlaub, R.P. Jansen, and D. Niessing. 2011. A cytoplasmic complex mediates specific mRNA recognition and localization in yeast. *PLoS Biol*. 9:e1000611.
- Olivier, C., G. Poirier, P. Gendron, A. Boisgontier, F. Major, and P. Chartrand. 2005. Identification of a conserved RNA motif essential for She2p recognition and mRNA localization to the yeast bud. *Mol Cell Biol*. 25:4752-4766.

- Pardee, J.D., and J.A. Spudich. 1982. Purification of muscle actin. *Methods Enzymol.* 85 Pt B:164-181.
- Sage, D., F.R. Neumann, F. Hediger, S.M. Gasser, and M. Unser. 2005. Automatic tracking of individual fluorescence particles: application to the study of chromosome dynamics. *IEEE Trans Image Process.* 14:1372-1383.
- Shen, Z., N. Paquin, A. Forget, and P. Chartrand. 2009. Nuclear shuttling of She2p couples ASH1 mRNA localization to its translational repression by recruiting Loc1p and Puf6p. *Mol Biol Cell.* 20:2265-2275.
- Sil, A., and I. Herskowitz. 1996. Identification of asymmetrically localized determinant, Ash1p, required for lineage-specific transcription of the yeast HO gene. *Cell.* 84:711-722.
- Takizawa, P.A., A. Sil, J.R. Swedlow, I. Herskowitz, and R.D. Vale. 1997. Actin-dependent localization of an RNA encoding a cell-fate determinant in yeast. *Nature.* 389:90-93.
- Warshaw, D.M., G.G. Kennedy, S.S. Work, E.B. Krementsova, S. Beck, and K.M. Trybus. 2005. Differential labeling of myosin V heads with quantum dots allows direct visualization of hand-over-hand processivity. *Biophys J.* 88:L30-32.

SUPPORTING MATERIAL

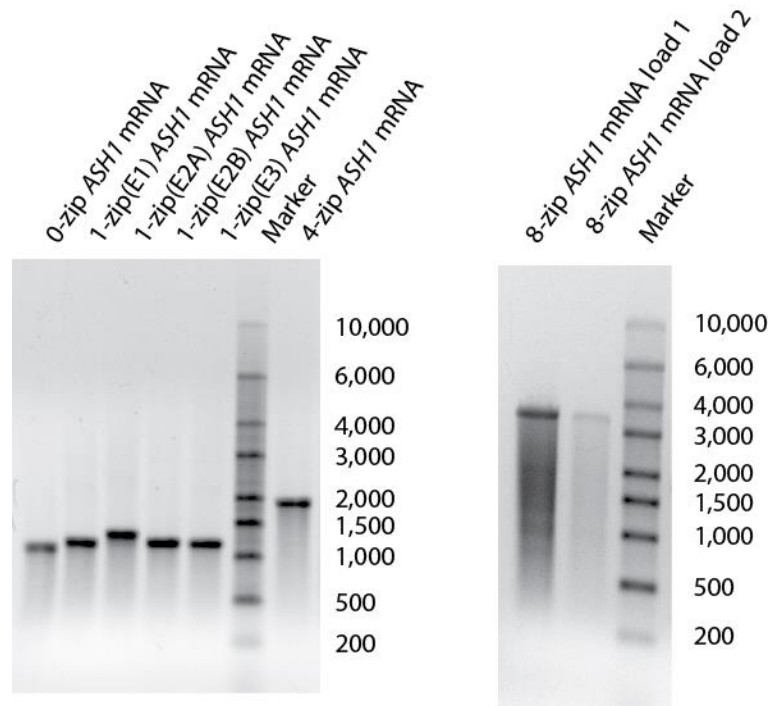


Figure 2-S1. Gel electrophoresis showing the relative sizes of Alexa-488 labeled *ASH1* mRNA constructs following *in vitro* synthesis. For the 8-zip *ASH1* mRNA construct, two loading amounts of mRNA are shown.

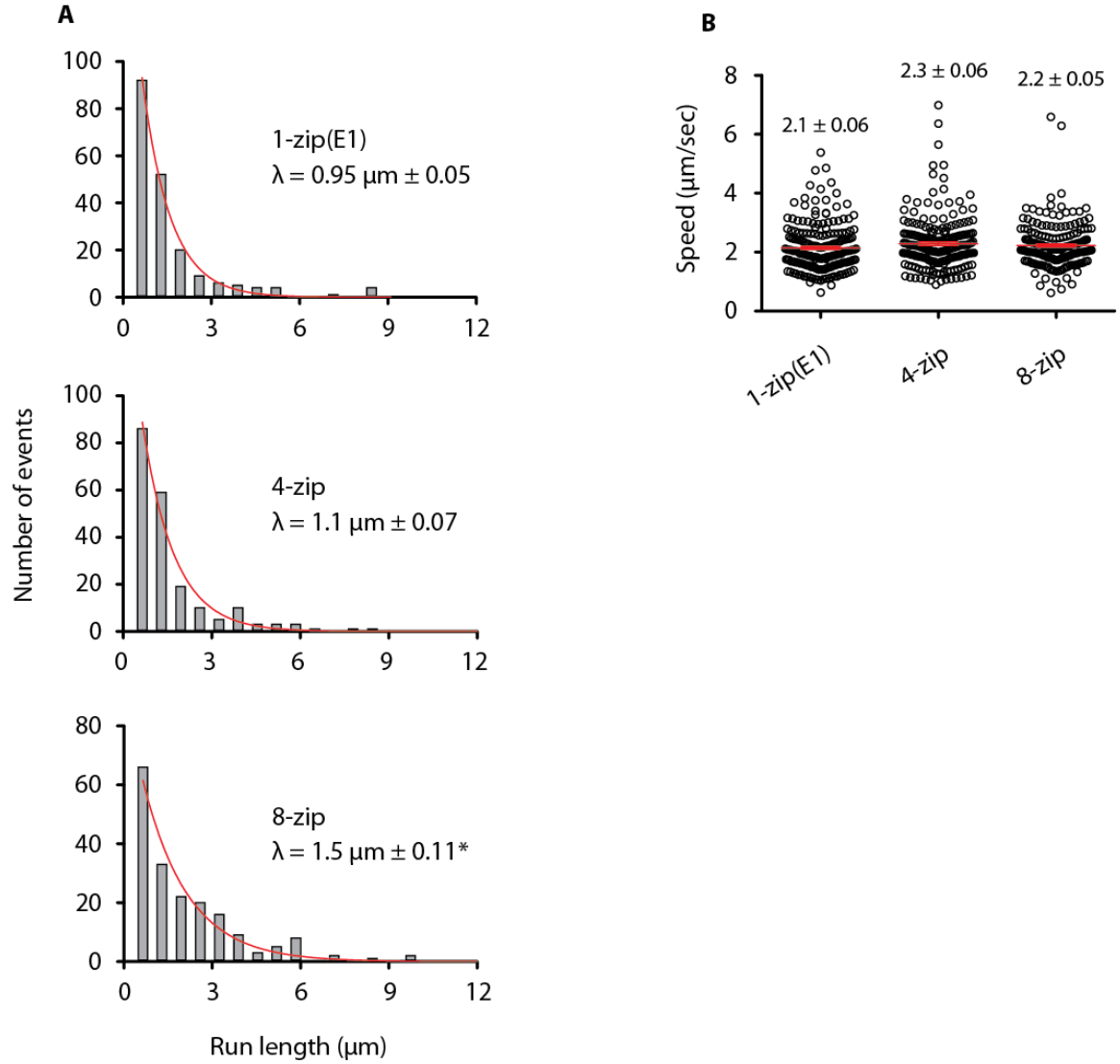


Figure 2-S2. Characteristic run length and speed of Myo4p mRNPs containing *ASH1* mRNA with the indicated number of zip codes. (A) Run length histograms of Myo4p mRNPs from a representative experiment comparing *ASH1* mRNA sequences containing, 1(E1), 4 or 8 zip codes. The 1-zip(E1) data are from a different data set than that shown in Table 1. Asterisk (*) indicates run lengths that are significantly different from the 1-zip(E1) and the 4-zip construct with $P < 0.001$ (Kolmogorov-Smirnov Test). **(B)** Speed distributions of Myo4p motile mRNPs. The mean speed is indicated with a red line. Error is in s.e.m. Conditions: 140 mM KCl, pH 7.4, 1 mM MgATP.

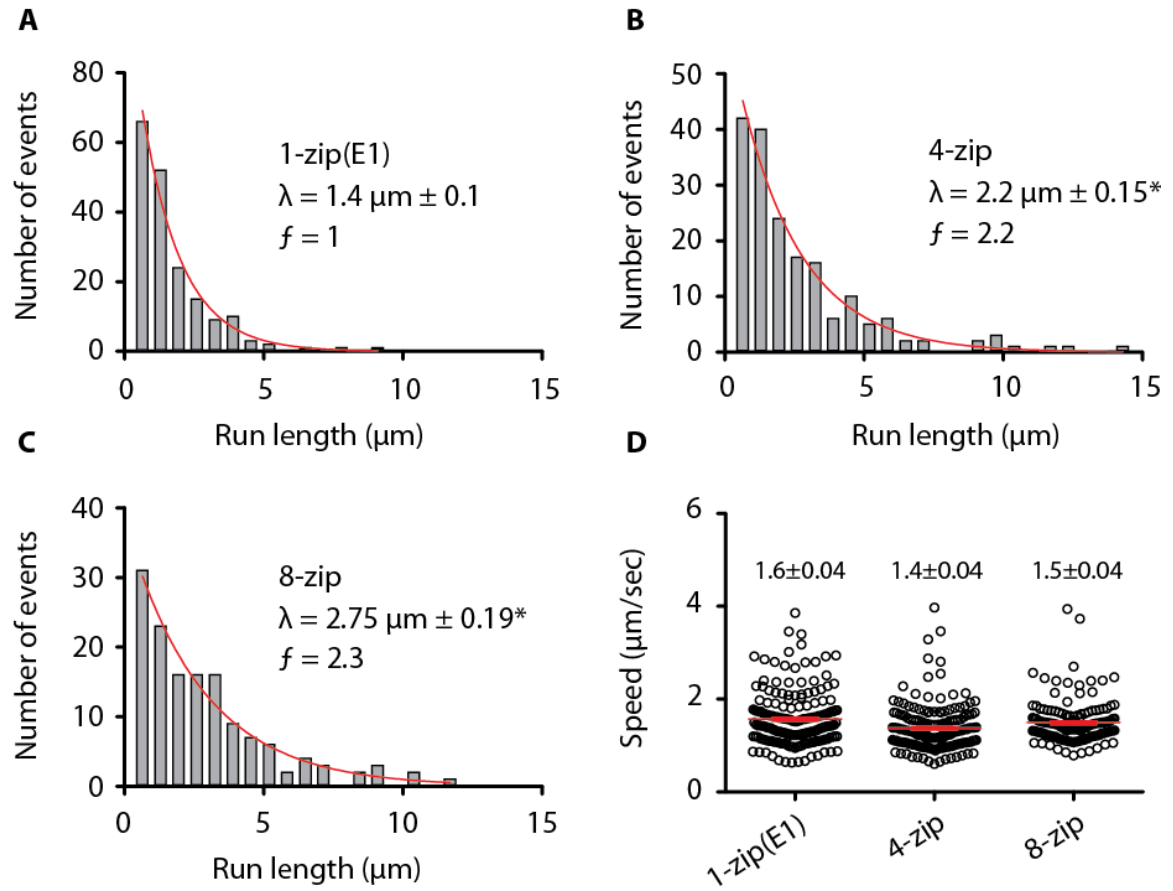


Figure 2-S3. Characteristic run length and speed of labeled Myo4p mRNPs in the presence of excess unlabeled motor and *ASH1* mRNA to promote zip code occupancy. Run length histograms of Myo4p mRNPs containing (A) 1(E1), (B) 4 and (C) 8 zip codes. Reactions included 0.35 nM labeled *ASH1* mRNA, 10 nM unlabeled *ASH1* mRNA, and 250 nM Myo4p. Asterisk (*) indicates run lengths that are significantly different from the 1-zip(E1) *ASH1* construct with $P < 0.001$ (Kolmogorov-Smirnov Test). The run frequency (number of runs per μM Myo4p per μm actin per sec) with 1-zip(E1) is normalized to one. (D) Speed distributions of Myo4p motile mRNPs in the presence of excess unlabeled Myo4p and *ASH1* mRNA. The mean speed is indicated with a red line. Error is in s.e.m. Conditions: 140 mM KCl, pH 7.4, 1 mM MgATP.

Table 2-S1. Sequences constituting the four native *ASH1* mRNA zip codes

E1 zip code
T ₆₁₈ ATCAAGACTATGTTAAAATACGCGAAGAAGTGGCTCATTTCAAGCCATT AAGTATACCCAACCTTAATAATAATCAAAAATAAT ₇₀₂
E2A zip code
A ₁₁₀₂ AATTGCTTGCGAATAGAGACATTCTATCGAACAATTCCAAATCTAATG TAAGGAAACCATCTAAGAACAAAATCTCAAAGCAA ₁₁₈₅
E2B zip code
T ₁₂₅₈ CTGCATCTTCATCTCCATCTCCCTCCACACCGACGAAAAGTGGCAAGA TGAGATCAAGATCATCCTCACCTGTGCGTCCCAAG ₁₃₄₁
E3 zip code
T ₁₇₆₅ GATACATGGATAACTGAATCTCTTTCAACTAATAAGAGACATTATCAC GAAACAATTGTACATTT ₁₈₃₀

Table 2-S2. Nucleotide sequences present or base pair changes made to ablate zip code elements for each *ASH1* mRNA construct

<i>ASH1</i> Construct	<i>ASH1</i> Sequence
0-zip	1-618, 703-1104
1-zip	1-1104
2-zip(E2A,E2B)	1-617, 703-1590
3-zip(E1,E2A,E2B)	1-1590
4-zip	1-1837
8-zip	4-zip concatenated (1-1827, 382-1837)
2-zip(E1,E3)	C ₆₄₁ GA → TAA and C ₁₈₁₃ GA → TGA

Movie legends

Movies are available at

<http://www.nature.com/nsmb/journal/v20/n8/full/nsmb.2614.html#supplementary-information>

Movie 2-S1. No movement of mRNPs containing an *ASH1* mRNA construct without zip code elements on yeast actin–tropomyosin tracks. mRNA, green. Actin, red. Conditions: 140 mM KCl, 1mM MgATP. Movie time, 17 s. Image width, 7 μ m.

Movie 2-S2. Movement of mRNPs containing the native four zip code *ASH1* mRNA construct on yeast actin–tropomyosin tracks. mRNA, green. Actin, red. Conditions: 140 mM KCl, 1mM MgATP. Movie time, 17 s. Image width, 7 μ m.

Movie 2-S3. Movement of mRNPs containing an *ASH1* mRNA construct with a single (E1) zip code element on yeast actin–tropomyosin tracks. Run frequency is 1/3 that of native *ASH1*. mRNA, green. Actin, red. Conditions: 140 mM KCl, 1mM MgATP. Movie time, 17 s. Image width, 7 μ m.

Movie 2-S4. Movement of mRNPs containing an *ASH1* mRNA construct with eight zip code elements on yeast actin–tropomyosin tracks. Run frequency is 2-fold higher than with the native *ASH1*. mRNA, green. Actin, red. Conditions: 140 mM KCl, 1mM MgATP. Movie time, 17 s. Image width, 7 μ m.

CHAPTER 3: SINGLE-MOLECULE RECONSTITUTION OF A MICROTUBULE-BASED mRNA TRANSPORT COMPLEX

Thomas E. Sladewski¹, Carol S. Bookwalter¹, Neil Billington², Elena B. Krementsova¹, Hailong M. Lu, Yusuf M. Ali, Stephanie A. Ketcham³, Trina A. Schroer³ & Kathleen M. Trybus^{1,3}

¹Department of Molecular Physiology & Biophysics, University of Vermont, Burlington, VT 05405. ²National Institutes of Health, NHLBI, Bethesda, Maryland. ³Johns Hopkins, Department of Biology, Baltimore, Maryland. ³Correspondence should be addressed to K.M.T.

To be submitted to *eLife*

Correspondence:
Kathleen M. Trybus
Health Science Research Facility 130
149 Beaumont Avenue
Department of Molecular Physiology & Biophysics
University of Vermont
Burlington VT 05405
phone: 802-656-8750
kathleen.trybus@uvm.edu
<http://physiology.med.uvm.edu/trybus>

This work was supported by funds from the US National Institutes of Health (GM078097 to K.M.T.).

Subject terms: Motor proteins, RNA transport, Single-molecule biophysics

ABSTRACT

It has recently been shown that dynein-dynactin can be converted into an ultra-processive motor in the presence of a truncated fragment of the cargo adapter protein Bicaudal D2 (BicD2) (McKenney et al., 2014; Schlager et al., 2014a). Full-length BicD, in contrast, is not recruited by dynein-dynactin (Hoogenraad et al., 2003). Here we investigate the role of downstream binding partners of BicD in activation of dynein-dynactin. As cargo, we used a synthesized localizing mRNA found in *Drosophila* (*K10*), and the mRNA binding protein Egalitarian, to fully reconstitute a messenger ribonucleoprotein (mRNP) complex *in vitro*. Negative stain electron microscopy showed that full-length BicD exhibits a folded looped conformation, with the C-terminal region interacting with more N-terminal regions, likely prohibiting interaction with dynein-dynactin. Single molecule *in vitro* assays show that only mRNA-bound Egalitarian activates dynein-dynactin for ultra-processive runs, which may be the result of Egalitarian-mRNA disrupting the inhibitory looped structure of BicD. The presence of the cargo mRNA is thus the trigger to activate mRNP motility.

INTRODUCTION

Mammalian cytoplasmic dynein is a 1.4MDa molecular motor complex of the AAA+ ATPase family that provides essential cellular functions including transport of vesicles, organelles, and mRNA (reviewed in (Roberts et al., 2013)). Dynein is the predominant minus-end directed microtubule-based motor that traffics cellular cargos for many microns at speeds of $\sim 1 \mu\text{m}/\text{sec}$ (Allan, 2011). Molecular motors that transport cargo typically exhibit processive behavior when assayed *in vitro*, meaning that single motors remain bound to the polymer track for long distances without dissociating. Thus, it was surprising when *in vitro* studies showed that single molecules of mammalian dynein not attached to beads are at best weakly processive, even in the presence of the multi-subunit dynactin complex that is needed for most cellular functions of dynein (King and Schroer, 2000; McKenney et al., 2014; Miura et al., 2010; Ross et al., 2006; Schlager et al., 2014a; Trokter et al., 2012; Wang et al., 1995). It was not initially recognized that dynein, like other molecular motors, exists in an auto-inhibited state (McKenney et al., 2014; Schlager et al., 2014a; Torisawa et al., 2014). Electron microscope images of single dynein motors showed that in the inhibited state, the motor domain rings are closely stacked together in a structure called the phi particle. Several non-physiologic mechanisms of disrupting this interaction, including coupling multiple dyneins to a DNA origami (Torisawa et al., 2014), or binding to a large bead (Belyy et al., 2016; King and Schroer, 2000; Mallik et al., 2004), converts dynein from a diffusive to a processive motor.

A major advance in understanding dynein function came from two recent single molecule studies. Both studies showed that single dynein-dynactin complexes showed

ultra-processive behavior when a truncated fragment of the native dynein cargo adapter protein Bicaudal-D2 (BicD2^{CC1}) was bound. A signature feature of this motor complex is that it moves to the end of the microtubule and accumulates (McKenney et al., 2014; Schlager et al., 2014a). In addition, the dynein-dynactin-BicD^{CC1} complex (DDB^{CC1}) produced 4.3 pN of force (Belyy et al., 2016), in contrast to earlier reports for dynein alone which were in the range of 0.5-1.5 pN, implying that dynein was a weak motor (Mallik et al., 2004; McKenney et al., 2010; Ori-McKenney et al., 2010; Rai et al., 2013). The higher force of the activated dynein complex is able to successfully engage in a tug-of-war with a single kinesin (Belyy et al., 2016).

Cargo adapter proteins such as BicD are thus central to understanding how dynein is activated in the cell. BicD2 is composed of three coiled-coil domains; the N-terminal coiled-coil domains (CC1 and part of CC2) domains are involved with dynein-dynactin binding and activation (Urnavicius et al., 2015), while the C-terminal coiled-coil (CC3) binds adapter proteins that link dynein to cargo. Unlike the constitutively activated BicD2^{CC1} fragment, the full-length BicD molecule fails to recruit dynein (Hoogenraad et al., 2001; Hoogenraad et al., 2003). Yeast-2-hybrid studies showed that the CC1 domain interacts with the CC3 domain, leading to a model in which BicD forms N- to C-terminal auto-inhibitory interactions (Hoogenraad et al., 2001). Metal shadowed images of BicD, in contrast, appear more consistent with a CC2-CC3 interaction (Stuurman et al., 1999). One hypothesis for cellular activation of dynein-dynactin by BicD is that cargo adapter proteins that bind to BicD may relieve its auto-inhibition. To test this model *in vitro*, we relied on a well-characterized model system for studying dynein-driven microtubule-based transport, namely localization of *K10* mRNA in *Drosophila*. During development, *K10*

mRNA is transported by dynein from nurse cells to the *Drosophila* oocyte, where it localizes to the anterior margin to establish dorsal polarity (Cheung et al., 1992). *K10* contains a single 44 base-pair localization element (TLS) in its 3'UTR that binds the mRNA adapter protein Egalitarian (Dienstbier et al., 2009; Serano and Cohen, 1995). Egalitarian links *K10* mRNA to dynein by associating with the CC3 of BicD (Dienstbier et al., 2009).

To understand the molecular basis for dynein activation by cargo and full-length cargo adapters, we fully reconstituted a mRNP (messenger ribonucleotide protein) complex *in vitro* from tissue-purified dynein and dynactin, baculovirus expressed full-length adapters BicD and Egalitarian, and synthesized *K10* mRNA. Negatively stained electron microscope images show that full-length BicD forms a looped, folded conformation that persists upon Egalitarian binding. Using single molecule techniques, we show that only mRNA-bound Egalitarian supports the recruitment of dynein-dynactin to BicD, and activation of mRNA transport *in vitro*. The requirement of mRNA for activation may be its ability to recruit a molecule of Egalitarian to the CC3 domain of each chain of the BicD coiled-coil dimer. We previously demonstrated that mRNA cargo also activates a yeast class V myosin motor for processivity on actin filaments (Sladewski et al., 2013), albeit by a different mechanism. Thus, activation of motors by mRNA cargo is a conserved mechanism in yeast and higher eukaryotes, which ensures that only cargo-bound motors become activated for transport.

MATERIALS AND METHODS

K10 mRNA constructs

DNA base pairs in the 3'UTR of *Drosophila K10* mRNA (NM_058143.3), 105-1165 past the stop codon were cloned behind the SP6 promoter in the pSP72 vector (Promega) followed by a poly16A tail and an EcoRV site to allow the vector to be bluntly opened for use as a template for RNA transcription. The 43 nt transport/localization signal (TLS) zip code starts 679 base pairs from the start of the 3'UTR (Serano and Cohen, 1995). Thus, *K10* mRNA constructs contain 575 bases before and 443 bases after the TLS. For the *K10* no zip construct, the TLS element (CTTGATTGTATTTTAAATTAATTCTTAAAACTACAAATTAA) was removed. A minimal *K10* mRNA construct (*K10min*) (433 base pairs in length) contains 195 base pairs on either side of the TLS element. A minimal *K10* mRNA construct lacking the zip code (*K10min no zip*) is the same sequence without the TLS and contain an additional 43 bases of 3'UTR sequence immediately following *K10min* to ensure that *K10min* and *K10min no zip* are the same size.

Protein constructs

Full-length *Drosophila* BicD (NP_724056.1 or NM_165220.3) was cloned into pACSG2 for *Sf9*/baculovirus expression. A FLAG tag was added to the C-terminus to facilitate purification. Where indicated, constructs contained an N-terminal monomeric YFP, or a biotin tag for conjugation to a streptavidin-Qdot (Invitrogen). The biotin tag is a 88 amino acid piece of the biotin carboxyl carrier protein (Cronan, 1990). Constitutively active human BicD2^{CC1} (NM_015250 and NP_056065.1) contains amino acids 25-398 and

was cloned into bacterial expression vector pET19 with either an N-terminal HIS and biotin tag, or an N-terminal HIS and monomeric YFP tag. Human BicD2^{CC1} aligns with *Mus musculus* BicD amino acids 25-400. Other *Drosophila* BicD truncation constructs were cloned with an N-terminal FLAG and biotin tag, or an N-terminal FLAG and monomeric YFP tag, and inserted into pACSG2 for *Sf9*/baculovirus expression. BicD CC2 contains the second coil-coiled region (amino acids L318-Q557). BicD CC2 + CC3 contains also the third coil-coiled region (amino acids L318-F782). *Drosophila* Egalitarian (AAB49975.2 and U86404.2) was cloned into pACSG2 with either a C-terminal FLAG, or C-biotin followed by a HIS tag. *Drosophila* Rab6 (NM_057824.5) containing a Q71L point mutation was cloned into a pET19 bacterial expression vector with an N-terminal HIS and biotin tag. This point mutation causes Rab6 to slowly hydrolyse GTP (Bergbrede et al., 2005). The N-terminal 402 amino acids of mouse kinesin (NP_032475 and NM_008449.2) with a point mutation (G235A) was cloned into pET21b to express a rigor kinesin that was used for attachment of microtubules to the surface of flow chambers.

Protein expression and purification

Cytoplasmic dynein and dynactin was purified from bovine brain as described previously (Bingham et al., 1998), except that the preparation was scaled down to 1.5 brains (~375 g) of starting material. Bovine tubulin was purified as described previously (Castoldi and Popov, 2003). BicD^{CC1} containing a N-terminal HIS and biotin tag was expressed in 0.5 L of BL21(DE3) bacterial cells and induced with 0.7 mM IPTG overnight at room temperature in LB broth containing 0.024 mg/mL biotin (Sigma B4639). Cells were harvested by pelleting 5,500 x g for 10 min. The pellet was re-suspended in 30mL

HIS lysis buffer (10 mM NaPO₄, pH 7.4, 0.3 M NaCl, 0.5% glycerol, 7% sucrose, 7 mM BME, 0.5 mM 4-(2-aminoethyl)benzenesulfonyl fluoride, 5 µg/ml leupeptin). Cells were lysed by sonication and centrifuged 33,000 x g for 30 min and passed over a 3.5 mL HIS-Select column at 0.75 mL/min. Column was then washed with 10 mM imidazole wash buffer (10 mM NaPO₄, pH 7.4, 0.3 M NaCl, 10 mM Imidazole) followed by 12mL of 30 mM imidazole wash buffer (10 mM NaPO₄, pH 7.4, 0.3 M NaCl, 10 mM Imidazole). Protein was eluted in elution buffer (10 mM NaPO₄, pH 7.4, 0.3 M NaCl, 200 mM Imidazole) and concentrated using a Millipore Amicon Ultra-15 centrifugal filter. Purified protein was clarified 487,000 x g for 20 min and dialyzed in storage buffer (25 mM Imidazole, pH 7.4, 300 mM NaCl, 1 mM EGTA, 50% glycerol, 1 mM DTT, 0.1 µg/mL leupeptin) for storage at -20°C.

For full-length *Drosophila* BicD purification, two billion *Sf9* cells in 0.33 L *Sf9* medium (Gibco 10902-088) supplemented with 1 parts to 20 fetal bovine serum (Sigma F0926), 1 parts to 100 PEN STREP (Gibco 15140-122), 1 parts to 1000 Gentamicin Sulfate (Corning 30-005-CR), and 1 parts to 500 Amphotericin B (Gibco 15290-98) were infected with virus coding for BicD with either an N-terminal biotin or YFP tag and an N- or C-terminal FLAG tag for FLAG affinity purification. For constructs with a biotin tag, 0.2 mg/mL biotin was added to the media. Cells were grown for ~76 hours at 27°C, and then harvested by spinning at 1,800 x g for 10 min. The pellet was re-suspended in 40 mL FLAG lysis buffer (10 mM imidazole, pH 7.4, 0.3 M NaCl, 1 mM EGTA, 2 mM DTT, 0.5 mM 4-(2-aminoethyl)benzenesulfonyl fluoride (AEBSF) (Fisher BioReagents 30827-99-7), 0.5 mM phenylmethylsulfonyl fluoride (PMSF) (Sigma P7626), 0.5 mM Tosyl-L-lysyl-

chloromethane hydrochloride (TLCK) (Sigma T7254), 0.5 mM Calpeptin, 5 µg/ml leupeptin (Thermo Scientific 78435), 1.3 mg/ml benzamidine (Sigma B6506)). Cells were lysed by sonication and the lysate was centrifuged 257,000 x g for 35 min. The clarified lysate was added to 4 mL FLAG affinity resin (Sigma A2220) and incubated with shaking at 4°C in a 50 mL falcon tube for 40 min. Resin was transferred to a column and washed with ~200 mL FLAG wash buffer (25 mM Imidazole, pH 7.4, 0.3 M NaCl, 1 mM EGTA) and eluted with FLAG wash buffer containing 0.1 mg/ml of FLAG peptide. Peak fractions were concentrated using a Millipore Amicon Ultra-15 centrifugal filter, clarified 487,000 x g for 20 min and dialyzed in storage buffer (25 mM Imidazole, pH 7.4, 300 mM NaCl, 1 mM EGTA, 50% glycerol, 1 mM DTT, 0.1 µg/mL Leupeptin) for storage at -20°C.

Egalitarian containing a C-terminal biotin and FLAG tag, or only a FLAG tag, was purified similarly except that cells were infected for only 48 hours. Lysis and wash steps were done at 1 M NaCl and protein was stored by snap freezing in liquid nitrogen and stored at -80°C. For Egalitarian-BicD co-purification, 2-3 billion *Sf9* cells in 0.33-0.5 L of *Sf9* medium with additives (see above) were co-infected with Egalitarian containing a C-terminal biotin and HIS tag, and BicD containing an N-terminal YFP and FLAG tag, or only an N-terminal FLAG tag. Following infection, cells were grown for 76 hours at 27°C temp and then harvested. The pellet was re-suspended in HIS lysis buffer (10 mM NaPO₄, pH 7.4, 0.25 M NaCl, 0.5% glycerol, 7% sucrose, 0.1% NP40, 0.5 mM DTT and protease inhibitors described earlier for purifying BicD). The cells were lysed by sonication and the lysate was centrifuged 257,000 x g for 35 min. A 5 mL HIS-Select column (Sigma P6611) was prepared by washing the resin with 5 column volumes of water followed by 3 column

volumes of 0.5 M imidazole pH 7.4. The column was washed with 20 column volumes of water and re-equilibrated in 5 column volumes of HIS lysis buffer without DTT and protease inhibitors. A high imidazole wash allows for subsequent use of DTT. The clarified lysate was incubated with resin for 45 min and then washed in a column with 40 mL of 10 mM imidazole wash buffer (10 mM NaPO₄, pH 7.4, 0.25 M NaCl, 10 mM Imidazole, 0.5 mM DTT) followed by 60 mL of 30 mM imidazole wash buffer (10 mM NaPO₄, pH 7.4, 0.3 M NaCl, 10 mM Imidazole, 0.5 mM DTT). Protein was eluted in elution buffer (10 mM NaPO₄, pH 7.4, 0.3 M NaCl, 200 mM Imidazole, 0.5 mM DTT) and dialyzed overnight in FLAG purification buffer (10 mM Imidazole, pH 7.4, 0.25 M NaCl, 0.5% glycerol, 0.1% NP40, 1 mM DTT, 0.1 µg/mL leupeptin). The dialyzed protein was then purified over a FLAG column to remove excess Egalitarian by incubating with 3.5mL FLAG affinity resin for 60 min, followed by washing and elution as described for BicD purification. Peak elution fractions were combined and snap frozen in liquid nitrogen and stored at -80°C. For negative stain electron microscopy, protein was dialyzed against buffer C (30 mM HEPES pH 7.2, 0.25 M KOAc, 2 mM MgOAc, 1 mM EGTA, 1 mM TCEP, 0.1 µg/mL leupeptin), centrifuged 487,000 x g for 20min, and drop frozen into liquid nitrogen.

Drosophila Rab6(Q71L) with a C-terminal biotin and HIS tag was expressed in BL21(DE3) bacteria and purified as previously described (Fuchs et al., 2005), except that protein was dialyzed against storage buffer (25 mM Imidazole, pH 7.4, 300 mM NaCl, 1 mM EGTA, 50% glycerol, 1 mM DTT, 0.1 µg/mL leupeptin) for storage at -20°C. Before use in experiments Rab6(Q71L) bound nucleotide was exchanged for GTP (Rab6^{GTP}). Rab6 was first diluted into buffer B300 (15 mM Imidazole, pH 7.4, 300 mM KCl, 4 mM

MgCl₂, 1 mM EGTA), and clarified at 400,000 x g for 20 min at 4°C. 50 µl of 2 µM Rab6 in B300 buffer was supplemented with 1 mg/mL BSA, 1 mM GTP and 10 mM EDTA and incubated for 25 min at room temperature. MgCl₂ was then added to 15 mM and the protein transferred to ice.

Rigor kinesin (G235A) was induced for expression overnight at room temperature in *E. coli* Rosetta (DE3) (Novagen) with 0.4 mM IPTG in Terrific Broth Media (Invitrogen 22711-022) containing Kanamycin. Cells were harvested by centrifugation and resuspended in lysis buffer (10 mM Hepes pH 7.5, 10 mM NaCl, 1 mM EGTA, 0.25 mM DTT with protease inhibitors AEBSF, TLCK at 0.5 mM and leupeptin at 5 µg/ml added) and sonicated for 4 min with 0.5 sec pulses in an ice bath. MgATP was added to a final concentration of 25 µM and centrifuged at 257,000 x g for 40 min. After clarification, the buffer was adjusted to a final concentration of 0.2 M NaCl and loaded onto a HIS-Select column (Sigma P6611) equilibrated with lysis buffer containing 0.2 M NaCl. The column was washed with the same buffer containing 10 mM Imidazole, then eluted with lysis buffer containing 0.2 M Imidazole. Peak fractions were dialyzed against storage buffer (50% glycerol, 10 mM Imidazole, 0.2 M NaCl, 1 mM EGTA, 1 mM DTT, 40 µM MgATP, and 5 µg/ml leupeptin) for storage at -20°C.

RNA synthesis

The DNA template was bluntly linearized at an EcoRV site situated directly after the polyA16 tail and transcribed using a phage SP6 RNA polymerase (RiboMAX system from Promega). Labeling of the *K10* RNA was achieved by adding a mixture of Alexa488

labeled UTP (Molecular Probes - Invitrogen) in a 1:10 molar ratio to unlabeled nucleotides thus allowing incorporation of the fluorophore during RNA synthesis.

Flow cell preparation

PEGylated coverslips were made using methods adapted from (Gestaut et al., 2008). Glass cover slides (Fisher Scientific 12-545-M) were plasma cleaned for 5 min and transferred to glass Coplin jars containing 1 M KOH and then placed in a sonicating water bath for 20 min. Using a squirt bottles, slides were rinsed thoroughly with nanopure water, then 95% ethanol and dried using a nitrogen stream. Slides were then placed in dry glass Coplin jars and a solution was added containing 1.73% 2-methoxy(polyethyleneoxy)propyltrimethoxysilane (Gelest, Inc SIM6492.7 – 25g) and 0.62% n-butylamine (Acros Organics 109-73-9) in anhydrous toluene (Sigma 244511), prepared using glass pipettes. Coplin jars containing slides were then placed in plastic bags, purged with nitrogen and incubated for 1.5 hours at room temperature. Following this incubation, the slides were dipped successively in two beakers containing anhydrous toluene and dried using a nitrogen stream. The slides were immediately made into flow chambers, placed in 50mL falcon tubes and stored at -20°C. This procedure produces a PEGylated slide surface that contains small gaps for the purpose of microtubule attachment.

Single molecule Total Internal Reflection Fluorescence (TIRF) microscopy assays

Bovine tubulin was thawed and centrifuged at 400,000 x g for 5 min at 2°C. Tubulin concentration was determined using a Bradford reagent and diluted to 100 µM in ice cold BRB80 (80 mM PIPES, pH 6.9, 1 mM EGTA, and 1 mM MgCl₂) and supplemented with

1 mM GTP. For generating labeled microtubules, unlabeled tubulin was mixed with 1 μ M rhodamine-labeled tubulin (Cytoskeleton, Denver, CO) for a final labeled/unlabeled ratio of 1:100. The tubulin mixture was polymerized by transferring to 37°C water bath for 20 min and stabilized by adding 10 μ M paxitaxol (Cytoskeleton, Denver, CO). Stabilized microtubules were kept at room temperature for experiments performed that day. Microtubules could be stored at 4°C for use in experiments within 3 days.

Labeled or unlabeled microtubules were adhered to PEGylated flow chambers using rigor kinesin for attachment. Rigor kinesin was diluted to 0.2 mg/mL in buffer B (30 mM HEPES, pH 7.4, 25 mM KOAc, 2 mM MgOAc, 1 mM EGTA, 10% glycerol, 10 mM DTT) and added to PEGylated flow chambers for 10 min at room temperature. Flow chambers were then washed three times in buffer B and blocked with buffer B containing 2 mg/mL BSA, 0.5 mg/mL κ -casein and 0.5% pluronic F68. Paxitaxol stabilized microtubules were diluted 100-fold to a final concentration of in buffer B containing 10 μ M paxitaxol, and added to flow chambers and incubated for 10 min at room temperature. Flow chambers were washed three times with buffer B containing 10 μ M paxitaxol to remove unbound microtubules.

For DDB^{CC1} single molecule motility, BicD^{CC1} containing an N-terminal biotin tag was diluted in buffer B300 (30 mM HEPES pH 7.4, 300 mM KOAc, 2 mM MgOAc, 1 mM EGTA, 0.5% pluronic F68, 20 mM DTT) and centrifuged 400,000 x g for 20 min. Protein concentration was determined by Bradford reagent and diluted to 1 μ M in B300. Dynein, dynactin and BicD^{CC1} were mixed to a final concentration of 100 nM in buffer Go50 (30 mM HEPES pH 7.4, 50 mM KOAc, 2 mM MgOAc, 1 mM EGTA, 10% glycerol, 2 mM

MgATP, 20 mM DTT, 8 mg/mL BSA, 0.5 mg/mL κ -casein, 0.5% pluronic F68, 10 μ M paxitaxol and an oxygen scavenger system (5.8 mg/mL glucose, 0.045 mg/mL catalase, and 0.067 mg/mL glucose oxidase; Sigma-Aldrich)). Streptavidin-conjugated 655 quantum dots (Invitrogen) were added at 200 nM and incubated with proteins on ice for 30 min. Samples were diluted in buffer Go50 for a final dynein concentration of 1 nM and added to microtubule adsorbed flow chambers for imaging.

For imaging complexes where *K10* mRNA is labeled, BicD was diluted in B300 and centrifuged 400,000 x g for 20 min. Egalitarian was diluted in B300 supplemented with 40 mM DTT and incubated on ice for 1 hour before centrifuging 400,000 x g for 20 min. Concentrations of BicD and Egalitarian was determined using Bradford reagent. BicD and Egalitarian were combined at 1 μ M in B300. 50 nM dynein and dynactin, 100 nM BicD-Egalitarian and 50 nM *K10* mRNA, synthesized with an Alexa 488 dUTP for visualization, was mixed in buffer Go150 (buffer Go50 adjusted to a final concentration of 150 mM KOAc) containing 10 units of RNase Inhibitor (Promega N261B) and 0.25 mg/mL tRNA from *E. coli* (Sigma R1753). The order of mixing is BicD-Egalitarian, dynein-dynactin, RNase Inhibitor, tRNA, *K10* mRNA. The mixture was incubated on ice for 45 min and diluted to a final dynein concentration of 1 nM in Go80 (buffer Go50 adjusted to a final concentration of 80 mM KOAc) before imaging.

For imaging of complexes where the adapters are labeled, either BicD or Egalitarian containing a biotin tag were used for conjugation to quantum dots for visualization. Mixtures contained 50 nM dynein and dynactin, 100 nM BicD and Egalitarian, 50 nM unlabeled *K10* mRNA and 200 nM Streptavidin-conjugated 655 quantum dots

(Invitrogen). Complexes were incubated on ice for 45 min and diluted to a final dynein concentration of 1 nM in Go80 before imaging.

For single molecule pull-downs showing co-localization of YFP-BicD and Egalitarian on microtubules, BicD fused to an N-terminal YFP tag and Egalitarian containing a C-terminal biotin tag were prepared as described above and pre-mixed at 1 μ M in B300. Mixtures containing 50 nM dynein and dynactin, 100 nM BicD-Egalitarian, 50 nM unlabeled *K10* mRNA and 200 nM streptavidin-conjugated 655 quantum dots (Invitrogen) were diluted in Go150 supplemented with 10 units of RNase Inhibitor (Promega N261B) and 0.25 mg/mL tRNA (Sigma R1753). Mixtures were diluted so that the final concentration of dynein is 1 nM and imaged. YFP was used to visualize YFP-BicD and 655 Qdots were used to visualize Egalitarian on rhodamine-labeled microtubules.

FLAG immunoprecipitation

BicD partial constructs *Drosophila* CC2 (amino acids L318-Q557) *Drosophila* BicD CC2 + CC3 (amino acids L318-F782) and human BicD^{CC1} were diluted in BB (30 mM HEPES, pH 7.4, 150 mM KOAc, 2 mM MgOAc, 1 mM EGTA, 1 mM DTT, 0.5% Tween-20 and 1 μ g/mL leupeptin), clarified at 400,000 x g for 20 min, and concentration determined by Bradford reagent. In 250 μ l BB, BicD constructs were diluted to 1.5 μ M and samples were taken for running 'inputs' on a gel. BSA was then added to 1 mg/mL and 40 μ L of a 1:1 slurry of FLAG affinity resin equilibrated in BB was added. Mixtures were rocked for 1 hour at room temperature, washed 4 times with 500 μ l of BB and eluted by boiling in 50 μ l of 2x SDS loading buffer. 10 μ l of input and 20 μ l of elution were loaded on a 4-12% SDS gel and run at 150 V till the dye front migrated to the bottom of

the gel. The gel was stained with Coomassie for visualization of inputs and immunoprecipitation.

Imaging and data analysis

Complexes were imaged using TIRF microscopy at room temperature using an inverted microscope (Eclipse Ti-U; Nikon, Melville, NY) equipped with a 100x plan apochromatic objective lens (1.49 NA) and auxiliary 1.5x magnification. Data were collected as described previously (Krementsova et al., 2011). Alexa Fluor488 and Qdots (655 nm) were excited with a 488-nm argon laser. For single molecule pull-downs, YFP was excited with a 488-nm laser line. Microtubules were visualized using Epi fluorescence. Data were typically collected at 5 to 10 frames per second. Motile mRNPs were tracked with labeled mRNA or with adapters labeled with a Qdot, and run lengths were measured with ImageJ and the particle-tracking plug-in MTrackJ (Meijering et al., 2012). For all processivity assays, frequencies were generated by counting the total number of runs in movies acquired no more than 15 min after dilution of the mRNP mixture. The total number of runs was divided by the total microtubule length, time and final dynein concentration to generate a run frequency. Speeds were measured by tracking run trajectories every 0.2 sec with ImageJ using the particle-tracking plug-in SpotTracker (Sage et al., 2005).

Analytical ultracentrifugation

Sedimentation coefficients of BicD, YFP-BicD and YFP-BicD-Rab6^{GTP} complex were determined using an analytical ultracentrifuge (Optima XL-I; Beckman Coulter). To determine if BicD unfolds at high ionic strength, sedimentation velocity runs were

performed with BicD in buffer C (10 mM Hepes, pH 7.4, 1 mM EGTA and 1 mM DTT) containing 0.1 M KCl or 0.5 M KCl. To determine if Rab6^{GTP} binding unfolds BicD, sedimentation velocity runs comparing YFP-BicD, Rab6^{GTP} and the YFP-BicD-Rab6^{GTP} complex were performed in buffer D (30 mM Hepes, pH 7.4, 0.15 M KOAc, 2 mM MgOAc, 1 mM EGTA, 10 μ M GTP and 1 mM DTT). All runs were performed in the An-60 Ti rotor at 40,000 rpm and 20°C. Sedimentation coefficients were determined by curve fitting to one or more species using the dc/dt program (Philo, 2000).

Negative stain electron microscopy

YFP-BicD was imaged in 150 mM KOAc by diluting to 25 nM in buffer E (30 mM HEPES, pH 7.2, 150 mM KOAc, 2 mM MgOAc 1 mM EGTA, 1 mM TCEP) or containing 500 mM KOAc by diluting in buffer F (10 mM MOPS (pH 7.0), 0.1 mM EGTA, 2 mM MgCl₂, 500 mM KCl, 1 mM TCEP). The BicD-Rab6^{GTP} complex was prepared by mixing 2 μ M YFP-BicD dimer and 4 μ M Rab6^{GTP} in buffer E containing 1 mM GTP. The complex was diluted to 25 nM in buffer E for imaging. 3 μ L volume of diluted samples were applied to UV-treated, carbon-coated copper grids and stained with 1% uranyl acetate. Micrographs were recorded using an AMT XR-60 CCD camera at room temperature on a JEOL 1200EX II microscope at a nominal magnification of 40,000. Catalase crystals were used as a size calibration standard. Image processing was performed using SPI DER software as described previously (Burgess et al., 2004).

RESULTS

Full-length BicD is auto-inhibited for dynein-dynactin recruitment

We determined if full-length *Drosophila* BicD binds to tissue purified dynein-dynactin *in vitro* using a single molecule pull-down assay. Dynein-dynactin complexes were added to either bacterially expressed YFP-BicD2^{CC1}, or full-length YFP-BicD expressed using the *Sf9*/baculovirus system (**Fig. 3-1, A and B**). Complexes were applied to flow cells with surface-adhered labeled microtubules in the presence of the MgATP analog AMP-PNP, which causes dynein to bind strongly to microtubules. Thus, YFP-BicD associations with microtubules is a measure of BicD complex formation with dynein-dynactin. Total internal reflection fluorescence (TIRF) microscopy was used to visualize dynein-dynactin complexes bound to YFP-BicD2^{CC1} (**Fig. 3-1, C**) or YFP-BicD (**Fig. 3-1, D**). In both 50 and 80 mM KOAc, YFP-BicD2^{CC1} shows a 13-fold enhanced recruitment to dynein-dynactin-bound microtubules compared with full-length BicD (**Fig. 3, E**). As controls, YFP-BicD2^{CC1} and full-length BicD were shown to not interact non-specifically with microtubules at the concentrations used in single molecule assays.

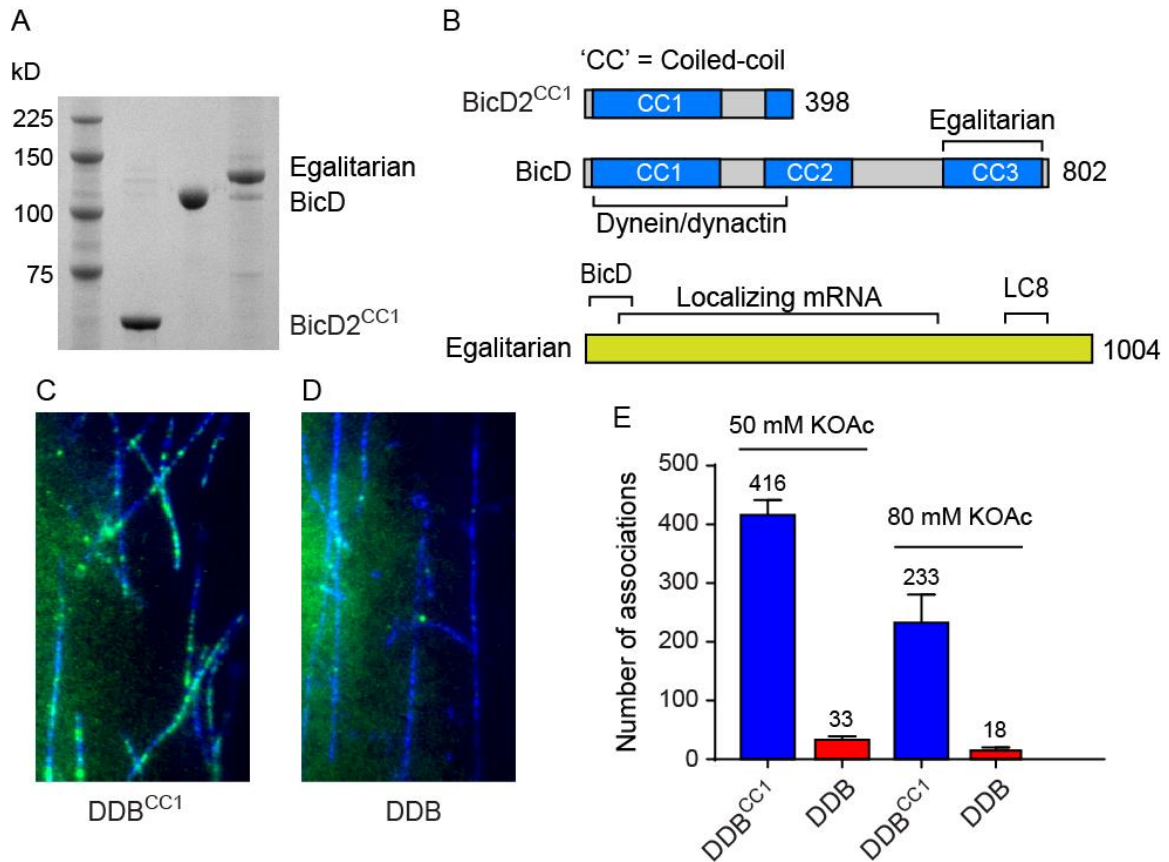


Figure 3-1. Truncated but not full-length BicD binds dynein and dynactin.

(A) SDS PAGE gel of truncated BicD (BicD2^{CC1}), full-length BicD and Egalitarian. (B) BicD contains three coiled-coil (CC) domains. CC1 binds dynein and dynactin and CC3 binds Egalitarian. BicD2^{CC1} lacks the cargo binding CC3 domain. Egalitarian has an N-terminal BicD-binding domain and interacts with dynein light chain (LC8) at its C-terminus. mRNA binding is mediated through a large number (~800) of amino acids. (C-D) Single molecule pull-downs on microtubules (blue) show that dynein and dynactin associates with (C) YFP-BicD2^{CC1} (green) but not with (D) full-length YFP-BicD (green) in the presence of 6 mM AMP-PNP. YFP is used to visualize BicD constructs. (E) Data were quantified to show the number of dynein-dependent associations of complexes containing BicD2^{CC1} (blue) or full-length BicD (red) to microtubules, normalized to microtubule length and dynein concentration. Data are shown for 50 mM KOAc (left) and 80 mM KOAc (right) ionic strength conditions.

BicD forms a folded looped conformation

Electron microscopy was used to determine if BicD auto-inhibition results from N- to C-terminal interactions. Negatively stained EM images of YFP-BicD (**Fig. 3-2, A**) reveals two distinct globular densities at the N-terminus corresponding to YFP, showing that BicD forms a parallel coiled-coil dimer. The YFP densities join a thin CC1 region, followed by a flexible break in the coiled-coil from which CC2 projects and the CC3 loops back to a point close to the first bend. Class averages of YFP BicD where the loop is aligned shows a structure that forms a “D” shape (**Fig. 3-2, B**). Pull-downs indicate that the CC1 domain interacts with a construct containing the CC2 and CC3 domains, but not with one containing only the CC2 domain (**Fig. 3-2, C**). Thus, CC3 likely binds to the C-terminal end of CC1 leaving N-terminal regions of CC1 exposed (**Fig. 3-2, D and E**). We tested whether increasing ionic strength from 0.15 M KOAc to 0.5 M KOAc results in disrupting the auto-inhibitory intramolecular interaction but found no changes in the appearance of the loop (data not shown), consistent with sedimentation velocity analysis showing that YFP-BicD has similar sedimentation coefficients in buffers containing 0.1 M and 0.5 M KOAc (**Fig. 3-2, F**).

BicD extends when bound to Egalitarian but not Rab6^{GTP}

We tested if adapter proteins that bind to the CC3 of BicD promote an extended conformation. A Rab6 mutation (Q71L) that suppresses GTP hydrolysis (Rab6^{GTP}) (Bergbrede et al., 2005) serves as a model CC3-binding protein (**Appendix II - Fig 3**). Complexes formed from YFP-BicD and Rab6^{GTP} in a 1:6 molar ratio (1 BicD dimer: 6 Rab6^{GTP} monomers) were negatively stained and imaged by EM (**Fig. 3-2, G and H**).

Structures of the BicD-Rab6^{GTP} complex show that it persists in a folded conformation, and that the C-terminal loop is collapsed in most images (**Fig. 3-2, G and H**). We confirmed that Rab6^{GTP} does not promote an extended conformation of BicD by comparing the sedimentation coefficients of YFP-BicD alone, Rab6^{GTP} alone, and the YFP-BicD-Rab6^{GTP} complex (**Fig. 3-2, I**). The sedimentation coefficient (S) is a measure of how fast a protein moves through a gradient. Proteins that are elongated will have a large frictional coefficient (f). Because S is inversely proportional to f, proteins that are in a compact folded conformation will have a large sedimentation coefficient and transition to an extended conformation will be followed by a smaller S value. We observed no decrease in S value for BicD in the presence of Rab6^{GTP}, as would occur if BicD became elongated in the presence of Rab6^{GTP}. Taken together these data support the idea that binding of Rab6^{GTP} to the C-terminus of BicD does not induce large scale conformational changes that suggest an extending of the CC2-CC3 loop.

We next tested if Egalitarian binding to BicD results in an extended conformation. Using sedimentation velocity analyses, we show that BicD-Egalitarian complex gives a 44% decrease in sedimentation coefficient compared to BicD alone (**Fig. 3-2, J**). A decrease in S value is consistent with a transition to an extended conformation of BicD when bound to Egalitarian.

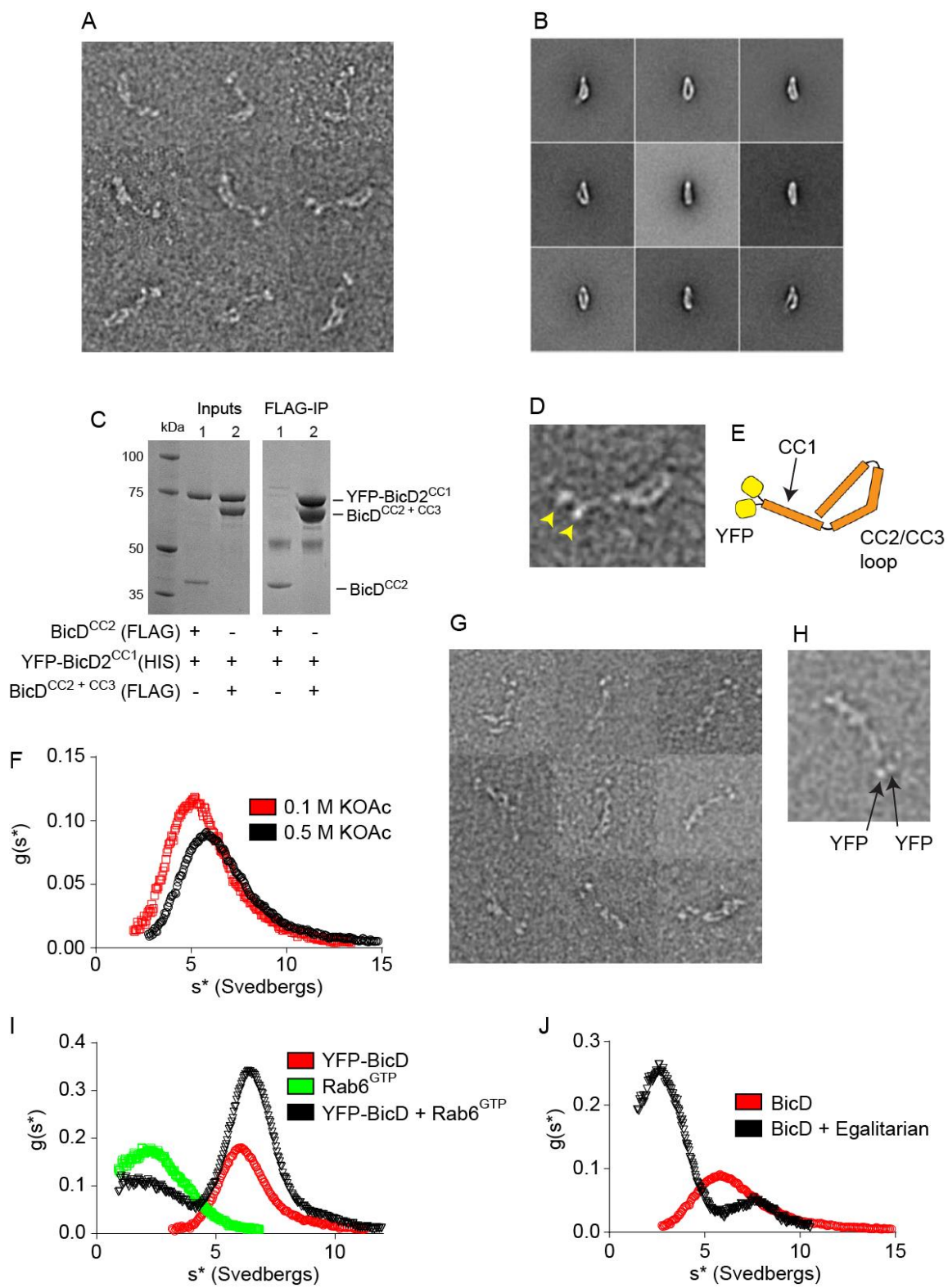


Figure 3-2. Conformation of BicD alone and when bound to Rab6^{GTP} or Egalitarian. (A) Gallery of negatively stained EM images of YFP-BicD. (B) EM class averages of YFP-BicD obtained by aligning the CC2/CC3 loop. (C) FLAG immunoprecipitation (IP) showing inputs of 1.5 μ M purified protein constructs of FLAG-tagged BicD containing CC2 or CC2 + CC3 domains and HIS-tagged BicD2^{CC1}. The CC1 domain interacts with CC2 + CC3 domains but not with CC2 alone. (D) EM image of BicD with YFP labeled (yellow arrowheads). (E) Cartoon illustration of what is seen in the image of BicD with YFP, CC1 and the CC2/CC3 loop labeled. (F) Sedimentation coefficient of BicD in solvents containing 0.1 M KOAc (5.4S) and 0.5 M KOAc (6.1S). (G) Gallery of EM images of a protein complex containing YFP-BicD and Rab6^{GTP}. Rab6^{GTP} is added at 2-molar excess over YFP-BicD dimer. (H) Image of a single YFP-BicD-Rab6^{GTP} complex labeled to show the location of an N-terminal YFP tag. (I) Sedimentation coefficient of YFP-BicD (6.0S), Rab6^{GTP} (2.6S) and a YFP-BicD-Rab6^{GTP} complex (2.6S + 6.4S + 8.5S) in a buffer containing 0.15 M KOAc. Rab6^{GTP} is added at 6-molar excess over YFP-BicD dimer. (J) Sedimentation coefficient of BicD (5.4S) and the BicD-Egalitarian complex (3.0S major peak, 7.7S minor peak) in a buffer containing 0.25 M KOAc. Sedimentation coefficients were calculated using the dc/dt program (Philo, 2000). Fits are not shown.

mRNA cargo is needed for dynein-dynactin recruitment to BicD-Egalitarian in single molecule in vitro assays

Single molecule pull-downs were used to determine the requirements for BicD to bind to dynein-dynactin. Complexes were first reconstituted from dynein-dynactin, YFP-BicD and Egalitarian that contained a C-terminal biotin tag for quantum dot attachment. Dynein complexes were recruited to the microtubules by 6 mM AMP-PNP. Neither BicD nor Egalitarian were recruited to microtubule-bound dynein-dynactin (**Fig. 3-3, A**) implying that Egalitarian alone did not activate BicD for dynein-dynactin binding. We thus tested the hypothesis that an mRNA cargo bound to Egalitarian is necessary for BicD activation. An mRNP consisting of dynein-dynactin, BicD, Egalitarian and a *K10* mRNA transcript was reconstituted. The presence of *K10* mRNA dramatically enhances

Egalitarian and BicD co-localization with microtubules under conditions where dynein is in a strongly-bound state (**Fig. 3-3, B**). This observation implies that mRNA is needed for Egalitarian to activate BicD for dynein-dynactin recruitment. Next, we tested whether the presence of a zip code in *K10* mRNA (TLS) is needed for dynein-dynactin recruitment to BicD-Egalitarian complexes. We reconstituted mRNPs containing a mutant *K10* mRNA transcript lacking the transport/localization sequence (TLS). We observed a ~3-fold reduction in the number of BicD-Egalitarian complexes associated with microtubule-bound dynein (**Fig. 3-3, C**). Thus, Egalitarian binds primarily to the TLS zip code, and more weakly to other regions of the mRNA.

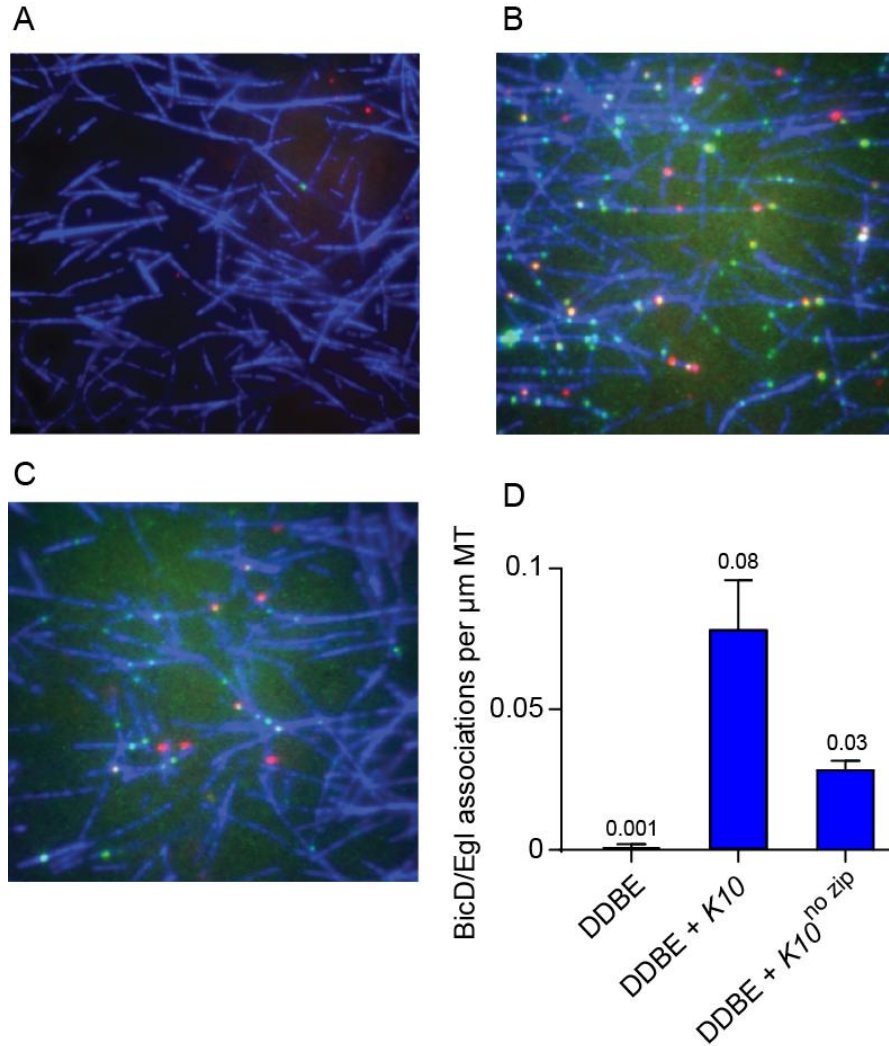


Figure 3-3. *K10* mRNA is needed for BicD-Egalitarian to recruit dynein-dynactin.

(A-C) Single molecule pull-downs of YFP-BicD (green) and quantum dot-bound Egalitarian (red) associated with dynein-dynactin strongly bound to microtubules (blue) in the presence of 6 mM AMP-PNP and (A) no mRNA (B) *K10* mRNA and (C) *K10* mRNA lacking the TLS zip code. (D) Quantification of single molecule pull-down data showing the number of co-localized BicD-Egalitarian complexes bound to dynein-dynactin normalized per μm microtubule length in the absence of mRNA (DDBE), in the presence of *K10* mRNA (DDBE + *K10*) or *K10* without the TLS zip code (DDBE + *K10*^{no zip}).

K10 mRNA activates mRNPs for processive movement and fast speeds

We tested if reconstituted mRNPs bound to *K10* mRNA are activated for long processive runs. mRNPs were reconstituted with either Qdot-labeled adapter proteins or *K10* mRNA synthesized with Alexa Fluor 488-5 dUTP for visualization. TIRF microscopy was used to track mRNP movement on labeled microtubules. In the absence of either BicD or Egalitarian, no movement of labeled *K10* mRNA was observed (**Fig. 3-4, A**). In the absence of mRNA, where the adapters are labeled, we observe a low frequency of runs. Addition of *K10* mRNA to the dynein-dynactin-BicD-Egalitarian complex enhanced run frequency 5-fold. For robust localization of *K10* mRNA in the cell, the TLS zip code is needed. Consistent with single molecule pull-downs, *K10* mRNA constructs lacking the TLS showed a reduced run frequency compared with wild type transcripts. Motility of reconstituted complexes required PEGylation of glass surfaces, excessive protein blocking (8mg/mL BSA and 0.1 mg/mL κ -casein) and tRNA blocking (0.25 mg/mL total tRNA isolated from *E. coli*). Thus, complex formation and motility from *K10* mRNA or *K10* lacking the TLS zip code is specific to *K10* sequences as tRNA is not sufficient to activate mRNP complex formation and motility. Lastly, we tested is a mutant of BicD (K730M) which has reduced association with Egalitarian. This mutant supports motility with a reduced frequency compared with wild type BicD. As an additional control, we confirmed that motile *K10* mRNA complexes were bound to Egalitarian, by simultaneously tracking labeled *K10* mRNA and Qdot-labeled Egalitarian. Consistent with our data showing that Egalitarian is needed for mRNP motility, *K10* and Egalitarian are shown to co-localize in motile mRNP complexes on microtubules (**Fig. 3-4, B**).

Both the constitutively activated DDB^{CC1} complex and the fully reconstituted mRNP complex show long processive runs and accumulation at the minus-end of microtubules (**Fig. 3-4, C and D**). To accurately determine if there are differences in run speed between dynein-dynactin bound to BicD^{CC1} versus dynein-dynactin bound to full-length BicD, Egalitarian, and *K10* mRNA, we tracked motile complexes with high temporal (0.2 ms) resolution. *K10* mRNP motility is significantly faster compared with the minimal DDB^{CC1} complex (**Fig. 3-4, E**). However, no significant differences in run lengths are evident (P of 0.036, using Kolmogorov–Smirnov test) (**Fig. 3-4, F**).

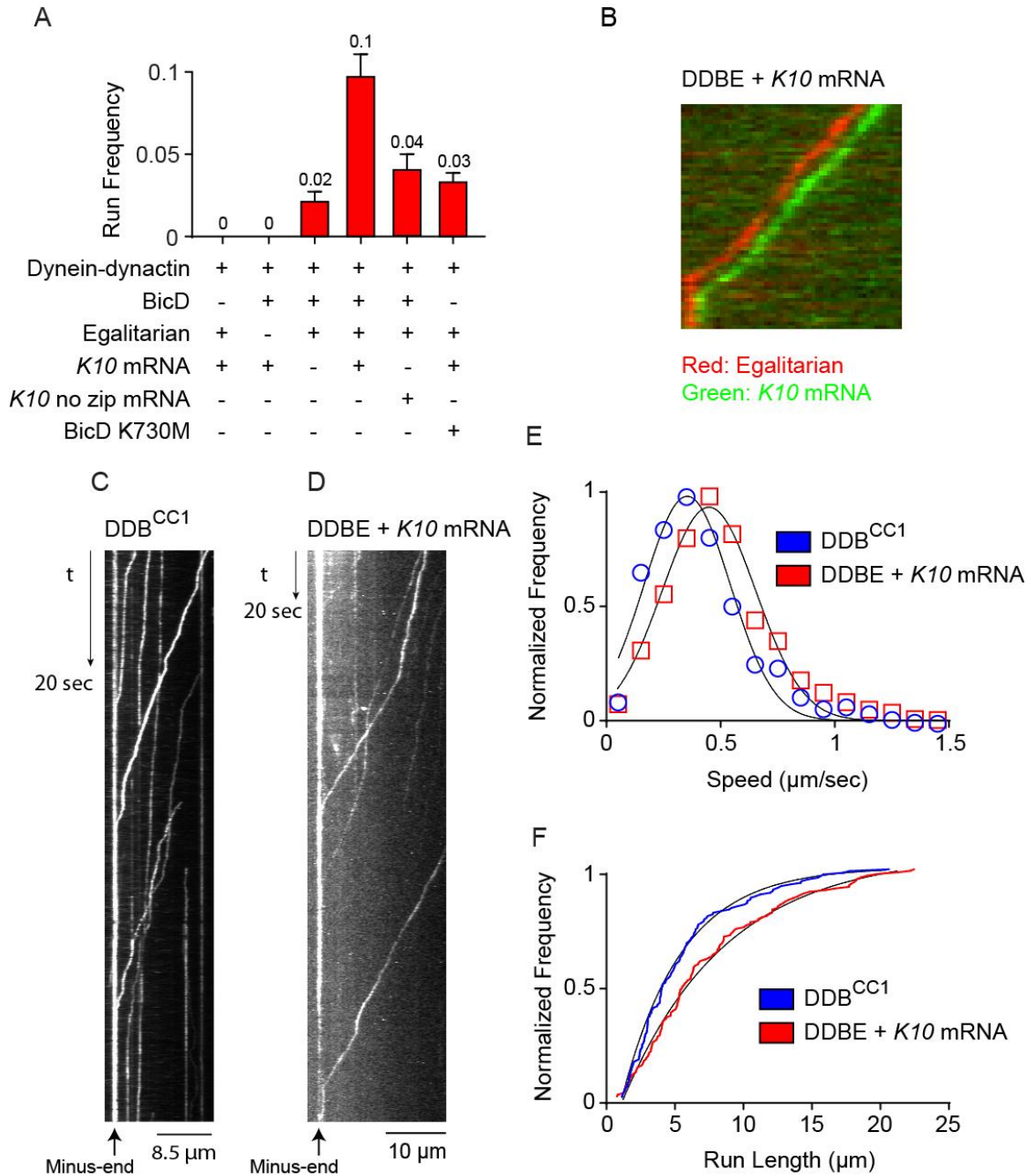


Figure 3-4. Comparison of the motile properties of DDB^{CC1} and *K10* mRNPs.

(A) Representative experiment showing run frequencies (n runs per μm dynein per μm microtubule length per s) of motile mRNPs. (Left to right) Movement of labeled *K10* mRNA is not observed in the absence of either BicD or Egalitarian. A small number of events are observed for mRNPs lacking mRNA, labeled with a Qdot on Egalitarian. Fully reconstituted mRNPs have dramatically enhanced run frequency while mRNPs reconstituted without the TLS zip code show reduced run frequencies. mRNPs

reconstituted with a mutant of BicD (BicDK730M) that has impaired Egalitarian binding shows fewer events than wild type Egalitarian. Error bars, s.e.m.; $n \geq 4$ movies. Data is representative of 3 independent preparation of dynein-dynactin. **(B)** Kymograph showing DDBE + *K10* mRNA dual labeled with Egalitarian bound to a Qdot (red) and *K10* mRNA labeled with Alexa488 dUTP (Green). Color channels are offset for presentation purposes. **(C)** Kymograph (time vs displacement) of a minimal dynein-dynactin-BicD2^{CC1} (DDB^{CC1}) complex. BicD2^{CC1} is bound to a Qdot. The straight vertical line at the left of the kymograph shows that complexes accumulate at the minus-end microtubules. **(D)** Kymograph of motile complexes containing dynein, dynactin, full-length BicD, Egalitarian and *K10* mRNA labeled with Alexa488 dUTP. **(E)** Speed distributions showing that DDBE + *K10* mRNA ($0.45 \pm 0.21 \mu\text{m/sec}$; $n = 1126$) has a significantly faster speed average speed compared to DDB^{CC1} ($0.35 \pm 0.19 \mu\text{m/sec}$; $n = 1147$) with $P < 0.05$ (t-test), from 50 representative run trajectories for each condition. The Y-axis is shown as normalized frequency so that the shape of the two distributions can be compared. **(F)** Cumulative frequency distribution of run lengths for DDB^{CC1} ($4.36 \mu\text{m} \pm 0.31$; $n = 137$) and DDBE + *K10* mRNA ($7.54 \mu\text{m} \pm 0.697$; $n = 142$) at 2 mM MgATP and 22°C. Run lengths are significantly different with P of 0.011 (Kolmogorov–Smirnov test). Run lengths, λ , were determined by fitting the distributions to an exponential function (black line). Error represents an error of the fit.

mRNPs contain multiple copies of Egalitarian and are dynamic

We previously showed that a localizing mRNA in budding yeast, *ASH1* mRNA, activates a class V motor complex by stabilizing a double-headed complex. We wondered if mRNA functions similarly in *Drosophila* to activate BicD by stabilizing an Egalitarian dimer. To test this idea, we separately labeled two pools of Egalitarian containing a biotin tag with either streptavidin conjugated to Alexa Fluor 635 (red), or Alexa Fluor 488 (green), then blocked with excess biotin to prevent re-binding. *K10* mRNPs were then reconstituted with red and green labeled Egalitarian (**Fig. 3-5, A**). Using single molecule pull-downs, we observe a number of complexes that contained both red and green fluorophores co-localized on microtubules (visualized as yellow), indicating that at least two Egalitarian molecules are present in *K10* mRNPs (**Fig. 3-5, B**).

A common theme of localizing mRNA transcripts is the ability to recruit multiple motors for transport. For a subset of motile mRNPs we observe distinctive merging (**Fig. 3-5, C**) and splitting (**Fig. 3-5, D**) events indicating that mRNPs assemble and disassemble. This property provides a mechanism to increase the number of bound motors per mRNA that may enhance transport properties of localizing mRNAs in the cell.

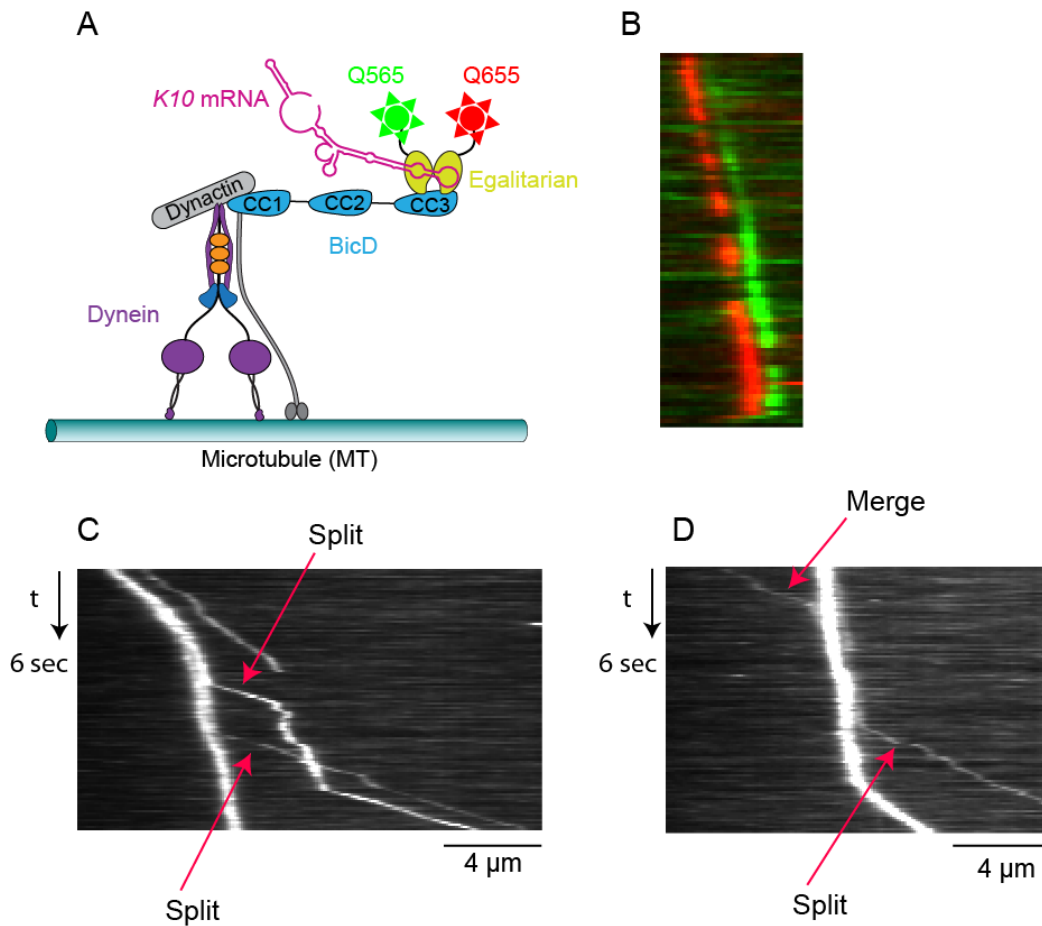


Figure 3-5. Imaging of multiple Egalitarian proteins and dynamics of motile mRNPs. (A) Diagram showing experimental setup for imaging multiple Egalitarian molecules associated with stationary *K10* mRNP complexes in single molecule pull-down assays. (B) Kymograph showing a DDBE + *K10* mRNA dual labeled with two Egalitarian adapters associated with a single motile mRNP, each bound to a 655 Qdot (red) and 565 Qdot (green) respectively. Color channels are offset for presentation purposes. (C-D) Kymograph (time vs displacement) of motile *K10* mRNP showing (C) split and (D) merge-split events.

DISCUSSION

We reconstituted *in vitro* an mRNP composed of dynein-dynactin, BicD, Egalitarian, and *K10* mRNA, a localizing mRNA found in *Drosophila*. Using single molecule techniques, we showed that unlike BicD2^{CC1}, full-length BicD does not bind to dynein-dynactin due to auto-inhibitory N- to C-terminal interactions. Negatively stained images of BicD show that the C-terminal CC2 and CC3 regions form a looped conformation that interacts with the distal end of CC1. This intramolecular interaction may sterically prevent dynein-dynactin from binding the CC1 domain. Preliminary hydrodynamic analysis showed that binding of Egalitarian, but not Rab6^{GTP}, promotes an extended conformation of BicD, likely by competing for interactions that stabilize the folded loop conformation. Despite this apparent conformational change, Egalitarian does not effectively activate BicD for dynein-dynactin recruitment at the nM concentrations used in single molecule assays. Importantly, when *K10* mRNA cargo is added to the reconstitution, dynein-dynactin becomes activated for long processive runs on microtubules, with enhanced speeds compared to a minimal DDB^{CC1} complex. Multiple Egalitarian molecules associate with *K10* mRNP complexes, indicating that mRNA may

activate transport by favoring the recruitment of multiple Egalitarian molecules necessary for BicD activation.

Dynein processivity is coupled to mRNA cargo recruitment via BicD. We show that BicD^{CC1} forms a complex with dynein-dynactin, consistent with previous *in vitro* studies (McKenney et al., 2014; Schlager et al., 2014a). Unlike BicD^{CC1}, full-length BicD is auto-inhibited and does not bind or activate dynein-dynactin. These *in vitro* data are consistent with *in vivo* studies showing that human BicD^{CC1} fused to mitochondria or peroxisome anchoring sequences support robust dynein-driven motility in HeLa cells, while full-length BicD has only a mild effect on organelle relocalization (Hoogenraad et al., 2003).

Yeast-2-hybrid studies indicated that the BicD CC1 domain interacts with the CC3 domain, which led to a model where BicD is auto-inhibited due to N- to C- terminal intramolecular interactions (Hoogenraad et al., 2001). In contrast, metal shadowed images of purified *Drosophila* BicD showed structures with a CC2-CC3 interaction (Stuurman et al., 1999). Using negative stain electron microscopy and class averages, we show that the CC1 of full-length is exposed, while the C-terminal CC2 and CC3 domains form a folded loop conformation that touches back onto CC1. Using immunoprecipitations, we confirmed that BicD CC1 sequences interact with CC3 sequences. Thus, the CC3 interaction likely occurs with C-terminal sequences in the CC1 domain. The site of interaction was obscured in metal-shadowed images because the loop structure was collapsed.

A recent atomic resolution structure of dynactin in complex with BicD and the dynein tail show that 275 amino acids (~35 nm) of BicD is necessary for binding along dynactin (Urnavicius et al., 2015). We show that CC1 sequences are exposed but because full-length BicD fails to recruit dynein-dynactin, the CC1-CC3 interaction may block critical residues needed for BicD to form a complex with dynein-dynactin. We tested whether cargo adapter proteins that bind the CC3 of BicD may promote an extended active conformation. Using Rab6^{GTP} as a model CC3-binding cargo adapter protein, we show by EM and analytical ultracentrifugation that Rab6^{GTP} binding does not show conformational changes consistent with BicD unfolding. In contrast, preliminary hydrodynamic analysis showed that the S value of a co-expressed BicD-Egalitarian complex is smaller than BicD alone, consistent with a more asymmetric conformation of BicD that may result from unfolding of the loop (i.e. activation of BicD). This result is exciting because it suggests that BicD activation is consistent with unfolding mechanism, but this data is still preliminary. Because we cannot obtain a sedimentation coefficient for Egalitarian alone, the slow sedimenting 3S peak may correspond unbound Egalitarian. Future experiments using a YFP-BicD fusion is necessary to confirm that BicD is present in a complex that sediments at 3S by tracking YFP absorbance in sedimentation velocity analysis. The different results obtained for Rab6^{GTP} and Egalitarian was surprising because they share the same binding site on the BicD CC3 domain (Liu et al., 2013). Additional experiments are needed to fully understand if Rab6^{GTP} and Egalitarian have different requirements for BicD activation.

Single molecule assays of reconstituted mRNPs reveal that Egalitarian binding to BicD does not fully activate BicD. One possibility is that the Egalitarian-BicD interaction required stabilization by an mRNA cargo at the nanomolar concentrations used in our single molecule assays. Addition of a *K10* mRNA cargo to dynein-dynactin-BicD-Egalitarian complexes activated dynein-dynactin for long processive runs in single molecule assays. A low frequency of events was observed without *K10* mRNA. Thus, there is likely a small number of activated BicD-Egalitarian complexes, an idea supported by sedimentation velocity analysis implying that in the absence of a localizing mRNA, Egalitarian can unfold BicD.

To test whether a zip code is required for activation we reconstituted mRNPs containing labeled *K10* mRNA, or *K10* lacking the TLS zip code. Single molecule pull downs and motility show that the TLS zip code enhances BicD activation but it not required, implying that Egalitarian may also bind to sequences outside the TLS. This interaction is specific to the *K10* mRNA transcript because tRNA used in single molecule reconstitutions is not capable of activating DDBE complexes. The idea that the TLS zip code is not essential for assembly and activation of *K10* mRNPs is supported by single molecule *in vitro* assays showing that *K10* lacking the TLS zip code is capable of recruiting dynein in cell extracts, but shows defects in dynein recruitment and motility (Amrute-Nayak and Bullock, 2012). We also see defects in dynein recruitment, evidenced by decreases in mRNP run frequency in processivity assays, and reduced complex associations in single molecule pull-downs. Thus, the function of zip codes in *Drosophila* differs from budding yeast mRNA transport, where zip codes in *ASH1* are necessary for

recruitment of motors to the adapter protein She2p for processive movement in single molecule assays at physiological ionic strength (Sladewski et al., 2013).

Previous studies show that multiple Rab6^{GTP} adapters can bind to the CC3 domain of BicD with a stoichiometry of 1 BicD dimer to 2 Rab6^{GTP} monomers by associating with opposite faces of the BicD coiled-coil (Liu et al., 2013). However, binding affinity of this complex is weak ($K_d = 0.9 \mu\text{M}$) and two Rab6^{GTP} monomers are not likely to associate with BicD under conditions used in our single molecule assays. Thus, while two Rab6^{GTP} monomers can bind to a BicD dimer, the complex likely requires additional binding partners for stability. Egalitarian may also bind opposite faces of BicD to promote activation and mRNA may be required to stabilize this interaction at nanomolar concentrations. Using Egalitarian labeled with two different colors, we showed that multiple Egalitarians are associated with mRNPs. We were unable to determine if Egalitarian forms a dimer on its own because Egalitarian expressed by itself aggregates when expressed without BicD, and thus unsuitable for sedimentation velocity analysis. However, it is unlikely that Egalitarian forms a dimer in isolation because it has no clear coiled-coil dimerization motifs (Coils) and contains a large (~200 amino acids) disordered region (Globplot2). Thus, one potential mechanism to explain why *K10* mRNA is needed to activate mRNP motility is that it stabilizes the association of two Egalitarian proteins per BicD dimer.

The speeds of fully reconstituted mRNPs are significantly faster compared to BicD^{CC1} complexes. The human dynein activator, BicDR1 shows a nearly 2-fold enhancement of Rab6 vesicle speed *in vivo* compared to human BicD2 (Schlager et al., 2014b). In addition,

single molecule studies of dynein activators, Hook1 and Hook3 also show at least 2-fold enhanced speeds compared to BicD^{CC1} (Olenick et al., 2016; Schroeder and Vale, 2016). It is possible that the enhancements in speed we see with fully reconstituted mRNPs result from additional interactions between C-terminal sequences of BicD or the Egalitarian-*K10* mRNA complex with dynein-dynactin. Alternatively, mRNPs may recruit multiple motors to generate enhanced speeds. A recent study showed that multiple yeast dynein motors coupled by a flexible DNA origami support faster speeds compared to a single motor (Driller-Colangelo et al., 2016). Furthermore, coupling two mammalian dyneins activates the ensemble for unidirectional motility (Torisawa et al., 2014).

Dynein transitions between an auto-inhibited state, where the heads are stacked and an activated state where the heads are separated. In the absence of coiled-coil activators, the stacked state is favored and in the presence of activators, the unstacked state is favored. Thus, one explanation why DDB^{CC1} complexes have slower speeds compared to other coiled-coil adapters, is that the adapters differentially regulate the equilibrium between these two states and reduced speeds with DDB^{CC1} may result from a diffusional component. One exciting possibility is that different adapters may change extent of dynein activation by preventing the heads from stacking during a run to further enhance run speeds. We provide evidence of recruitment of multiple motors. mRNPs show split and merge events, suggesting that some mRNA particles are able to oligomerize to form complexes with multiple mRNAs and motors.

ACKNOWLEDGMENTS

The authors thank G. Kennedy for technical assistance, D. Warshaw for use of the TIRF microscope, M. Sckolnick, P. Fagnant and S. Lowey for helpful discussions. This work was supported by funds from the US National Institutes of Health (GM078097 to K.M.T.).

REFERENCES

- Allan, V.J. 2011. Cytoplasmic dynein. *Biochem Soc Trans.* 39:1169-1178.
- Amrute-Nayak, M., and S.L. Bullock. 2012. Single-molecule assays reveal that RNA localization signals regulate dynein-dynactin copy number on individual transcript cargoes. *Nat Cell Biol.* 14:416-423.
- Belyy, V., M.A. Schlager, H. Foster, A.E. Reimer, A.P. Carter, and A. Yildiz. 2016. The mammalian dynein-dynactin complex is a strong opponent to kinesin in a tug-of-war competition. *Nat Cell Biol.* 18:1018-1024.
- Bergbrede, T., O. Pylypenko, A. Rak, and K. Alexandrov. 2005. Structure of the extremely slow GTPase Rab6A in the GTP bound form at 1.8Å resolution. *J Struct Biol.* 152:235-238.
- Bingham, J.B., S.J. King, and T.A. Schroer. 1998. Purification of dynactin and dynein from brain tissue. *Methods Enzymol.* 298:171-184.
- Burgess, S.A., M.L. Walker, K. Thirumurugan, J. Trinick, and P.J. Knight. 2004. Use of negative stain and single-particle image processing to explore dynamic properties of flexible macromolecules. *J Struct Biol.* 147:247-258.
- Castoldi, M., and A.V. Popov. 2003. Purification of brain tubulin through two cycles of polymerization-depolymerization in a high-molarity buffer. *Protein Expr Purif.* 32:83-88.
- Cheung, H.K., T.L. Serano, and R.S. Cohen. 1992. Evidence for a highly selective RNA transport system and its role in establishing the dorsoventral axis of the *Drosophila* egg. *Development.* 114:653-661.
- Cronan, J.E., Jr. 1990. Biotination of proteins in vivo. A post-translational modification to label, purify, and study proteins. *J Biol Chem.* 265:10327-10333.

- Dienstbier, M., F. Boehl, X. Li, and S.L. Bullock. 2009. Egalitarian is a selective RNA-binding protein linking mRNA localization signals to the dynein motor. *Genes Dev.* 23:1546-1558.
- Driller-Colangelo, A.R., K.W. Chau, J.M. Morgan, and N.D. Derr. 2016. Cargo rigidity affects the sensitivity of dynein ensembles to individual motor pausing. *Cytoskeleton (Hoboken)*.
- Fuchs, E., B. Short, and F.A. Barr. 2005. Assay and properties of rab6 interaction with dynein-dynactin complexes. *Methods Enzymol.* 403:607-618.
- Gestaut, D.R., B. Graczyk, J. Cooper, P.O. Widlund, A. Zelter, L. Wordeman, C.L. Asbury, and T.N. Davis. 2008. Phosphoregulation and depolymerization-driven movement of the Dam1 complex do not require ring formation. *Nat Cell Biol.* 10:407-414.
- Hoogenraad, C.C., A. Akhmanova, S.A. Howell, B.R. Dortland, C.I. De Zeeuw, R. Willemsen, P. Visser, F. Grosveld, and N. Galjart. 2001. Mammalian Golgi-associated Bicaudal-D2 functions in the dynein-dynactin pathway by interacting with these complexes. *EMBO J.* 20:4041-4054.
- Hoogenraad, C.C., P. Wulf, N. Schiefermeier, T. Stepanova, N. Galjart, J.V. Small, F. Grosveld, C.I. de Zeeuw, and A. Akhmanova. 2003. Bicaudal D induces selective dynein-mediated microtubule minus end-directed transport. *EMBO J.* 22:6004-6015.
- King, S.J., and T.A. Schroer. 2000. Dynactin increases the processivity of the cytoplasmic dynein motor. *Nat Cell Biol.* 2:20-24.
- Krementsova, E.B., A.R. Hodges, C.S. Bookwalter, T.E. Sladewski, M. Travaglia, H.L. Sweeney, and K.M. Trybus. 2011. Two single-headed myosin V motors bound to a tetrameric adapter protein form a processive complex. *J Cell Biol.* 195:631-641.
- Liu, Y., H.K. Salter, A.N. Holding, C.M. Johnson, E. Stephens, P.J. Lukavsky, J. Walshaw, and S.L. Bullock. 2013. Bicaudal-D uses a parallel, homodimeric coiled coil with heterotypic registry to coordinate recruitment of cargos to dynein. *Genes Dev.* 27:1233-1246.
- Mallik, R., B.C. Carter, S.A. Lex, S.J. King, and S.P. Gross. 2004. Cytoplasmic dynein functions as a gear in response to load. *Nature.* 427:649-652.
- McKenney, R.J., W. Huynh, M.E. Tanenbaum, G. Bhabha, and R.D. Vale. 2014. Activation of cytoplasmic dynein motility by dynactin-cargo adapter complexes. *Science.* 345:337-341.

- McKenney, R.J., M. Vershinin, A. Kunwar, R.B. Vallee, and S.P. Gross. 2010. LIS1 and NudE induce a persistent dynein force-producing state. *Cell*. 141:304-314.
- Meijering, E., O. Dzyubachyk, and I. Smal. 2012. Methods for cell and particle tracking. *Methods Enzymol*. 504:183-200.
- Miura, M., A. Matsubara, T. Kobayashi, M. Edamatsu, and Y.Y. Toyoshima. 2010. Nucleotide-dependent behavior of single molecules of cytoplasmic dynein on microtubules in vitro. *FEBS Lett*. 584:2351-2355.
- Olenick, M.A., M. Tokito, M. Boczkowska, R. Dominguez, and E.L. Holzbaur. 2016. Hook Adaptors Induce Unidirectional Processive Motility by Enhancing the Dynein-Dynactin Interaction. *J Biol Chem*. 291:18239-18251.
- Ori-McKenney, K.M., J. Xu, S.P. Gross, and R.B. Vallee. 2010. A cytoplasmic dynein tail mutation impairs motor processivity. *Nat Cell Biol*. 12:1228-1234.
- Philo, J.S. 2000. A method for directly fitting the time derivative of sedimentation velocity data and an alternative algorithm for calculating sedimentation coefficient distribution functions. *Anal Biochem*. 279:151-163.
- Rai, A.K., A. Rai, A.J. Ramaiya, R. Jha, and R. Mallik. 2013. Molecular adaptations allow dynein to generate large collective forces inside cells. *Cell*. 152:172-182.
- Roberts, A.J., T. Kon, P.J. Knight, K. Sutoh, and S.A. Burgess. 2013. Functions and mechanics of dynein motor proteins. *Nat Rev Mol Cell Biol*. 14:713-726.
- Ross, J.L., K. Wallace, H. Shuman, Y.E. Goldman, and E.L. Holzbaur. 2006. Processive bidirectional motion of dynein-dynactin complexes in vitro. *Nat Cell Biol*. 8:562-570.
- Sage, D., F.R. Neumann, F. Hediger, S.M. Gasser, and M. Unser. 2005. Automatic tracking of individual fluorescence particles: application to the study of chromosome dynamics. *IEEE Trans Image Process*. 14:1372-1383.
- Schlager, M.A., H.T. Hoang, L. Urnavicius, S.L. Bullock, and A.P. Carter. 2014a. In vitro reconstitution of a highly processive recombinant human dynein complex. *EMBO J*. 33:1855-1868.
- Schlager, M.A., A. Serra-Marques, I. Grigoriev, L.F. Gumy, M. Esteves da Silva, P.S. Wulf, A. Akhmanova, and C.C. Hoogenraad. 2014b. Bicaudal d family adaptor proteins control the velocity of Dynein-based movements. *Cell Rep*. 8:1248-1256.
- Schroeder, C.M., and R.D. Vale. 2016. Assembly and activation of dynein-dynactin by the cargo adaptor protein Hook3. *J Cell Biol*. 214:309-318.

- Serano, T.L., and R.S. Cohen. 1995. A small predicted stem-loop structure mediates oocyte localization of *Drosophila* K10 mRNA. *Development*. 121:3809-3818.
- Sladewski, T.E., C.S. Bookwalter, M.S. Hong, and K.M. Trybus. 2013. Single-molecule reconstitution of mRNA transport by a class V myosin. *Nat Struct Mol Biol*. 20:952-957.
- Stuurman, N., M. Haner, B. Sasse, W. Hubner, B. Suter, and U. Aebi. 1999. Interactions between coiled-coil proteins: *Drosophila* lamin Dm0 binds to the bicaudal-D protein. *Eur J Cell Biol*. 78:278-287.
- Torisawa, T., M. Ichikawa, A. Furuta, K. Saito, K. Oiwa, H. Kojima, Y.Y. Toyoshima, and K. Furuta. 2014. Autoinhibition and cooperative activation mechanisms of cytoplasmic dynein. *Nat Cell Biol*.
- Trocter, M., N. Mucke, and T. Surrey. 2012. Reconstitution of the human cytoplasmic dynein complex. *Proc Natl Acad Sci U S A*. 109:20895-20900.
- Urnavicius, L., K. Zhang, A.G. Diamant, C. Motz, M.A. Schlager, M. Yu, N.A. Patel, C.V. Robinson, and A.P. Carter. 2015. The structure of the dynactin complex and its interaction with dynein. *Science*. 347:1441-1446.
- Wang, Z., S. Khan, and M.P. Sheetz. 1995. Single cytoplasmic dynein molecule movements: characterization and comparison with kinesin. *Biophys J*. 69:2011-2023.

CHAPTER 4: DISCUSSION

Mechanisms of mRNA transport in budding yeast

Myo4p is unlike other class V myosin motors because it forms a single-headed complex with the adapter protein She3p. Thus, Myo4p is non-processive because it cannot take coordinated steps on actin. We show that at low ionic strength, the tetrameric mRNA-binding protein She2p recruits two Myo4p-She3p complexes forming a double-headed motor complex that steps processively on actin filaments *in vitro* (Krementsova et al., 2011). However, this complex is not stable at ionic strength conditions that approximate physiological. Thus, we hypothesized that mRNA cargo is required for stabilizing the double-headed complex, ensuring that only cargo bound motors move processively in the cell. To test this hypothesis, we reconstituted a messenger ribonucleoprotein (mRNP) by adding *ASH1* mRNA, a localizing mRNA in budding yeast, to the Myo4p motor complex. At physiological ionic strength (140 mM KCl), we show that *ASH1* mRNA is required to stabilize the double-headed complex, which moves processively on actin (Sladewski et al., 2013) (**Fig. 4-1, A**). Under the same conditions, the Myo4p-She3p-She2p complex (no mRNA) tracked by a YFP tag on She2p fails to assemble and is non-motile (Sladewski et al., 2013). Thus, mRNA triggers the assembly of a processive complex by enhancing the stability of the Myo4p-She3p-She2p complex.

Mechanisms of mRNA transport in Drosophila

Next we wished to determine if the principles of mRNA transport in budding yeast are conserved in higher eukaryotes. Unlike budding yeast dynein, *in vitro* studies of

mammalian dynein show that it is weakly processive (King and Schroer, 2000; McKenney et al., 2014; Miura et al., 2010; Ross et al., 2006; Schlager et al., 2014; Trokter et al., 2012; Wang et al., 1995). Dynein can be activated for transport by coupling at least two motors together on artificial cargoes (Torisawa et al., 2014). Alternatively, recent studies indicate that dynein binding to dynactin and an N-terminal fragment of BicD (BicD2^{CC1}) activates single molecules of dynein for long processive runs on microtubules (McKenney et al., 2014; Schlager et al., 2014). Using single molecule techniques, we confirm that dynein, dynactin and BicD2^{CC1} forms a processive complex (**Chapter 3**). However, we show that full-length BicD does not activate dynein-dynactin motility because it is auto-inhibited due to N- to C-terminal interactions that prevent dynein and dynactin from binding BicD. Full-length BicD contains a C-terminal coiled-coil cargo binding region (CC3) that links cargo to dynein through its interaction with adapter proteins. One adapter, Egalitarian, is a mRNA binding protein that links dynein to localizing mRNAs in *Drosophila*. Thus, we hypothesized that dynein activation by full-length BicD requires cargo binding that is mediated by the binding of adapter proteins to the CC3 of BicD. To test this hypothesis, we reconstituted a messenger ribonucleotide protein (mRNP) complex from purified dynein, dynactin, BicD, Egalitarian and *K10* mRNA, a localizing mRNA found in *Drosophila*. We show that Egalitarian binding alone does not fully activate BicD. Only in the presence of localizing mRNA do we observe full activation of BicD for dynein recruitment and activation of processivity *in vitro* (**Fig. 4-1, B**). Interestingly, speeds of mRNA-dynein complexes are faster than those observed for dynein activation by a truncated N-terminal BicD construct, implying that dynein activity is enhanced when bound to native full-length adapters and cargo.

Taken together, our work on yeast and *Drosophila* mRNA transport show that mRNA cargo activation of molecular motors is a conserved mechanism that ensures only cargo bound motors are activated for transport.

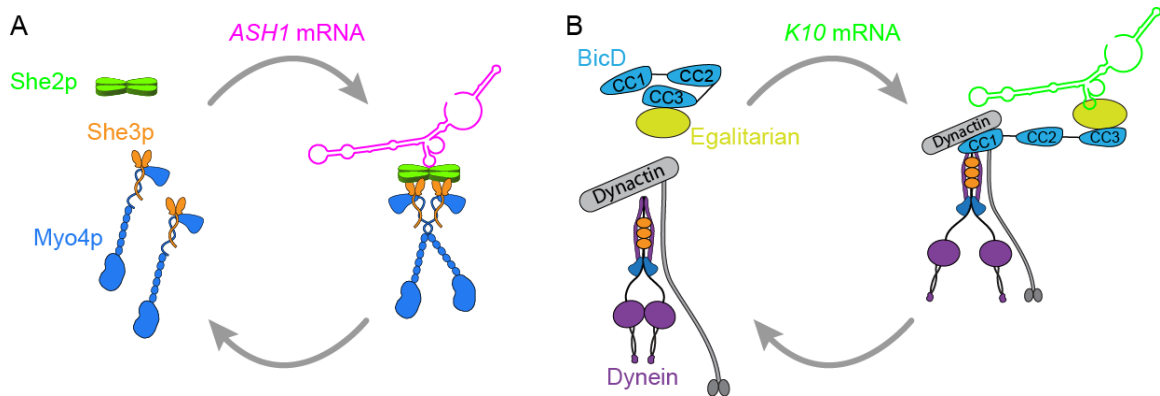


Figure 4-1. Mechanisms for mRNA transport in budding yeast and *Drosophila*. (A) Diagram showing She2p- and mRNA-dependent dimerization of Myo4p–She3p for activation of mRNA transport in budding yeast. (B) Diagram showing mRNA-dependent activation of a BicD–Egalitarian complex and recruitment of dynein/dynactin for activation of mRNA transport in *Drosophila*.

Comparison of yeast and Drosophila mRNA transport mechanisms

We now have a unique opportunity to compare the mechanisms of mRNA transport in two distinct systems. In budding yeast, mRNA is transported on actin cables by a class V myosin. In *Drosophila*, mRNA is transported on microtubules by cytoplasmic dynein. Despite using an entirely different set of molecular motors and tracks, they share a number of conserved mechanisms. (1) The motors are auto-inhibited in the absence of cargo. (2) Motor activation requires two adapter proteins, to ensure that activity is coupled to cargo selection, and (3) Recruitment of multiple motor/adapter complexes to the mRNA promotes their motility *in vitro* and *in vivo*. While these themes are conserved, the details

of motor activation differ. Here, I will compare these differences to gain insight into the mechanisms of mRNA transport. These themes will likely apply more broadly to other cargo systems.

Molecular motors involved in cargo transport are auto-inhibited

Both Myo4p and dynein are non-processive and require activation by cargo and adapter proteins. Similar mechanisms have been proposed for other cargo transporters, including mammalian class V myosins and members of the kinesin family of motor proteins. We show that budding yeast Myo4p is single-headed and inactive, but dimerization mediated by the mRNA binding adapter protein She2p activates the motor for processive motion. This is an unusual mechanism to regulate processivity among class V myosin motors. The most well studied class V myosin, mammalian myosin Va (MyoVa) is auto-inhibited by a head-tail interaction that is disrupted by cargo binding. In the absence of cargo, MyoVa forms a stable dimer that folds into an auto-inhibited 14S conformation that has reduced actin-activated ATPase activity (Krementsov et al., 2004; Li et al., 2004; Wang et al., 2004). This folded conformation is stabilized through an interaction between basic residues in the globular tail and acidic residues in the motor domain near the MgATP binding pocket. It is interesting to note that yeast Myo4p lacks these conserved residues because it does not use a folding mechanism for regulation (Hodges et al., 2008). The MyoVa head-to-tail interaction can be destabilized at high ionic strength concentrations (300 mM NaCl) resulting in an extended ~11S conformation with restored ATPase activity (Liu et al., 2006). The extent of activation at high ionic strength is similar to a constitutively activated construct lacking the regulatory globular tail domain (HMM) that moves

processively on actin *in vitro* (Mehta et al., 1999). One popular hypothesis is that cargo binding to MyoVa activates the motor by promoting its extended conformation. In support of this hypothesis, addition of the cargo adapter protein melanophilin to MyoVa activates the motor for long processive runs and supports stepping on actin consistent with an unfolding mechanism (Sckolnick et al., 2013).

Kinesin-1 is a plus-end directed microtubule-based motor composed of dimers of two ~120 kDa heavy chains that each associate with ~70 kDa light chains (Bloom et al., 1988; Kuznetsov et al., 1988). Just like MyoVa, full-length kinesin adopts a folded conformation stabilized by head-to-tail interactions that is associated with reduced ATPase activity (Hackney et al., 1992). This interaction is destabilized at high ionic strength conditions that promote an extended active conformation of kinesin (Hackney et al., 1992). Folding of kinesin requires a flexible hinge 2 region and deleting this hinge results in activation of both ATPase activity and processivity (Friedman and Vale, 1999). The activity of this construct is equivalent to a bacterially expressed truncation construct of kinesin lacking the regulatory globular tail domain (Vale et al., 1996). Thus, similar mechanisms of cargo activation have been proposed for kinesin and myosin whereby adapter proteins promote their active extended conformation, which ensures motor activity is coupled to cargo recruitment.

An additional level of regulation of molecular motors is via the track. Myo2p is a class V myosin in budding yeast that was shown to be non-processive on bare skeletal muscle actin *in vitro* (Reck-Peterson et al., 2001). More recently, it was shown that Myo2p is processive on actin tracks that are bound with yeast tropomyosin (Hodges et al., 2012).

This selection mechanism ensures that activated motors are targeted to the appropriate tracks in the cell. Mammalian MyoVc is another class V myosin that was characterized as non-processive on single actin filaments *in vitro* (Gunther et al., 2014; Takagi et al., 2008; Watanabe et al., 2008). We explored whether MyoVc is processive under more physiological conditions. Recently it was shown that secretory zymogen granules are transported on parallel actin bundles nucleated from the cell periphery (Geron et al., 2013) and MyoVc has been implicated in this transport (Jacobs et al., 2009). Using single molecule techniques, we showed that MyoVc is non-processive on bare actin filaments but moves processively on actin bundles, which mimic the actin cables found in secretory cells (Sladewski et al., 2016). Thus, in addition to auto-regulatory mechanisms, the actin track restricts the activity of motors within the cell by regulating their ability to move processively.

This mechanism is not limited to actin-based motors. Post translational modifications of the carboxy-terminal tails (CTT) of tubulin (known as the ‘tubulin code’) affects the processive properties of kinesin and dynein. For example, kinesin-1 run length is enhanced by polyglutamylation of alpha-tubulin tails, and kinesin-2 motility requires detyrosination of alpha-tubulin tails (Sirajuddin et al., 2014). Similarly, motility of activated dynein complexes is dramatically decreased on de-tyrosinated microtubules by decreasing the affinity of the p150 subunit of dynactin to microtubules (McKenney et al., 2016).

The auto-regulatory mechanisms of cytoplasmic dynein appear far more complex compared to class V myosins and kinesin. Despite recent single molecule and structural

studies of dynein/dynactin in complex with coiled-coil activators, we still have an incomplete understanding of how dynein auto-inhibition is relieved. The auto-inhibited state of dynein appears to be associated with a stacked-head conformation that is generally non-processive and produces little force (Belyy et al., 2016; Mallik et al., 2004; Ross et al., 2006; Torisawa et al., 2014; Trokter et al., 2012). Recently it was shown that dynein and dynactin can be activated for long processive runs *in vitro*, by binding an N-terminal fragment of BicD (BicD2^{CC1}). BicD2^{CC1} is able to activate dynein processivity because it creates a functional interface between dynein and dynactin that likely disrupts head-head stacking. Evidence suggests that dynein activation by BicD also requires undocking of p150 from the Arp filament of dynactin (Tripathy et al., 2014; Urnavicius et al., 2015). In addition, it has been shown that coupling as few as two dynein motors on artificial scaffolds is sufficient for activation (Torisawa et al., 2014).

Thus, a general feature of cargo transporters is that they are auto-inhibited. However, activation mechanisms differ greatly even within families of motors (e.g. Myo4p versus MyoVa), and cargo adapters are likely to use different mechanisms to ensure that motor activation is coupled to cargo selection.

Two adapters couple motor activation with cargo selection

Budding yeast Myo4p is only stable when co-expressed with She3p (Hodges et al., 2008; Kremtsova et al., 2011). The requirement of both Myo4p and She3p to form a homogeneous high-affinity complex suggests that She3p functions as an essential subunit of Myo4p and provides the motor with additional binding sites for other cargo adapters. She2p is an mRNA binding adapter protein that links localizing mRNAs to Myo4p by

interacting with She3p (Krementsova et al., 2011; Muller et al., 2009). She2p ultimately couples cargo selection with motor activation by recruiting two Myo4p-She3p complexes, and this interaction is mRNA-dependent.

An interesting finding from these studies is that the double-headed Myo4p motor complex shows regular hand-over-hand stepping on actin, which suggests that the heads are coordinated. How is this possible, when the motor is dimerized distally by adapter proteins? Myo4p contains four heptads of coiled-coil propensity at the base of the rod. One hypothesis is that this region dimerizes when two heavy chains are recruited by She2p. Similar mechanisms of cargo-mediated dimerization have been previously proposed for vertebrate myosin VI (Phichith et al., 2009). Myosin VI also exists as a monomer in isolation and its dimerization has been proposed to occur by recruitment of two motors to the dimeric adapter protein optineurin, forming a double-headed complex (Phichith et al., 2009). Myosin VI contains a proximal dimerization domain that is predicted to form a coiled-coil only when two heavy chains are brought into close proximity (Park et al., 2006). Thus, it is possible that this coiled-coil may be necessary to stabilize a double-headed complex and provides a mechanism that ensures the heads are coordinated. Alternatively, dimerization at the C-terminus of Myo4p may be sufficient to cause the development of intramolecular strain causing a resistive load on the lead head and assistive load on the trailing head that coordinate the ATPase cycles of the two heads as shown for MyoVa (Kad et al., 2008; Veigel et al., 2005).

The short coiled-coil in Myo4p may operate similarly to ensure that the motor steps in a coordinated fashion on actin. The importance of the Myo4p coiled-coil region in

promoting motor coordination can be addressed by mutating key residues needed for stabilizing the coiled-coil and comparing its single molecule stepping to wild type. Ultimately, an atomic structure of the entire complex would address how the complex is stabilized and optimized for mRNA transport.

Dynein is linked to mRNA cargo in *Drosophila* through the adapters BicD and Egalitarian. BicD interacts with the motor directly and an N-terminal fragment containing CC1 and part of CC2 is sufficient for dynein activation. However, full-length BicD is auto-inhibited and cannot interact with dynein without activation. Previous studies suggest that this auto-inhibition is due to an intramolecular interaction between the CC1 and CC3 domains (Hoogenraad et al., 2001). However, metal shadowed images of *Drosophila* BicD suggest a CC2 to CC3 interaction (Stuurman et al., 1999). Our negatively stained images of YFP-BicD (**Chapter 3**) may be consistent with both studies because they show that the N-terminus of the CC1 domain is exposed and a loop is formed due to an interaction that likely occurs between CC3 and C-terminal regions in CC1. Egalitarian binds the CC3 domain of BicD. Thus, one hypothesis is that Egalitarian binding relieves BicD auto-inhibition and allows it to recruit and activate dynein for processivity. Thus, in *Drosophila*, Egalitarian couples cargo selection to dynein activation. But it does so by different mechanisms compared to She2p. Rather than dimerizing the motor, Egalitarian is responsible for activating BicD for dynein recruitment and can only do so when bound to a localizing mRNA cargo.

There are a number of other examples where two adapters are needed to link motors to their cargo. Rab27A and melanophilin are two cargo adapters that link MyoVa to

melanosomes (Wu et al., 2002). Recent work has shown that melanophilin binding to full-length MyoVa through the alternately spliced exon F and the globular tail activates the motor for processive runs (Sckolnick et al., 2013). One interesting question is how cargo influences the properties of this complex. Our data show that cargo recruitment is linked to activation. Thus, it would be interesting to see how Rab27A bound to a vesicular cargo influences the properties of a MyoVa/melanophilin complex.

Kinesin-1 uses a similar folding mechanism for its auto-inhibition and studies show that transition from a folded to an extended conformation requires binding of two adapter proteins. c-Jun N-terminal kinase-interacting protein 1 (JIP1) functions as a scaffolding protein that links kinesin-1 to vesicular cargoes by binding the kinesin light chain (Verhey and Rapoport, 2001). The kinesin-1 heavy chain binds to the fasciculation and elongation protein ζ (FEZ). Studies show that both proteins cooperate to activate kinesin-1 for processive motility *in vivo* and *in vitro* (Verhey and Rapoport, 2001). These examples show that the use of two adapter proteins to link motors to cargo and activate them for transport is a conserved theme that ensures that motor activity is linked to cargo recruitment.

Models of BicD activation by cargo binding adapters

We propose two alternative models for how Egalitarian and an mRNA cargo activate BicD for dynein/dynactin recruitment: one by unfolding a bent/looped conformation of BicD and the other by a shift in heptad registry of BicD (**Fig. 4-2, A and B**). An unfolding mechanism is based on our data showing that negatively stained EM images of YFP-BicD form an N- to C-terminal interaction (**Chapter 3**). Using single molecule pull-downs, we show that full-length BicD cannot activate dynein/dynactin like

the N-terminal BicD truncation because it fails to interact (**Chapter 3**). Thus, it is possible that the BicD intramolecular interaction sterically prevents dynein and dynactin from forming a tripartite complex with full-length BicD. One possible mechanism for BicD activation is that Egalitarian/mRNA binding displaces this auto-inhibitory interaction to allow dynein/dynactin recruitment and activation of the motor (**Fig. 4-2, A**). Negatively stained EM images of YFP-BicD show that the N-terminus is exposed (**Chapter 3**) but it is not clear what length of BicD is sufficient to form a functional interface with dynein and dynactin. An atomic resolution structure of dynactin in complex with BicD and the dynein tail shows that 275 amino acids (~35 nm) of BicD is necessary for binding along dynactin (Urnavicius et al., 2015). It is difficult to determine from our images the location of the BicD CC1-CC3 interaction but it could potentially block critical regions needed for DDB^{CC1} complex formation. We used sedimentation velocity to determine if BicD can adopt an extended conformation under certain condition. We find that YFP-BicD sediments with an S-value of ~6S at 150 mM KCl. We tested if increasing ionic strength unfolds BicD similar to myosin Va (Krementsov et al., 2004). At 300 mM KCl, we observed no change in S value consistent with a compact folded structure at high ionic strength (**Chapter 3**). This is also consistent with our results showing that the majority of negatively stained EM images of YFP-BicD form an intramolecular loop at 500 mM KOAc (**Chapter 3**). Taken together, these data show that BicD does not unfold into an extended conformation at high ionic strength conditions, implying that electrostatic interactions do not stabilize the bent form. EM also shows that BicD is retained in a compact conformation when bound to Egalitarian (**Chapter 3**). Assuming an unfolding model for activation, these data are consistent with our single molecule assays showing that

Egalitarian binding to BicD is not sufficient for activation in the absence of an mRNA cargo. One possibility is that BicD is only activated when Egalitarian is also bound to a localizing mRNA.

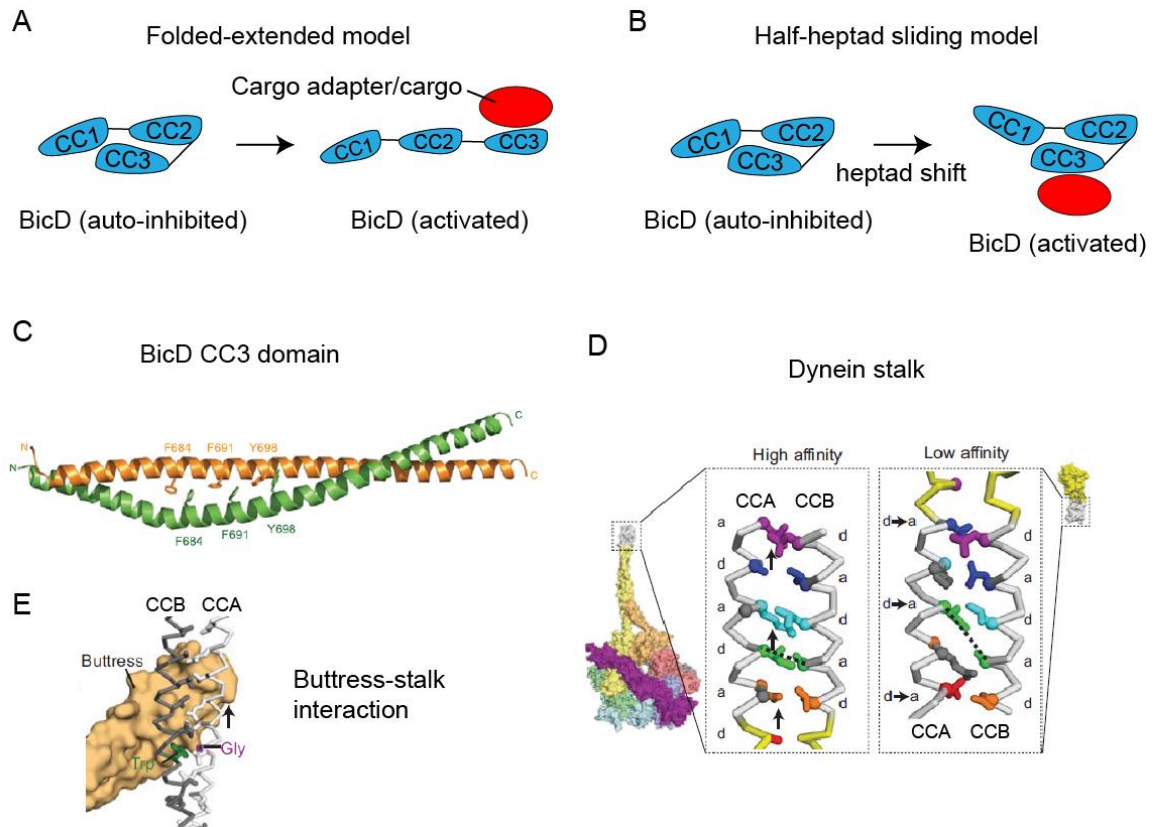


Figure 4-2. Models of BicD activation. (A) Illustration showing that BicD activation for dynein/dynactin recruitment may result because of a transition from a folded, auto-inhibited state to active extended state upon cargo adapter/cargo binding. (B) Alternatively, BicD may be activated through mechanisms involving a shift in the heptad registry. (C) Crystal structure of the cargo binding CC3 domain of BicD (amino acids 656-745) with aromatic side chains that disrupt homotypic coiled-coil packing labeled (Liu et al., 2013). (D) Illustration of the dynein coiled-coil stack showing that it exists in two states: a high microtubule-binding affinity state and a low affinity state where one alpha helix in the coiled-coil (CCA) slides relative to the other (CCB) by half of a heptad repeat. (E) Illustration showing that the dynein buttress domain (tan) acts on the base of the stalk near a conserved tryptophan and glycine residue which destabilizes homotypic packing in the low microtubule-binding affinity state (Carter, 2013). Image C was reused with permission from Genes and Development (Liu et al., 2013). Images D-E were adapted with permission from the Journal of Cell Science (Carter, 2013) DOI 10.1242/jcs.120725.

A second model is that small conformational changes in BicD may control dynein/dynactin recruitment (**Fig. 4-2, B**). This idea comes from structural data of the cargo-binding CC3 domain of BicD, which forms a coiled-coil with a heterotypic registry (Liu et al., 2013) (**Fig. 4-2, C**). Coiled-coils are composed of two alpha-helices that wrap around each other. They are normally stabilized by a heptad repeat, described as patterns of seven amino acids (abcdef) where the 'a' and 'd' position are hydrophobic and pack together to form a hydrophobic core. The CC3 domain of BicD does not assume this packing because large aromatic residues are present where the alpha helices pack together push the coiled-coil out of registry by half of a heptad (four residues) (Liu et al., 2013) (**Fig. 4-2, C**). In contrast, the crystal structure of the human BicD1 CC3 domain reveals a homotypic registry (Terawaki et al., 2015). One possibility for the observed difference is that the *Drosophila* structure may represent the auto-inhibited conformation while the human structure may have captured the activated conformation of BicD.

Coincidentally, a heterotypic registry has also been observed for the dynein stalk and is important for transmitting signals from the motor domain to the microtubule-binding domain (Carter, 2013) (**Fig. 4-2, D**). MgATP binding to AAA1 in the dynein motor domain causes a structural conformation that is communicated through the stalk to decrease the affinity of the microtubule binding domain (Imamula et al., 2007). The current model for this communication is that one alpha helix in the coiled-coil stalk slides against the other by half of a heptad (Carter and Vale, 2010; Gibbons et al., 2005) (**Fig. 4-2, D**). This sliding results in structural changes in the microtubule-binding domain that alters its affinity for microtubules (Redwine et al., 2012). Structural changes in the motor domain are

transmitted to the stalk by the buttress which interacts with two highly conserved residues at the base of the stalk, a tryptophan and a glycine (**Fig. 4-2, E**). The buttress is thought to induce sliding of the alpha helix by pushing the bulky tryptophan residue into the core of the coiled-coil, melting alpha helix A (CCA) at the glycine residue and causing CCA to migrate toward the microtubule-binding domain (Carter, 2013) (**Fig. 4-2, D and E**).

A similar type of communication could occur with BicD. For instance, Egalitarian and/or cargo binding to the CC3 could signal the presence of cargo through a ‘half heptad sliding’ mechanism. Thus, the resulting changes in the heptad registry could induce structural changes in the N-terminus of BicD to recruit dynein/dynactin for transport (**Fig. 4-2, B**). In support of this model, classic dominant BicD mutations that are characteristic of enhanced dynein recruitment and minus-end directed mRNA transport in the cell destroy this heterotypic packing (Liu et al., 2013).

Future work is needed to distinguish between these models. In principle, unfolding of BicD can be easily observed using analytical ultracentrifugation or EM, because this transition is associated with a large conformational change. However, we find that BicD does not unfold at high ionic strength and it is still unclear if unfolding is accompanied by Egalitarian binding (**Chapter 3**). mRNA cargo may be required for unfolding. However, these changes are difficult to detect in the presence of cargo due to the complexity of the sample. Constructs of BicD and adapter proteins that are constitutively activated for dynein recruitment in the absence of cargo may have to be created for these types of analyses.

One way to address whether BicD uses a heptad-shift mechanism for activation is to use a disulfide cross-linking approach. This method was previously used to show how

the dynein stalk communicates structural information from the motor domain to the microtubule binding domain. Kon *et al*, engineered cysteines into the dynein stalk to lock the coiled-coil into different heptad registries and showed that microtubule binding affinity is associated with the different registries (Kon et al., 2009). The structure of the BicD CC3 domain is known (Liu et al., 2013) so it is feasible to similarly engineer cysteines into the coiled-coil and oxidize them to potentially trap BicD into different heptad registries. Then a single molecule pull-down approach (described in **Chapter 3**) can be used to determine if dynein/dynactin is recruited depending on the heptad registry of BicD.

The requirement of mRNA cargo for activation of motor processivity

BicD and Egalitarian form a tight complex in the absence of mRNA. This contrasts with the yeast system where binding of She3p to She2p requires mRNA at physiological ionic strength conditions (Sladewski et al., 2013). Thus, mRNA is required in both systems for activation but their mechanisms differ. In yeast, mRNA is needed to stabilize a double-headed complex but in *Drosophila*, mRNA is needed to fully activate BicD for dynein/dynactin recruitment and activation. It is not clear why mRNA is needed for activation of the dynein complex. One idea is that mRNA induces an allosteric change in Egalitarian that promotes a functional interaction with BicD. An alternative explanation is that mRNA is needed to dimerize Egalitarian or recruit two Egalitarian molecules for BicD activation. This idea comes from our data showing that multiple Egalitarian molecules are associated with *K10* mRNPs (**Chapter 3**). This result is consistent with previous studies showing that multiple Rab6^{GTP} adapters can bind to the CC3 domain of BicD with a stoichiometry of 1 BicD dimer to 2 Rab6^{GTP} monomers by associating with opposite faces

of the BicD coiled-coil (Liu et al., 2013). However, the binding affinity of this complex is weak ($K_d = 0.9 \mu\text{M}$) and two Rab6^{GTP} monomers are not likely to associate with BicD under conditions used in our single molecule assays. Thus, while two Rab6^{GTP} monomers can bind to a BicD dimer, the complex likely requires additional binding partners for stability.

Egalitarian and Rab6^{GTP} bind similar residues in BicD because a single point mutation in the cargo binding CC3 domain (K730M) disrupts binding of both (Dienstbier et al., 2009; Liu et al., 2013). The implication is that two Egalitarian monomers have the potential to bind BicD, but the complex likely requires stabilization by mRNA cargo. Thus, we propose that mRNA is required for activation of BicD by stabilizing a dimer of Egalitarian that is needed to interact functionally with the CC3 domain of BicD by binding opposite faces of the coiled-coil. We favor this model because it is more or less consistent with the function of mRNA in budding yeast. *ASH1* mRNA stabilizes a dimer of Myo4p-She3p complexes and *K10* mRNA functions to stabilize a dimer of Egalitarian.

Implications for other cargo systems

We showed that Rab6^{GTP} binds full-length BicD but does not activate it for recruitment of dynein and dynactin for processive movement on microtubules in *in vitro* motility assays (**Appendix II**). We propose that a vesicular cargo is required for this activation and may function similarly to mRNA and Egalitarian by stabilizing a functional Rab6^{GTP} dimer so that it can associate with BicD for activation of vesicular transport by recruiting and activating dynein/dynactin. Rab proteins are generally monomers. However, Rabs have been shown to dimerize under conditions used for crystallography (Pasqualato

et al., 2004). When multiple Rab proteins are inserted into a lipid membrane it increases their local concentration which may facilitate oligomerization. Thus, the requirement for a vesicular cargo for recruiting and clustering multiple adapters would ensure that only cargo bound Rab is capable of activating BicD for dynein/dynactin recruitment and transport.

Fragile X mental retardation protein (FMRP) is an mRNA cargo adapter that also interacts with the CC3 of BicD (Bianco et al., 2010). Similar to Rab6, we find that FMRP does not activate BicD for dynein recruitment and activation. Surprisingly, we find that FMRP undergoes a phase transition to form protein droplets *in vitro* (**Appendix II**) as found for other mRNA binding proteins (Zhang et al., 2015). At physiological ionic strength we find that phase transitions require the presence of a localizing mRNA. Thus, one idea is that FMRP oligomerization into microdomains may allow it to functionally interact with BicD and activate it for dynein recruitment and transport. Future studies are needed to understand how these adapters activate BicD by studying them in the presence of a cargo.

We can directly test whether the dimerization of adapters is sufficient for BicD activation by expressing either Egalitarian or Rab6^{GTP} with a C-terminal biotin tag. Addition of streptavidin at half the molar ratio should recruit multiple adapter proteins, effectively forcing them to dimerize. Alternatively, either Egalitarian or Rab6^{GTP} can be expressed with a C-terminal leucine zipper. Forced dimers can be added to BicD and tested for dynein/dynactin recruitment in single molecule pull-down assays (described in **Chapter 3**). If dimerization of cargo adapters is sufficient to activate BicD, then this would

serve as a useful construct to test whether BicD uses an unfolding mechanism for activation by either visualizing at the complex by EM or sedimentation velocity analysis.

Mechanisms for speed enhancements with multiple dynein motors

One interesting result from our studies of mRNA transport *in vitro* is that the speed of fully reconstituted mRNPs containing dynein, dynactin, BicD, Egalitarian and a localizing mRNA is significantly faster compared to minimal activated complexes containing only dynein, dynactin and an N-terminal truncation of BicD (BicD2^{CC1}) (**Chapter 3**). Reported average DDB^{CC1} speeds range between 350-600 nm/sec with broad distributions (Belyy et al., 2016; McKenney et al., 2014; Olenick et al., 2016; Schlager et al., 2014). Interestingly, dynein/dynactin interact with a number of other BicD-like cargo adapters. Similar to BicD, Rab11-FIP3, Spindly and Hook proteins activate dynein and dynactin for processivity (McKenney et al., 2014; Olenick et al., 2016). Rab11-FIP3 links dynein to recycling endosomes (Horgan and McCaffrey, 2012), spindly to kinetochores (Griffis et al., 2007) and Hook3 to early endosomes (Bielska et al., 2014; Zhang et al., 2014). Single molecule studies of Hook1 and Hook3 complexes with dynein and dynactin show that they support at least 2-fold enhanced speeds compared to BicD2^{CC1} (Olenick et al., 2016; Schroeder and Vale, 2016). These data suggest that dynein/dynactin is only partially activated by BicD2^{CC1}. Dynein transitions between an auto-inhibited state, where the heads are stacked and an activated state where in the heads are separated. In the absence of coiled-coil activators, the stacked state is favored and in the presence of activators, the unstacked state is favored. Thus, one explanation why DDB^{CC1} complexes have slower speeds compared to other coiled-coil adapters, is that the adapters differentially regulate

the equilibrium between these two states and reduced speeds with DDB^{CC1} may result from a diffusional component. Depending on the dynein-bound coiled-coil activator, differences in dynein speeds may serve a biological purpose. The kinesin superfamily has been shown to support a large range of speeds (Steinberg and Schliwa, 1996). It is not clear why kinesins and dynein associated with different coiled-coil adapters have different speeds, but it is tempting to speculate that motor speed may be optimized for their biological roles.

Our results showing enhancements in speed with the fully reconstituted mRNP suggests that additional factors present in our fully reconstituted complexes promote dynein activation possibly by shifting the equilibrium to the activated conformation. One possibility is that additional interactions between full-length adapters and the motor promote activation. In support of multiple interactions that favor dynactin activation, Hook proteins have an N-terminal extension that interacts with the dynein light intermediate chain and is shown to be necessary for dynein activation (Olenick et al., 2016; Schroeder and Vale, 2016). Full-length BicD has been shown to interact directly with the C-terminus of the dynein light intermediate chain (Schroeder et al., 2014). Future studies that clearly define the domains in BicD necessary for this interaction will be informative to determine if this interaction is necessary for dynein/dynactin activation.

An interesting finding is that adapter proteins that bind to the CC3 domain of BicD often contain dynein light chain interaction motifs. For example, Rab6 binds dynein light chain, LC7 (Wanschers et al., 2008) and Egalitarian binds LC8 (Navarro et al., 2004). Previous studies have indicated a role for dynein light chains in promoting protein dimerization (Benison and Barbar, 2009). Thus, future studies are needed to determine if

adapters associate with dynein through the light chains or if adapters have access to a cytoplasmic pool of light chains to promote their dimerization. We have preliminary data showing that a mutant of Egalitarian that cannot associate with the dynein light chain (Navarro et al., 2004) shows enhanced speeds compared to wild type. One complementary experiment is to add wild type Egalitarian to a minimal DDB^{CC1} complex to see if it slows dynein speeds. Full-length human dynein can be expressed in *Sf9* cells (McKenney et al., 2014; Schlager et al., 2014; Trokter et al., 2012), so another experiment that would address how Egalitarian binding affects dynein function is to express the motor without LC8 and determine if mRNPs reconstituted with this construct show enhanced speeds similar to the mutant Egalitarian. These experiments would more clearly define a role for dynein light chain interaction motifs in BicD cargo adapters.

An alternative mechanism for the enhanced activation of dynein by mRNA adapter proteins is that mRNA may recruit multiple dynein/dynactin complexes. Multiple myosin motors tethered to artificial cargoes support longer run lengths and slower speeds (Lu et al., 2012). In contrast to myosin, multiple dynein motors coupled through a cargo may result in faster speeds. A recent study showed that multiple yeast dynein motors coupled by a flexible DNA origami support faster speeds compared to a single motor (Driller-Colangelo et al., 2016). In addition, coupling two mammalian dyneins activates the ensemble for unidirectional motility (Torisawa et al., 2014). Thus, cargoes such as mRNA may promote dynein activation through BicD binding and by coupling motors to generate enhancements in speed. Further support for this model comes from structural studies showing that the BicD-like protein, BicDR1 supports dynein/dynactin speeds that are two-

fold faster than BicD2^{CC1} activation, and recruits two dynein motors per dynactin filament (Andrew Carter, personal communication). It would be of interest to determine if coupling two activated DDB^{CC1} complexes results in speed enhancements. This can be tested using a DNA origami approach (Torisawa et al., 2014) by attaching BicD2^{CC1} to two ends of a DNA scaffold through a biotin-streptavidin linkage. Dynein and dynactin can be added, forming a complex with the scaffold-attached BicD. If coupling two activated motors results in enhanced speeds, then this attachment strategy should give two speed distributions resulting from one- and two-motor complexes. Future work is needed to count the number of motors associated with mRNP complexes to determine if *K10* can recruit multiple motors. Imaging of mRNPs moving on microtubules show merge and split events, direct evidence that multiple motor complexes can form (**Chapter 3**). To more clearly define how many motors are associated with *K10* mRNA, dynein can be recombinantly expressed in *Sf9* cells with a tag for labeling. Motors can be labeled with two different color fluorophores and then added to BicD-Egalitarian-*K10* mRNA complexes. If the two colors are shown to merge, then this is good evidence that multiple dynein complexes are associated with mRNA cargoes. Alternatively, labeled dynein can be counted in mRNPs using a stepwise photobleaching method as previously done for counting dynein motors associated with mRNA complexes in *Drosophila* cell extracts (Amrute-Nayak and Bullock, 2012).

Recruitment of multiple motors to localizing mRNA

A theme of localizing mRNAs that is conserved in yeast and higher eukaryotes is the presence of multiple redundant zip codes. Zip code sequences are often duplicated in individual mRNA transcripts to promote targeting in the cell. For example, *ASH1* mRNA in budding yeast contains four zip codes. Three of these are in the coding region and one is in the 3'UTR. Each of these zip codes is sufficient to recruit She2p and support transport but all are necessary to restrict *ASH1* to the bud tip. Thus, multiple zip codes must cooperate to promote localization (Chartrand et al., 1999; Gonzalez et al., 1999). We provide a molecular understanding of why localizing mRNAs in yeast have multiple zip codes. Single molecule reconstitutions of motor-mRNA complexes show that mRNA transcripts with more zip codes recruit multiple Myo4p motor complexes leading to enhancements in run frequency and longer run lengths (Sladewski et al., 2013). Multiple motor recruitment is typically associated with enhancements in run length (Beeg et al., 2008). Thus, in yeast multiple zip codes promote mRNA localization by taking advantage of the collective properties of myosin motors.

In higher eukaryotes, there are a number of mechanisms to ensure that localizing mRNAs have multiple zip codes. Similar to *ASH1*, many transcripts contain duplicated copies of zip codes. For example, a single BLE1 element in *bicoid* is necessary for transport but it is not sufficient. This element is only competent for mRNA targeting when duplicated or expressed in combination with surrounding zip codes (Macdonald et al., 1993). In *Xenopus* oocytes, the 3'UTR of the *Vg1* transcript contains a 340 base-pair localization element containing clusters of zip codes that act synergistically to promote localization at

the vegetal hemisphere of the oocyte (Deshler et al., 1997; Lewis et al., 2004). In chicken embryo fibroblasts, the *β-actin* mRNA transcript encodes two localization elements in its 3'UTR that are both required for full localization to the lamellae (Kislauskis et al., 1994).

Some mRNA transcripts containing a single zip codes oligomerize to promote their transport. One hypothesis is that oligomerization clusters zip codes that is necessary to promote their targeting. The *Drosophila oskar* mRNA contains a dimerization domain in its 3'UTR and deletion of this domain disrupts dimerization and localization in the cell (Jambor et al., 2011). Transcript oligomerization has been visualized *in vivo*. Studies tracking individual *β-actin* mRNA transcripts in cultured neurons show that actively transporting mRNA messages merge and split in response to depolarization (Park et al., 2014). This observation shows that mRNA-motor complex assembly and disassembly is a regulated process.

Cell biological studies indicate that multiple zip codes are essential for promoting transport in higher eukaryotes but it is still unclear how. Similar to in yeast, multiple zip codes may recruit multiple motors to promote run length and engagement with the track (Sladewski et al., 2013). One interesting idea is that multiple zip codes can recruit multiple dynein motors to enhance activation and minus-end directed speed of mRNA complexes (**Chapter 3**). Activation by multiple dynein recruitment may be essential when considering that many mRNA complexes also associate with the plus-end directed motor, kinesin.

Bi-directional mRNA transport

Some localizing mRNAs in higher eukaryotes recruit both dynein and kinesin. *Oscar* mRNA contains two zip codes. The OES links the mRNA to dynein in early stages of *Drosophila* development for minus-end directed oocyte entry (Jambor et al., 2014). Then, the alternatively spliced SOLE links the mRNA to kinesin-1 for plus-end directed transport to the posterior at later stages of development (Hachet and Ephrussi, 2004). If *oskar* recruits opposing motors, then how is the direction of transport determined? One explanation is that motors are alternatively regulated so that their activities do not interfere with one other. This way, auto-regulation can be used as a regulatory mechanism to determine the direction of transport. One such mechanism has been proposed for amyloid precursor protein (AAP) motility in axons. Phosphorylated JNK-interacting protein 1 (JIP1) binds and relieves kinesin 1 auto-inhibition, but the p150^{Glued} subunit of dynactin competes for this interaction when JIP1 is unphosphorylated. Two mutually exclusive active motor complexes are thus formed. Ultimately, the phosphorylation status of JIP1 dictates the direction of APP transport by determining the extent of kinesin 1 activation and dynein recruitment (Fu and Holzbaur, 2013). Similar regulatory mechanisms likely apply to bias the direction of *oskar* mRNA transport.

Surprisingly, all localizing mRNAs in *Drosophila* move bi-directionally. This includes mRNAs that contain only zip codes specifying dynein recruitment. One explanation is that kinesin is recruited to dynein-mRNA complexes independent of kinesin-specific zip codes, and cooperates to promote mRNA transport. Support for dynein-kinesin cooperation comes from knock-down studies in *Drosophila* S2 cells showing that depleting

either dynein or the kinesin-1 heavy chain inhibits the motility of FMRP-containing mRNA granules in both retrograde and anterograde directions, suggesting a tight coupling between kinesin and dynein (Ling et al., 2004). This property is observed in a number of other cargoes in *Drosophila* (Ally et al., 2009; Gross et al., 2002; Martin et al., 1999; Pilling et al., 2006; Uchida et al., 2009; Waterman-Storer et al., 1997). If there are no zip codes specifying kinesin recruitment how does this motor associate with mRNA transport complexes? Studies show that kinesin-1 directly associates with the second coiled-coil (CC2) in BicD (Grigoriev et al., 2007). However, we have data showing that kinesin-1 may associate with third coiled-coil (CC3) (**Appendix II**). To understand the molecular basis of motor coupling, we added a quantum dot labeled kinesin construct to reconstitutions containing dynein, dynactin, BicD and Egalitarian (**Appendix II**). We find that kinesin promotes associations of dynein complexes to the microtubule in the absence of a localizing mRNA transcript. The presence of Egalitarian was necessary to observe kinesin associations with microtubules indicating that only Egalitarian-bound BicD recruits kinesin. The requirement of Egalitarian for kinesin association with BicD may be consistent with our pull-downs showing that, unlike Egalitarian and Rab6, kinesin associates with fragments of BicD but not full-length BicD (**Appendix II**). Importantly, addition of kinesin to dynein complexes gives bi-directional motility (i.e. plus-end and minus-end directed runs) with no net bias in direction (**Appendix II**). Thus, a localizing mRNA may be required to bias the direction of transport by recruiting cellular factors for selective activation of motors. We have shown that *K10* mRNA activates dynein for processive transport (**Chapter 3**). One hypothesis is that *K10* determines its localization in the cell by activating dynein to bias the direction of transport to the minus-end of the

microtubule. This possibility can be tested adding a labeled *K10* mRNA to bi-directionally moving complexes. We predict that the selective activation of dynein would bias the complex to minus-end of the microtubule. To determine the extent of activation of kinesin in these complexes, bi-directionally moving mRNA complexes can be reconstituted with a mutation in full-length kinesin (Kinesin Δ H2) that renders it constitutively activated for transport but retains cargo binding capacity (Friedman and Vale, 1999). We predict that upregulating kinesin activity will shift the direction of transport to the plus-end of the microtubule. Experiments should be repeated with mRNA transcripts that contain zip codes that promote kinesin-driven plus-end directed transport such as those that bind the kinesin adapter protein Staufin (Ferrandon et al., 1994). These experiments highlight the utility of using mRNA to study molecular motors in the context of their native adapters and cargoes and will provide unique insight into the regulatory mechanisms that determine how cellular cargoes are sorted.

LITERATURE CITED

- Allan, V.J. 2011. Cytoplasmic dynein. *Biochem Soc Trans.* 39:1169-1178.
- Ally, S., A.G. Larson, K. Barlan, S.E. Rice, and V.I. Gelfand. 2009. Opposite-polarity motors activate one another to trigger cargo transport in live cells. *J Cell Biol.* 187:1071-1082.
- Amrute-Nayak, M., and S.L. Bullock. 2012a. Single-molecule assays reveal that RNA localization signals regulate dynein-dynactin copy number on individual transcript cargoes. *Nat Cell Biol.* 14:416-423.
- Amrute-Nayak, M., and S.L. Bullock. 2012b. Single-molecule assays reveal that RNA localization signals regulate dynein-dynactin copy number on individual transcript cargoes. *Nat Cell Biol.*

- Aniento, F., N. Emans, G. Griffiths, and J. Gruenberg. 1993. Cytoplasmic dynein-dependent vesicular transport from early to late endosomes. *J Cell Biol.* 123:1373-1387.
- Arn, E.A., B.J. Cha, W.E. Theurkauf, and P.M. Macdonald. 2003. Recognition of a bicoid mRNA localization signal by a protein complex containing Swallow, Nod, and RNA binding proteins. *Dev Cell.* 4:41-51.
- Baron, A.T., and J.L. Salisbury. 1988. Identification and localization of a novel, cytoskeletal, centrosome-associated protein in PtK2 cells. *J Cell Biol.* 107:2669-2678.
- Bashirullah, A., R.L. Cooperstock, and H.D. Lipshitz. 2001. Spatial and temporal control of RNA stability. *Proc Natl Acad Sci U S A.* 98:7025-7028.
- Beeg, J., S. Klumpp, R. Dimova, R.S. Gracia, E. Unger, and R. Lipowsky. 2008. Transport of beads by several kinesin motors. *Biophys J.* 94:532-541.
- Belyy, V., M.A. Schlager, H. Foster, A.E. Reimer, A.P. Carter, and A. Yildiz. 2016. The mammalian dynein-dynactin complex is a strong opponent to kinesin in a tug-of-war competition. *Nat Cell Biol.* 18:1018-1024.
- Benison, G., and E. Barbar. 2009. NMR analysis of dynein light chain dimerization and interactions with diverse ligands. *Methods Enzymol.* 455:237-258.
- Bergbrede, T., O. Pylypenko, A. Rak, and K. Alexandrov. 2005. Structure of the extremely slow GTPase Rab6A in the GTP bound form at 1.8Å resolution. *J Struct Biol.* 152:235-238.
- Bertrand, E., P. Chartrand, M. Schaefer, S.M. Shenoy, R.H. Singer, and R.M. Long. 1998. Localization of ASH1 mRNA particles in living yeast. *Mol Cell.* 2:437-445.
- Bianco, A., M. Dienstbier, H.K. Salter, G. Gatto, and S.L. Bullock. 2010. Bicaudal-D regulates fragile X mental retardation protein levels, motility, and function during neuronal morphogenesis. *Curr Biol.* 20:1487-1492.
- Bielska, E., M. Schuster, Y. Roger, A. Berepiki, D.M. Soanes, N.J. Talbot, and G. Steinberg. 2014. Hook is an adapter that coordinates kinesin-3 and dynein cargo attachment on early endosomes. *J Cell Biol.* 204:989-1007.
- Bingham, J.B., S.J. King, and T.A. Schroer. 1998. Purification of dynactin and dynein from brain tissue. *Methods Enzymol.* 298:171-184.

- Blobel, G., and B. Dobberstein. 1975. Transfer of proteins across membranes. I. Presence of proteolytically processed and unprocessed nascent immunoglobulin light chains on membrane-bound ribosomes of murine myeloma. *J Cell Biol.* 67:835-851.
- Bloom, G.S., M.C. Wagner, K.K. Pfister, and S.T. Brady. 1988. Native structure and physical properties of bovine brain kinesin and identification of the ATP-binding subunit polypeptide. *Biochemistry.* 27:3409-3416.
- Bobola, N., R.P. Jansen, T.H. Shin, and K. Nasmyth. 1996. Asymmetric accumulation of Ash1p in postanaphase nuclei depends on a myosin and restricts yeast mating-type switching to mother cells. *Cell.* 84:699-709.
- Bohl, F., C. Kruse, A. Frank, D. Ferring, and R.P. Jansen. 2000. She2p, a novel RNA-binding protein tethers ASH1 mRNA to the Myo4p myosin motor via She3p. *EMBO J.* 19:5514-5524.
- Boldogh, I.R., and L.A. Pon. 2007. Mitochondria on the move. *Trends Cell Biol.* 17:502-510.
- Bookwalter, C.S., M. Lord, and K.M. Trybus. 2009. Essential features of the class V myosin from budding yeast for ASH1 mRNA transport. *Mol Biol Cell.* 20:3414-3421.
- Brendza, R.P., L.R. Serbus, J.B. Duffy, and W.M. Saxton. 2000. A function for kinesin I in the posterior transport of oskar mRNA and Staufen protein. *Science.* 289:2120-2122.
- Bullock, S.L., and D. Ish-Horowicz. 2001. Conserved signals and machinery for RNA transport in *Drosophila* oogenesis and embryogenesis. *Nature.* 414:611-616.
- Bullock, S.L., A. Nicol, S.P. Gross, and D. Zicha. 2006. Guidance of bidirectional motor complexes by mRNA cargoes through control of dynein number and activity. *Curr Biol.* 16:1447-1452.
- Bullock, S.L., M. Stauber, A. Prell, J.R. Hughes, D. Ish-Horowicz, and U. Schmidt-Ott. 2004. Differential cytoplasmic mRNA localisation adjusts pair-rule transcription factor activity to cytoarchitecture in dipteran evolution. *Development.* 131:4251-4261.
- Burgess, S.A., M.L. Walker, K. Thirumurugan, J. Trinick, and P.J. Knight. 2004. Use of negative stain and single-particle image processing to explore dynamic properties of flexible macromolecules. *J Struct Biol.* 147:247-258.
- Carter, A.P. 2013. Crystal clear insights into how the dynein motor moves. *J Cell Sci.* 126:705-713.

- Carter, A.P., and R.D. Vale. 2010. Communication between the AAA+ ring and microtubule-binding domain of dynein. *Biochem Cell Biol.* 88:15-21.
- Castoldi, M., and A.V. Popov. 2003. Purification of brain tubulin through two cycles of polymerization-depolymerization in a high-molarity buffer. *Protein Expr Purif.* 32:83-88.
- Chang, P., J. Torres, R.A. Lewis, K.L. Mowry, E. Houliston, and M.L. King. 2004. Localization of RNAs to the mitochondrial cloud in *Xenopus* oocytes through entrapment and association with endoplasmic reticulum. *Mol Biol Cell.* 15:4669-4681.
- Chartrand, P., X.H. Meng, S. Huttelmaier, D. Donato, and R.H. Singer. 2002. Asymmetric sorting of *ash1p* in yeast results from inhibition of translation by localization elements in the mRNA. *Mol Cell.* 10:1319-1330.
- Chartrand, P., X.H. Meng, R.H. Singer, and R.M. Long. 1999. Structural elements required for the localization of *ASH1* mRNA and of a green fluorescent protein reporter particle in vivo. *Curr Biol.* 9:333-336.
- Chen, L.Y., C.S. Rex, M.S. Casale, C.M. Gall, and G. Lynch. 2007. Changes in synaptic morphology accompany actin signaling during LTP. *J Neurosci.* 27:5363-5372.
- Cheung, H.K., T.L. Serano, and R.S. Cohen. 1992. Evidence for a highly selective RNA transport system and its role in establishing the dorsoventral axis of the *Drosophila* egg. *Development.* 114:653-661.
- Chowdhury, S., S.A. Ketcham, T.A. Schroer, and G.C. Lander. 2015. Structural organization of the dynein-dynactin complex bound to microtubules. *Nat Struct Mol Biol.*
- Chung, S., and P.A. Takizawa. 2010. Multiple Myo4 motors enhance *ASH1* mRNA transport in *Saccharomyces cerevisiae*. *J Cell Biol.* 189:755-767.
- Churchman, L.S., Z. Okten, R.S. Rock, J.F. Dawson, and J.A. Spudich. 2005. Single molecule high-resolution colocalization of Cy3 and Cy5 attached to macromolecules measures intramolecular distances through time. *Proc Natl Acad Sci U S A.* 102:1419-1423.
- Cianfrocco, M.A., M.E. DeSantis, A.E. Leschziner, and S.L. Reck-Peterson. 2015. Mechanism and Regulation of Cytoplasmic Dynein. *Annu Rev Cell Dev Biol.*

- Coureux, P.D., H.L. Sweeney, and A. Houdusse. 2004. Three myosin V structures delineate essential features of chemo-mechanical transduction. *EMBO J.* 23:4527-4537.
- Coureux, P.D., A.L. Wells, J. Menetrey, C.M. Yengo, C.A. Morris, H.L. Sweeney, and A. Houdusse. 2003. A structural state of the myosin V motor without bound nucleotide. *Nature.* 425:419-423.
- Cripe, L., E. Morris, and A.B. Fulton. 1993. Vimentin mRNA location changes during muscle development. *Proc Natl Acad Sci U S A.* 90:2724-2728.
- Cronan, J.E., Jr. 1990. Biotination of proteins in vivo. A post-translational modification to label, purify, and study proteins. *J Biol Chem.* 265:10327-10333.
- Darnell, J.C., C.E. Fraser, O. Mostovetsky, G. Stefani, T.A. Jones, S.R. Eddy, and R.B. Darnell. 2005. Kissing complex RNAs mediate interaction between the Fragile-X mental retardation protein KH2 domain and brain polyribosomes. *Genes Dev.* 19:903-918.
- Davis, I., and D. Ish-Horowicz. 1991. Apical localization of pair-rule transcripts requires 3' sequences and limits protein diffusion in the *Drosophila* blastoderm embryo. *Cell.* 67:927-940.
- De La Cruz, E.M., A.L. Wells, S.S. Rosenfeld, E.M. Ostap, and H.L. Sweeney. 1999. The kinetic mechanism of myosin V. *Proc Natl Acad Sci U S A.* 96:13726-13731.
- Deshler, J.O., M.I. Highett, and B.J. Schnapp. 1997. Localization of *Xenopus* Vg1 mRNA by Vera protein and the endoplasmic reticulum. *Science.* 276:1128-1131.
- Dictenberg, J.B., S.A. Swanger, L.N. Antar, R.H. Singer, and G.J. Bassell. 2008. A direct role for FMRP in activity-dependent dendritic mRNA transport links filopodial-spine morphogenesis to fragile X syndrome. *Dev Cell.* 14:926-939.
- Dienstbier, M., F. Boehl, X. Li, and S.L. Bullock. 2009. Egalitarian is a selective RNA-binding protein linking mRNA localization signals to the dynein motor. *Genes Dev.* 23:1546-1558.
- Dodding, M.P., and M. Way. 2011. Coupling viruses to dynein and kinesin-1. *EMBO J.* 30:3527-3539.
- Driller-Colangelo, A.R., K.W. Chau, J.M. Morgan, and N.D. Derr. 2016. Cargo rigidity affects the sensitivity of dynein ensembles to individual motor pausing. *Cytoskeleton (Hoboken).*

- Du, T.G., S. Jellbauer, M. Muller, M. Schmid, D. Niessing, and R.P. Jansen. 2008. Nuclear transit of the RNA-binding protein She2 is required for translational control of localized ASH1 mRNA. *EMBO Rep.* 9:781-787.
- Du, Y., M. Pypaert, P. Novick, and S. Ferro-Novick. 2001. Aux1p/Swa2p is required for cortical endoplasmic reticulum inheritance in *Saccharomyces cerevisiae*. *Mol Biol Cell.* 12:2614-2628.
- Dunn, B.D., T. Sakamoto, M.S. Hong, J.R. Sellers, and P.A. Takizawa. 2007. Myo4p is a monomeric myosin with motility uniquely adapted to transport mRNA. *J Cell Biol.* 178:1193-1206.
- Eberwine, J., B. Belt, J.E. Kacharina, and K. Miyashiro. 2002. Analysis of subcellularly localized mRNAs using in situ hybridization, mRNA amplification, and expression profiling. *Neurochem Res.* 27:1065-1077.
- Edgar, B.A., G.M. Odell, and G. Schubiger. 1987. Cytoarchitecture and the patterning of fushi tarazu expression in the *Drosophila* blastoderm. *Genes Dev.* 1:1226-1237.
- Estrada, P., J. Kim, J. Coleman, L. Walker, B. Dunn, P. Takizawa, P. Novick, and S. Ferro-Novick. 2003. Myo4p and She3p are required for cortical ER inheritance in *Saccharomyces cerevisiae*. *J Cell Biol.* 163:1255-1266.
- Ferrandon, D., L. Elphick, C. Nusslein-Volhard, and D. St Johnston. 1994. Stauf protein associates with the 3'UTR of bicoid mRNA to form particles that move in a microtubule-dependent manner. *Cell.* 79:1221-1232.
- Foissner, I., I.K. Lichtscheidl, and G.O. Wasteneys. 1996. Actin-based vesicle dynamics and exocytosis during wound wall formation in characean internodal cells. *Cell Motil Cytoskeleton.* 35:35-48.
- Forrest, K.M., and E.R. Gavis. 2003. Live imaging of endogenous RNA reveals a diffusion and entrapment mechanism for nanos mRNA localization in *Drosophila*. *Curr Biol.* 13:1159-1168.
- Friedman, D.S., and R.D. Vale. 1999. Single-molecule analysis of kinesin motility reveals regulation by the cargo-binding tail domain. *Nat Cell Biol.* 1:293-297.
- Fu, M.M., and E.L. Holzbaur. 2013. JIP1 regulates the directionality of APP axonal transport by coordinating kinesin and dynein motors. *J Cell Biol.* 202:495-508.
- Fuchs, E., B. Short, and F.A. Barr. 2005. Assay and properties of rab6 interaction with dynein-dynactin complexes. *Methods Enzymol.* 403:607-618.

- Fukazawa, Y., Y. Saitoh, F. Ozawa, Y. Ohta, K. Mizuno, and K. Inokuchi. 2003. Hippocampal LTP is accompanied by enhanced F-actin content within the dendritic spine that is essential for late LTP maintenance in vivo. *Neuron*. 38:447-460.
- Gagnon, J.A., and K.L. Mowry. 2011. Molecular motors: directing traffic during RNA localization. *Crit Rev Biochem Mol Biol*. 46:229-239.
- Genz, C., J. Fundakowski, O. Hermesh, M. Schmid, and R.P. Jansen. 2013. Association of the yeast RNA-binding protein She2p with the tubular endoplasmic reticulum depends on membrane curvature. *J Biol Chem*. 288:32384-32393.
- Geron, E., E.D. Schejter, and B.Z. Shilo. 2013. Directing exocrine secretory vesicles to the apical membrane by actin cables generated by the formin mDia1. *Proc Natl Acad Sci U S A*.
- Gestaut, D.R., B. Graczyk, J. Cooper, P.O. Widlund, A. Zelter, L. Wordeman, C.L. Asbury, and T.N. Davis. 2008. Phosphoregulation and depolymerization-driven movement of the Dam1 complex do not require ring formation. *Nat Cell Biol*. 10:407-414.
- Ghaemmaghami, S., W.K. Huh, K. Bower, R.W. Howson, A. Belle, N. Dephoure, E.K. O'Shea, and J.S. Weissman. 2003. Global analysis of protein expression in yeast. *Nature*. 425:737-741.
- Gibbons, I.R., J.E. Garbarino, C.E. Tan, S.L. Reck-Peterson, R.D. Vale, and A.P. Carter. 2005. The affinity of the dynein microtubule-binding domain is modulated by the conformation of its coiled-coil stalk. *J Biol Chem*. 280:23960-23965.
- Gonsalvez, G.B., J.L. Little, and R.M. Long. 2004. ASH1 mRNA anchoring requires reorganization of the Myo4p-She3p-She2p transport complex. *J Biol Chem*. 279:46286-46294.
- Gonzalez, I., S.B. Buonomo, K. Nasmyth, and U. von Ahsen. 1999. ASH1 mRNA localization in yeast involves multiple secondary structural elements and Ash1 protein translation. *Curr Biol*. 9:337-340.
- Griffis, E.R., N. Stuurman, and R.D. Vale. 2007. Spindly, a novel protein essential for silencing the spindle assembly checkpoint, recruits dynein to the kinetochore. *J Cell Biol*. 177:1005-1015.
- Grigoriev, I., D. Splinter, N. Keijzer, P.S. Wulf, J. Demmers, T. Ohtsuka, M. Modesti, I.V. Maly, F. Grosveld, C.C. Hoogenraad, and A. Akhmanova. 2007. Rab6 regulates transport and targeting of exocytotic carriers. *Dev Cell*. 13:305-314.

- Gross, S.P., M.C. Tuma, S.W. Deacon, A.S. Serpinskaya, A.R. Reilein, and V.I. Gelfand. 2002. Interactions and regulation of molecular motors in *Xenopus melanophores*. *J Cell Biol.* 156:855-865.
- Grosshans, B.L., D. Ortiz, and P. Novick. 2006. Rabs and their effectors: achieving specificity in membrane traffic. *Proc Natl Acad Sci U S A.* 103:11821-11827.
- Gunther, L.K., K. Furuta, J. Bao, M.K. Urbanowski, H. Kojima, H.D. White, and T. Sakamoto. 2014. Coupling of two non-processive myosin 5c dimers enables processive stepping along actin filaments. *Sci Rep.* 4:4907.
- Hachet, O., and A. Ephrussi. 2004. Splicing of oskar RNA in the nucleus is coupled to its cytoplasmic localization. *Nature.* 428:959-963.
- Hackney, D.D., J.D. Levitt, and J. Suhan. 1992. Kinesin undergoes a 9 S to 6 S conformational transition. *J Biol Chem.* 267:8696-8701.
- Han, J.W., J.H. Park, M. Kim, and J. Lee. 1997. mRNAs for microtubule proteins are specifically colocalized during the sequential formation of basal body, flagella, and cytoskeletal microtubules in the differentiation of *Naegleria gruberi*. *J Cell Biol.* 137:871-879.
- He, B., and W. Guo. 2009. The exocyst complex in polarized exocytosis. *Curr Opin Cell Biol.* 21:537-542.
- Hendricks, A.G., E. Perlson, J.L. Ross, H.W. Schroeder, 3rd, M. Tokito, and E.L. Holzbaur. 2010. Motor coordination via a tug-of-war mechanism drives bidirectional vesicle transport. *Curr Biol.* 20:697-702.
- Heuck, A., I. Fetka, D.N. Brewer, D. Huls, M. Munson, R.P. Jansen, and D. Niessing. 2010. The structure of the Myo4p globular tail and its function in ASH1 mRNA localization. *J Cell Biol.* 189:497-510.
- Heym, R.G., D. Zimmermann, F.T. Edelmann, L. Israel, Z. Okten, D.R. Kovar, and D. Niessing. 2013. In vitro reconstitution of an mRNA-transport complex reveals mechanisms of assembly and motor activation. *J Cell Biol.* 203:971-984.
- Hodges, A.R., C.S. Bookwalter, E.B. Krementsova, and K.M. Trybus. 2009. A nonprocessive class V myosin drives cargo processively when a kinesin-related protein is a passenger. *Curr Biol.* 19:2121-2125.
- Hodges, A.R., E.B. Krementsova, C.S. Bookwalter, P.M. Fagnant, T.E. Sladewski, and K.M. Trybus. 2012. Tropomyosin is essential for processive movement of a class v Myosin from budding yeast. *Curr Biol.* 22:1410-1416.

- Hodges, A.R., E.B. Krementsova, and K.M. Trybus. 2008. She3p binds to the rod of yeast myosin V and prevents it from dimerizing, forming a single-headed motor complex. *J Biol Chem.* 283:6906-6914.
- Hoogenraad, C.C., A. Akhmanova, S.A. Howell, B.R. Dortland, C.I. De Zeeuw, R. Willemsen, P. Visser, F. Grosveld, and N. Galjart. 2001. Mammalian Golgi-associated Bicaudal-D2 functions in the dynein-dynactin pathway by interacting with these complexes. *EMBO J.* 20:4041-4054.
- Hoogenraad, C.C., P. Wulf, N. Schiefermeier, T. Stepanova, N. Galjart, J.V. Small, F. Grosveld, C.I. de Zeeuw, and A. Akhmanova. 2003. Bicaudal D induces selective dynein-mediated microtubule minus end-directed transport. *EMBO J.* 22:6004-6015.
- Horgan, C.P., and M.W. McCaffrey. 2012. Endosomal trafficking in animal cytokinesis. *Front Biosci (Schol Ed).* 4:547-555.
- Howard, J., and A.A. Hyman. 1993. Preparation of marked microtubules for the assay of the polarity of microtubule-based motors by fluorescence microscopy. *Methods Cell Biol.* 39:105-113.
- Huber, K.M., M.S. Kayser, and M.F. Bear. 2000. Role for rapid dendritic protein synthesis in hippocampal mGluR-dependent long-term depression. *Science.* 288:1254-1257.
- Imamula, K., T. Kon, R. Ohkura, and K. Sutoh. 2007. The coordination of cyclic microtubule association/dissociation and tail swing of cytoplasmic dynein. *Proc Natl Acad Sci U S A.* 104:16134-16139.
- Isaacs, W.B., and A.B. Fulton. 1987. Cotranslational assembly of myosin heavy chain in developing cultured skeletal muscle. *Proc Natl Acad Sci U S A.* 84:6174-6178.
- Isaacs, W.B., I.S. Kim, A. Struve, and A.B. Fulton. 1989. Biosynthesis of titin in cultured skeletal muscle cells. *J Cell Biol.* 109:2189-2195.
- Jacobs, D.T., R. Weigert, K.D. Grode, J.G. Donaldson, and R.E. Cheney. 2009. Myosin Vc is a molecular motor that functions in secretory granule trafficking. *Mol Biol Cell.* 20:4471-4488.
- Jambhekar, A., and J.L. Derisi. 2007. Cis-acting determinants of asymmetric, cytoplasmic RNA transport. *RNA.* 13:625-642.
- Jambhekar, A., K. McDermott, K. Sorber, K.A. Shepard, R.D. Vale, P.A. Takizawa, and J.L. DeRisi. 2005. Unbiased selection of localization elements reveals cis-acting determinants of mRNA bud localization in *Saccharomyces cerevisiae*. *Proc Natl Acad Sci U S A.* 102:18005-18010.

- Jambor, H., C. Brunel, and A. Ephrussi. 2011. Dimerization of oskar 3' UTRs promotes hitchhiking for RNA localization in the *Drosophila* oocyte. *RNA*. 17:2049-2057.
- Jambor, H., S. Mueller, S.L. Bullock, and A. Ephrussi. 2014. A stem-loop structure directs oskar mRNA to microtubule minus ends. *RNA*. 20:429-439.
- Jansen, R.P., C. Dowzer, C. Michaelis, M. Galova, and K. Nasmyth. 1996. Mother cell-specific HO expression in budding yeast depends on the unconventional myosin myo4p and other cytoplasmic proteins. *Cell*. 84:687-697.
- Januschke, J., E. Nicolas, J. Compagnon, E. Formstecher, B. Goud, and A. Guichet. 2007. Rab6 and the secretory pathway affect oocyte polarity in *Drosophila*. *Development*. 134:3419-3425.
- Jiang, H., S. Wang, Y. Huang, X. He, H. Cui, X. Zhu, and Y. Zheng. 2015. Phase transition of spindle-associated protein regulate spindle apparatus assembly. *Cell*. 163:108-122.
- Johnstone, O., and P. Lasko. 2001. Translational regulation and RNA localization in *Drosophila* oocytes and embryos. *Annu Rev Genet*. 35:365-406.
- Jorgensen, P., N.P. Edgington, B.L. Schneider, I. Rupes, M. Tyers, and B. Futcher. 2007. The size of the nucleus increases as yeast cells grow. *Mol Biol Cell*. 18:3523-3532.
- Kad, N.M., K.M. Trybus, and D.M. Warshaw. 2008. Load and Pi control flux through the branched kinetic cycle of myosin V. *J Biol Chem*. 283:17477-17484.
- Kim, C.H., and J.E. Lisman. 1999. A role of actin filament in synaptic transmission and long-term potentiation. *J Neurosci*. 19:4314-4324.
- King, S.J., and T.A. Schroer. 2000. Dynactin increases the processivity of the cytoplasmic dynein motor. *Nat Cell Biol*. 2:20-24.
- Kislauskis, E.H., X. Zhu, and R.H. Singer. 1994. Sequences responsible for intracellular localization of beta-actin messenger RNA also affect cell phenotype. *J Cell Biol*. 127:441-451.
- Kon, T., K. Imamula, A.J. Roberts, R. Ohkura, P.J. Knight, I.R. Gibbons, S.A. Burgess, and K. Sutoh. 2009. Helix sliding in the stalk coiled coil of dynein couples ATPase and microtubule binding. *Nat Struct Mol Biol*. 16:325-333.
- Kon, T., M. Nishiura, R. Ohkura, Y.Y. Toyoshima, and K. Sutoh. 2004. Distinct functions of nucleotide-binding/hydrolysis sites in the four AAA modules of cytoplasmic dynein. *Biochemistry*. 43:11266-11274.

- Kon, T., K. Sutoh, and G. Kurisu. 2011. X-ray structure of a functional full-length dynein motor domain. *Nat Struct Mol Biol.* 18:638-642.
- Krementsov, D.N., E.B. Krementsova, and K.M. Trybus. 2004. Myosin V: regulation by calcium, calmodulin, and the tail domain. *J Cell Biol.* 164:877-886.
- Krementsova, E.B., A.R. Hodges, C.S. Bookwalter, T.E. Sladewski, M. Travaglia, H.L. Sweeney, and K.M. Trybus. 2011. Two single-headed myosin V motors bound to a tetrameric adapter protein form a processive complex. *J Cell Biol.* 195:631-641.
- Krucker, T., G.R. Siggins, and S. Halpain. 2000. Dynamic actin filaments are required for stable long-term potentiation (LTP) in area CA1 of the hippocampus. *Proc Natl Acad Sci U S A.* 97:6856-6861.
- Kuznetsov, S.A., E.A. Vaisberg, N.A. Shanina, N.N. Magretova, V.Y. Chernyak, and V.I. Gelfand. 1988. The quaternary structure of bovine brain kinesin. *EMBO J.* 7:353-356.
- L'Ecuier, T.J., J.A. Noller, and A.B. Fulton. 1998. Assembly of tropomyosin isoforms into the cytoskeleton of avian muscle cells. *Pediatr Res.* 43:813-822.
- Lawrence, J.B., and R.H. Singer. 1986. Intracellular localization of messenger RNAs for cytoskeletal proteins. *Cell.* 45:407-415.
- Lecuyer, E., H. Yoshida, N. Parthasarathy, C. Alm, T. Babak, T. Cerovina, T.R. Hughes, P. Tomancak, and H.M. Krause. 2007. Global analysis of mRNA localization reveals a prominent role in organizing cellular architecture and function. *Cell.* 131:174-187.
- Levadoux, M., C. Mahon, J.H. Beattie, H.M. Wallace, and J.E. Hesketh. 1999. Nuclear import of metallothionein requires its mRNA to be associated with the perinuclear cytoskeleton. *J Biol Chem.* 274:34961-34966.
- Lewis, R.A., T.L. Kress, C.A. Cote, D. Gautreau, M.E. Rokop, and K.L. Mowry. 2004. Conserved and clustered RNA recognition sequences are a critical feature of signals directing RNA localization in *Xenopus* oocytes. *Mech Dev.* 121:101-109.
- Li, X., H. Kuromi, L. Briggs, D.B. Green, J.J. Rocha, S.T. Sweeney, and S.L. Bullock. 2010. Bicaudal-D binds clathrin heavy chain to promote its transport and augments synaptic vesicle recycling. *EMBO J.* 29:992-1006.

- Li, X.D., K. Mabuchi, R. Ikebe, and M. Ikebe. 2004. Ca^{2+} -induced activation of ATPase activity of myosin Va is accompanied with a large conformational change. *Biochem Biophys Res Commun.* 315:538-545.
- Ling, S.C., P.S. Fahrner, W.T. Greenough, and V.I. Gelfand. 2004. Transport of Drosophila fragile X mental retardation protein-containing ribonucleoprotein granules by kinesin-1 and cytoplasmic dynein. *Proc Natl Acad Sci U S A.* 101:17428-17433.
- Link, W., U. Konietzko, G. Kauselmann, M. Krug, B. Schwanke, U. Frey, and D. Kuhl. 1995. Somatodendritic expression of an immediate early gene is regulated by synaptic activity. *Proc Natl Acad Sci U S A.* 92:5734-5738.
- Liu, J., D.W. Taylor, E.B. Krementsova, K.M. Trybus, and K.A. Taylor. 2006. Three-dimensional structure of the myosin V inhibited state by cryoelectron tomography. *Nature.* 442:208-211.
- Liu, Y., H.K. Salter, A.N. Holding, C.M. Johnson, E. Stephens, P.J. Lukavsky, J. Walshaw, and S.L. Bullock. 2013. Bicaudal-D uses a parallel, homodimeric coiled coil with heterotypic registry to coordinate recruitment of cargos to dynein. *Genes Dev.* 27:1233-1246.
- Long, R.M., W. Gu, X. Meng, G. Gonsalvez, R.H. Singer, and P. Chartrand. 2001. An exclusively nuclear RNA-binding protein affects asymmetric localization of ASH1 mRNA and Ash1p in yeast. *J Cell Biol.* 153:307-318.
- Long, R.M., R.H. Singer, X. Meng, I. Gonzalez, K. Nasmyth, and R.P. Jansen. 1997. Mating type switching in yeast controlled by asymmetric localization of ASH1 mRNA. *Science.* 277:383-387.
- Lu, H., A.K. Efremov, C.S. Bookwalter, E.B. Krementsova, J.W. Driver, K.M. Trybus, and M.R. Diehl. 2012. Collective dynamics of elastically-coupled myosinV motors. *J Biol Chem.*
- Lu, H., E.B. Krementsova, and K.M. Trybus. 2006. Regulation of myosin V processivity by calcium at the single molecule level. *J Biol Chem.* 281:31987-31994.
- Lyford, G.L., K. Yamagata, W.E. Kaufmann, C.A. Barnes, L.K. Sanders, N.G. Copeland, D.J. Gilbert, N.A. Jenkins, A.A. Lanahan, and P.F. Worley. 1995. Arc, a growth factor and activity-regulated gene, encodes a novel cytoskeleton-associated protein that is enriched in neuronal dendrites. *Neuron.* 14:433-445.
- Macdonald, P.M., K. Kerr, J.L. Smith, and A. Leask. 1993. RNA regulatory element BLE1 directs the early steps of bicoid mRNA localization. *Development.* 118:1233-1243.

- Mach, J.M., and R. Lehmann. 1997. An Egalitarian-BicaudalD complex is essential for oocyte specification and axis determination in *Drosophila*. *Genes Dev.* 11:423-435.
- Mahowald, A.P., and J.M. Strassheim. 1970. Intercellular migration of centrioles in the germarium of *Drosophila melanogaster*. An electron microscopic study. *J Cell Biol.* 45:306-320.
- Mallik, R., B.C. Carter, S.A. Lex, S.J. King, and S.P. Gross. 2004. Cytoplasmic dynein functions as a gear in response to load. *Nature.* 427:649-652.
- Mallik, R., D. Petrov, S.A. Lex, S.J. King, and S.P. Gross. 2005. Building complexity: an in vitro study of cytoplasmic dynein with in vivo implications. *Curr Biol.* 15:2075-2085.
- Mallik, R., A.K. Rai, P. Barak, A. Rai, and A. Kunwar. 2013. Teamwork in microtubule motors. *Trends Cell Biol.* 23:575-582.
- Manseau, L.J., and T. Schupbach. 1989. cappuccino and spire: two unique maternal-effect loci required for both the anteroposterior and dorsoventral patterns of the *Drosophila* embryo. *Genes Dev.* 3:1437-1452.
- Martin, K.C., and R.S. Zukin. 2006. RNA trafficking and local protein synthesis in dendrites: an overview. *J Neurosci.* 26:7131-7134.
- Martin, M., S.J. Iyadurai, A. Gassman, J.G. Gindhart, Jr., T.S. Hays, and W.M. Saxton. 1999. Cytoplasmic dynein, the dynactin complex, and kinesin are interdependent and essential for fast axonal transport. *Mol Biol Cell.* 10:3717-3728.
- Martinez, O., C. Antony, G. Pehau-Arnaudet, E.G. Berger, J. Salamero, and B. Goud. 1997. GTP-bound forms of rab6 induce the redistribution of Golgi proteins into the endoplasmic reticulum. *Proc Natl Acad Sci U S A.* 94:1828-1833.
- Matanis, T., A. Akhmanova, P. Wulf, E. Del Nery, T. Weide, T. Stepanova, N. Galjart, F. Grosveld, B. Goud, C.I. De Zeeuw, A. Barnekow, and C.C. Hoogenraad. 2002. Bicaudal-D regulates COPI-independent Golgi-ER transport by recruiting the dynein-dynactin motor complex. *Nat Cell Biol.* 4:986-992.
- Matsuzaki, M., N. Honkura, G.C. Ellis-Davies, and H. Kasai. 2004. Structural basis of long-term potentiation in single dendritic spines. *Nature.* 429:761-766.
- Maytum, R., M.A. Geeves, and M. Konrad. 2000. Actomyosin regulatory properties of yeast tropomyosin are dependent upon N-terminal modification. *Biochemistry.* 39:11913-11920.

- McCaffrey, M.W., and A.J. Lindsay. 2012. Roles for myosin Va in RNA transport and turnover. *Biochem Soc Trans.* 40:1416-1420.
- McKenney, R.J., W. Huynh, M.E. Tanenbaum, G. Bhabha, and R.D. Vale. 2014. Activation of cytoplasmic dynein motility by dynactin-cargo adapter complexes. *Science.* 345:337-341.
- McKenney, R.J., W. Huynh, R.D. Vale, and M. Sirajuddin. 2016. Tyrosination of alpha-tubulin controls the initiation of processive dynein-dynactin motility. *EMBO J.* 35:1175-1185.
- McKenney, R.J., M. Vershinin, A. Kunwar, R.B. Vallee, and S.P. Gross. 2010. LIS1 and NudE induce a persistent dynein force-producing state. *Cell.* 141:304-314.
- Mehta, A.D., R.S. Rock, M. Rief, J.A. Spudich, M.S. Mooseker, and R.E. Cheney. 1999. Myosin-V is a processive actin-based motor. *Nature.* 400:590-593.
- Meijering, E., O. Dzyubachyk, and I. Smal. 2012. Methods for cell and particle tracking. *Methods Enzymol.* 504:183-200.
- Mercer, J.A., P.K. Seperack, M.C. Strobel, N.G. Copeland, and N.A. Jenkins. 1991. Novel myosin heavy chain encoded by murine dilute coat colour locus. *Nature.* 349:709-713.
- Miller, S., M. Yasuda, J.K. Coats, Y. Jones, M.E. Martone, and M. Mayford. 2002. Disruption of dendritic translation of CaMKIIalpha impairs stabilization of synaptic plasticity and memory consolidation. *Neuron.* 36:507-519.
- Miura, M., A. Matsubara, T. Kobayashi, M. Edamatsu, and Y.Y. Toyoshima. 2010. Nucleotide-dependent behavior of single molecules of cytoplasmic dynein on microtubules in vitro. *FEBS Lett.* 584:2351-2355.
- Mogami, T., T. Kon, K. Ito, and K. Sutoh. 2007. Kinetic characterization of tail swing steps in the ATPase cycle of Dictyostelium cytoplasmic dynein. *J Biol Chem.* 282:21639-21644.
- Mohler, J., and E.F. Wieschaus. 1986. Dominant maternal-effect mutations of *Drosophila melanogaster* causing the production of double-abdomen embryos. *Genetics.* 112:803-822.
- Moore, J.R., E.B. Krementsova, K.M. Trybus, and D.M. Warshaw. 2001. Myosin V exhibits a high duty cycle and large unitary displacement. *J Cell Biol.* 155:625-635.

- Muller, M., R.G. Heym, A. Mayer, K. Kramer, M. Schmid, P. Cramer, H. Urlaub, R.P. Jansen, and D. Niessing. 2011. A cytoplasmic complex mediates specific mRNA recognition and localization in yeast. *PLoS Biol.* 9:e1000611.
- Muller, M., K. Richter, A. Heuck, E. Kremmer, J. Buchner, R.P. Jansen, and D. Niessing. 2009. Formation of She2p tetramers is required for mRNA binding, mRNP assembly, and localization. *RNA.* 15:2002-2012.
- Munchow, S., C. Sauter, and R.P. Jansen. 1999. Association of the class V myosin Myo4p with a localised messenger RNA in budding yeast depends on She proteins. *J Cell Sci.* 112 (Pt 10):1511-1518.
- Navarro, C., H. Puthalakath, J.M. Adams, A. Strasser, and R. Lehmann. 2004. Egalitarian binds dynein light chain to establish oocyte polarity and maintain oocyte fate. *Nat Cell Biol.* 6:427-435.
- Nelson, S.R., K.M. Trybus, and D.M. Warshaw. 2014. Motor coupling through lipid membranes enhances transport velocities for ensembles of myosin Va. *Proc Natl Acad Sci U S A.* 111:E3986-3995.
- Ohashi, S., K. Koike, A. Omori, S. Ichinose, S. Ohara, S. Kobayashi, T.A. Sato, and K. Anzai. 2002. Identification of mRNA/protein (mRNP) complexes containing Puralpha, mStaufen, fragile X protein, and myosin Va and their association with rough endoplasmic reticulum equipped with a kinesin motor. *J Biol Chem.* 277:37804-37810.
- Olenick, M.A., M. Tokito, M. Boczkowska, R. Dominguez, and E.L. Holzbaur. 2016. Hook Adaptors Induce Unidirectional Processive Motility by Enhancing the Dynein-Dynactin Interaction. *J Biol Chem.* 291:18239-18251.
- Olivier, C., G. Poirier, P. Gendron, A. Boisgontier, F. Major, and P. Chartrand. 2005. Identification of a conserved RNA motif essential for She2p recognition and mRNA localization to the yeast bud. *Mol Cell Biol.* 25:4752-4766.
- Ori-McKenney, K.M., J. Xu, S.P. Gross, and R.B. Vallee. 2010. A cytoplasmic dynein tail mutation impairs motor processivity. *Nat Cell Biol.* 12:1228-1234.
- Pardee, J.D., and J.A. Spudich. 1982. Purification of muscle actin. *Methods Enzymol.* 85 Pt B:164-181.
- Park, H., B. Ramamurthy, M. Travaglia, D. Safer, L.Q. Chen, C. Franzini-Armstrong, P.R. Selvin, and H.L. Sweeney. 2006. Full-length myosin VI dimerizes and moves processively along actin filaments upon monomer clustering. *Mol Cell.* 21:331-336.

- Park, H.Y., H. Lim, Y.J. Yoon, A. Follenzi, C. Nwokafor, M. Lopez-Jones, X. Meng, and R.H. Singer. 2014. Visualization of dynamics of single endogenous mRNA labeled in live mouse. *Science*. 343:422-424.
- Pasqualato, S., F. Senic-Matuglia, L. Renault, B. Goud, J. Salamero, and J. Cherfils. 2004. The structural GDP/GTP cycle of Rab11 reveals a novel interface involved in the dynamics of recycling endosomes. *J Biol Chem*. 279:11480-11488.
- Phichith, D., M. Travaglia, Z. Yang, X. Liu, A.B. Zong, D. Safer, and H.L. Sweeney. 2009. Cargo binding induces dimerization of myosin VI. *Proc Natl Acad Sci U S A*. 106:17320-17324.
- Philo, J.S. 2000. A method for directly fitting the time derivative of sedimentation velocity data and an alternative algorithm for calculating sedimentation coefficient distribution functions. *Anal Biochem*. 279:151-163.
- Pilling, A.D., D. Horiuchi, C.M. Lively, and W.M. Saxton. 2006. Kinesin-1 and Dynein are the primary motors for fast transport of mitochondria in Drosophila motor axons. *Mol Biol Cell*. 17:2057-2068.
- Purcell, T.J., C. Morris, J.A. Spudich, and H.L. Sweeney. 2002. Role of the lever arm in the processive stepping of myosin V. *Proc Natl Acad Sci U S A*. 99:14159-14164.
- Rackham, O., and C.M. Brown. 2004. Visualization of RNA-protein interactions in living cells: FMRP and IMP1 interact on mRNAs. *EMBO J*. 23:3346-3355.
- Rai, A.K., A. Rai, A.J. Ramaiya, R. Jha, and R. Mallik. 2013. Molecular adaptations allow dynein to generate large collective forces inside cells. *Cell*. 152:172-182.
- Ramos, A., D. Hollingworth, S. Adinolfi, M. Castets, G. Kelly, T.A. Frenkiel, B. Bardoni, and A. Pastore. 2006. The structure of the N-terminal domain of the fragile X mental retardation protein: a platform for protein-protein interaction. *Structure*. 14:21-31.
- Reck-Peterson, S.L., M.J. Tyska, P.J. Novick, and M.S. Mooseker. 2001. The yeast class V myosins, Myo2p and Myo4p, are nonprocessive actin-based motors. *J Cell Biol*. 153:1121-1126.
- Reck-Peterson, S.L., and R.D. Vale. 2004. Molecular dissection of the roles of nucleotide binding and hydrolysis in dynein's AAA domains in *Saccharomyces cerevisiae*. *Proc Natl Acad Sci U S A*. 101:1491-1495.
- Reck-Peterson, S.L., A. Yildiz, A.P. Carter, A. Gennerich, N. Zhang, and R.D. Vale. 2006. Single-molecule analysis of dynein processivity and stepping behavior. *Cell*. 126:335-348.

- Redwine, W.B., R. Hernandez-Lopez, S. Zou, J. Huang, S.L. Reck-Peterson, and A.E. Leschziner. 2012. Structural basis for microtubule binding and release by dynein. *Science*. 337:1532-1536.
- Rex, C.S., C.Y. Lin, E.A. Kramar, L.Y. Chen, C.M. Gall, and G. Lynch. 2007. Brain-derived neurotrophic factor promotes long-term potentiation-related cytoskeletal changes in adult hippocampus. *J Neurosci*. 27:3017-3029.
- Roberts, A.J., T. Kon, P.J. Knight, K. Sutoh, and S.A. Burgess. 2013. Functions and mechanics of dynein motor proteins. *Nat Rev Mol Cell Biol*. 14:713-726.
- Ross, A.F., Y. Oleynikov, E.H. Kislauskis, K.L. Taneja, and R.H. Singer. 1997. Characterization of a beta-actin mRNA zipcode-binding protein. *Mol Cell Biol*. 17:2158-2165.
- Ross, J.L., K. Wallace, H. Shuman, Y.E. Goldman, and E.L. Holzbaur. 2006. Processive bidirectional motion of dynein-dynactin complexes in vitro. *Nat Cell Biol*. 8:562-570.
- Sage, D., F.R. Neumann, F. Hediger, S.M. Gasser, and M. Unser. 2005. Automatic tracking of individual fluorescence particles: application to the study of chromosome dynamics. *IEEE Trans Image Process*. 14:1372-1383.
- Sakamoto, T., A. Yildez, P.R. Selvin, and J.R. Sellers. 2005. Step-size is determined by neck length in myosin V. *Biochemistry*. 44:16203-16210.
- Schaeffer, C., B. Bardoni, J.L. Mandel, B. Ehresmann, C. Ehresmann, and H. Moine. 2001. The fragile X mental retardation protein binds specifically to its mRNA via a purine quartet motif. *EMBO J*. 20:4803-4813.
- Schlager, M.A., H.T. Hoang, L. Urnavicius, S.L. Bullock, and A.P. Carter. 2014a. In vitro reconstitution of a highly processive recombinant human dynein complex. *EMBO J*. 33:1855-1868.
- Schlager, M.A., L.C. Kapitein, I. Grigoriev, G.M. Burzynski, P.S. Wulf, N. Keijzer, E. de Graaff, M. Fukuda, I.T. Shepherd, A. Akhmanova, and C.C. Hoogenraad. 2010. Pericentrosomal targeting of Rab6 secretory vesicles by Bicaudal-D-related protein 1 (BICDR-1) regulates neuritogenesis. *EMBO J*. 29:1637-1651.
- Schlager, M.A., A. Serra-Marques, I. Grigoriev, L.F. Gumy, M. Esteves da Silva, P.S. Wulf, A. Akhmanova, and C.C. Hoogenraad. 2014b. Bicaudal d family adaptor proteins control the velocity of Dynein-based movements. *Cell Rep*. 8:1248-1256.

- Schmidt, H., and A.P. Carter. 2016. Review: Structure and mechanism of the dynein motor ATPase. *Biopolymers*. 105:557-567.
- Schroeder, C.M., J.M. Ostrem, N.T. Hertz, and R.D. Vale. 2014. A Ras-like domain in the light intermediate chain bridges the dynein motor to a cargo-binding region. *Elife*. 3:e03351.
- Schroeder, C.M., and R.D. Vale. 2016. Assembly and activation of dynein-dynactin by the cargo adaptor protein Hook3. *J Cell Biol*. 214:309-318.
- Schroer, T.A. 2004. Dynactin. *Annu Rev Cell Dev Biol*. 20:759-779.
- Sckolnick, M., E.B. Krementsova, D.M. Warshaw, and K.M. Trybus. 2013. More than just a cargo adapter, melanophilin prolongs and slows processive runs of myosin Va. *J Biol Chem*. 288:29313-29322.
- Serano, T.L., and R.S. Cohen. 1995. A small predicted stem-loop structure mediates oocyte localization of *Drosophila* K10 mRNA. *Development*. 121:3809-3818.
- Shen, Z., N. Paquin, A. Forget, and P. Chartrand. 2009. Nuclear shuttling of She2p couples ASH1 mRNA localization to its translational repression by recruiting Loc1p and Puf6p. *Mol Biol Cell*. 20:2265-2275.
- Shepard, K.A., A.P. Gerber, A. Jambhekar, P.A. Takizawa, P.O. Brown, D. Herschlag, J.L. DeRisi, and R.D. Vale. 2003. Widespread cytoplasmic mRNA transport in yeast: identification of 22 bud-localized transcripts using DNA microarray analysis. *Proc Natl Acad Sci U S A*. 100:11429-11434.
- Shi, H., N. Singh, F. Esselborn, and G. Blobel. 2014. Structure of a myosinbulletadaptor complex and pairing by cargo. *Proc Natl Acad Sci U S A*.
- Sil, A., and I. Herskowitz. 1996. Identification of asymmetrically localized determinant, Ash1p, required for lineage-specific transcription of the yeast HO gene. *Cell*. 84:711-722.
- Siomi, M.C., Y. Zhang, H. Siomi, and G. Dreyfuss. 1996. Specific sequences in the fragile X syndrome protein FMR1 and the FXR proteins mediate their binding to 60S ribosomal subunits and the interactions among them. *Mol Cell Biol*. 16:3825-3832.
- Sirajuddin, M., L.M. Rice, and R.D. Vale. 2014. Regulation of microtubule motors by tubulin isotypes and post-translational modifications. *Nat Cell Biol*. 16:335-344.
- Sivaram, M.V., M.L. Furgason, D.N. Brewer, and M. Munson. 2006. The structure of the exocyst subunit Sec6p defines a conserved architecture with diverse roles. *Nat Struct Mol Biol*. 13:555-556.

- Sladewski, T.E., C.S. Bookwalter, M.S. Hong, and K.M. Trybus. 2013. Single-molecule reconstitution of mRNA transport by a class V myosin. *Nat Struct Mol Biol.* 20:952-957.
- Sladewski, T.E., E.B. Krementsova, and K.M. Trybus. 2016. Myosin Vc Is Specialized for Transport on a Secretory Superhighway. *Curr Biol.*
- Sladewski, T.E., and K.M. Trybus. 2014. A single molecule approach to mRNA transport by a class V myosin. *RNA Biol.* 11:986-991.
- Snee, M.J., D. Harrison, N. Yan, and P.M. Macdonald. 2007. A late phase of Oskar accumulation is crucial for posterior patterning of the *Drosophila* embryo, and is blocked by ectopic expression of Bruno. *Differentiation.* 75:246-255.
- Soppina, V., A.K. Rai, A.J. Ramaiya, P. Barak, and R. Mallik. 2009. Tug-of-war between dissimilar teams of microtubule motors regulates transport and fission of endosomes. *Proc Natl Acad Sci U S A.* 106:19381-19386.
- Splinter, D., M.E. Tanenbaum, A. Lindqvist, D. Jaarsma, A. Flotho, K.L. Yu, I. Grigoriev, D. Engelsma, E.D. Haasdijk, N. Keijzer, J. Demmers, M. Fornerod, F. Melchior, C.C. Hoogenraad, R.H. Medema, and A. Akhmanova. 2010. Bicaudal D2, dynein, and kinesin-1 associate with nuclear pore complexes and regulate centrosome and nuclear positioning during mitotic entry. *PLoS Biol.* 8:e1000350.
- Steinberg, G., and M. Schliwa. 1996. Characterization of the biophysical and motility properties of kinesin from the fungus *Neurospora crassa*. *J Biol Chem.* 271:7516-7521.
- Steward, O., and W.B. Levy. 1982. Preferential localization of polyribosomes under the base of dendritic spines in granule cells of the dentate gyrus. *J Neurosci.* 2:284-291.
- Steward, O., C.S. Wallace, G.L. Lyford, and P.F. Worley. 1998. Synaptic activation causes the mRNA for the IEG Arc to localize selectively near activated postsynaptic sites on dendrites. *Neuron.* 21:741-751.
- Steward, O., and P.F. Worley. 2001. Selective targeting of newly synthesized Arc mRNA to active synapses requires NMDA receptor activation. *Neuron.* 30:227-240.
- Stuurman, N., M. Haner, B. Sasse, W. Hubner, B. Suter, and U. Aebi. 1999. Interactions between coiled-coil proteins: *Drosophila* lamin Dm0 binds to the bicaudal-D protein. *Eur J Cell Biol.* 78:278-287.

- Tadros, W., A.L. Goldman, T. Babak, F. Menzies, L. Vardy, T. Orr-Weaver, T.R. Hughes, J.T. Westwood, C.A. Smibert, and H.D. Lipshitz. 2007. SMAUG is a major regulator of maternal mRNA destabilization in *Drosophila* and its translation is activated by the PAN GU kinase. *Dev Cell*. 12:143-155.
- Takagi, Y., Y. Yang, I. Fujiwara, D. Jacobs, R.E. Cheney, J.R. Sellers, and M. Kovacs. 2008. Human myosin Vc is a low duty ratio, nonprocessive molecular motor. *J Biol Chem*. 283:8527-8537.
- Takizawa, P.A., A. Sil, J.R. Swedlow, I. Herskowitz, and R.D. Vale. 1997. Actin-dependent localization of an RNA encoding a cell-fate determinant in yeast. *Nature*. 389:90-93.
- Takizawa, P.A., and R.D. Vale. 2000. The myosin motor, Myo4p, binds Ash1 mRNA via the adapter protein, She3p. *Proc Natl Acad Sci U S A*. 97:5273-5278.
- Terawaki, S., A. Yoshikane, Y. Higuchi, and K. Wakamatsu. 2015. Structural basis for cargo binding and autoinhibition of Bicaudal-D1 by a parallel coiled-coil with homotypic registry. *Biochem Biophys Res Commun*. 460:451-456.
- TerBush, D.R., T. Maurice, D. Roth, and P. Novick. 1996. The Exocyst is a multiprotein complex required for exocytosis in *Saccharomyces cerevisiae*. *EMBO J*. 15:6483-6494.
- Torisawa, T., M. Ichikawa, A. Furuta, K. Saito, K. Oiwa, H. Kojima, Y.Y. Toyoshima, and K. Furuta. 2014. Autoinhibition and cooperative activation mechanisms of cytoplasmic dynein. *Nat Cell Biol*.
- Tripathy, S.K., S.J. Weil, C. Chen, P. Anand, R.B. Vallee, and S.P. Gross. 2014. Autoregulatory mechanism for dynactin control of processive and diffusive dynein transport. *Nat Cell Biol*. 16:1192-1201.
- Trocter, M., N. Mucke, and T. Surrey. 2012. Reconstitution of the human cytoplasmic dynein complex. *Proc Natl Acad Sci U S A*. 109:20895-20900.
- Trybus, K.M. 2008. Myosin V from head to tail. *Cell Mol Life Sci*. 65:1378-1389.
- Uchida, A., N.H. Alami, and A. Brown. 2009. Tight functional coupling of kinesin-1A and dynein motors in the bidirectional transport of neurofilaments. *Mol Biol Cell*. 20:4997-5006.
- Urnavicius, L., K. Zhang, A.G. Diamant, C. Motz, M.A. Schlager, M. Yu, N.A. Patel, C.V. Robinson, and A.P. Carter. 2015. The structure of the dynactin complex and its interaction with dynein. *Science*. 347:1441-1446.

- Vale, R.D., T. Funatsu, D.W. Pierce, L. Romberg, Y. Harada, and T. Yanagida. 1996. Direct observation of single kinesin molecules moving along microtubules. *Nature*. 380:451-453.
- Veigel, C., S. Schmitz, F. Wang, and J.R. Sellers. 2005. Load-dependent kinetics of myosin-V can explain its high processivity. *Nat Cell Biol*. 7:861-869.
- Veigel, C., F. Wang, M.L. Bartoo, J.R. Sellers, and J.E. Molloy. 2002. The gated gait of the processive molecular motor, myosin V. *Nat Cell Biol*. 4:59-65.
- Verhey, K.J., and T.A. Rapoport. 2001. Kinesin carries the signal. *Trends Biochem Sci*. 26:545-550.
- Wagner, W., S.D. Brenowitz, and J.A. Hammer, 3rd. 2011. Myosin-Va transports the endoplasmic reticulum into the dendritic spines of Purkinje neurons. *Nat Cell Biol*. 13:40-48.
- Wang, F., K. Thirumurugan, W.F. Stafford, J.A. Hammer, 3rd, P.J. Knight, and J.R. Sellers. 2004. Regulated conformation of myosin V. *J Biol Chem*. 279:2333-2336.
- Wang, Z., S. Khan, and M.P. Sheetz. 1995. Single cytoplasmic dynein molecule movements: characterization and comparison with kinesin. *Biophys J*. 69:2011-2023.
- Wanschers, B., R. van de Vorstenbosch, M. Wijers, B. Wieringa, S.M. King, and J. Fransen. 2008. Rab6 family proteins interact with the dynein light chain protein DYNLRB1. *Cell Motil Cytoskeleton*. 65:183-196.
- Warshaw, D.M., G.G. Kennedy, S.S. Work, E.B. Krementsova, S. Beck, and K.M. Trybus. 2005. Differential labeling of myosin V heads with quantum dots allows direct visualization of hand-over-hand processivity. *Biophys J*. 88:L30-32.
- Watanabe, S., T.M. Watanabe, O. Sato, J. Awata, K. Homma, N. Umeki, H. Higuchi, R. Ikebe, and M. Ikebe. 2008. Human myosin Vc is a low duty ratio nonprocessive motor. *J Biol Chem*. 283:10581-10592.
- Waterman-Storer, C.M., S.B. Karki, S.A. Kuznetsov, J.S. Tabb, D.G. Weiss, G.M. Langford, and E.L. Holzbaur. 1997. The interaction between cytoplasmic dynein and dynactin is required for fast axonal transport. *Proc Natl Acad Sci U S A*. 94:12180-12185.
- Wilkie, G.S., and I. Davis. 2001. Drosophila wingless and pair-rule transcripts localize apically by dynein-mediated transport of RNA particles. *Cell*. 105:209-219.

- Wilson, M.H., and E.L. Holzbaur. 2012. Opposing microtubule motors drive robust nuclear dynamics in developing muscle cells. *J Cell Sci.* 125:4158-4169.
- Wollert, T., D.G. Weiss, H.H. Gerdes, and S.A. Kuznetsov. 2002. Activation of myosin V-based motility and F-actin-dependent network formation of endoplasmic reticulum during mitosis. *J Cell Biol.* 159:571-577.
- Wu, X., B. Bowers, Q. Wei, B. Kocher, and J.A. Hammer, 3rd. 1997. Myosin V associates with melanosomes in mouse melanocytes: evidence that myosin V is an organelle motor. *J Cell Sci.* 110 (Pt 7):847-859.
- Wu, X.S., K. Rao, H. Zhang, F. Wang, J.R. Sellers, L.E. Matesic, N.G. Copeland, N.A. Jenkins, and J.A. Hammer, 3rd. 2002. Identification of an organelle receptor for myosin-Va. *Nat Cell Biol.* 4:271-278.
- Zhang, H., S. Elbaum-Garfinkle, E.M. Langdon, N. Taylor, P. Occhipinti, A.A. Bridges, C.P. Brangwynne, and A.S. Gladfelter. 2015. RNA Controls PolyQ Protein Phase Transitions. *Mol Cell.* 60:220-230.
- Zhang, J., R. Qiu, H.N. Arst, Jr., M.A. Penalva, and X. Xiang. 2014. HookA is a novel dynein-early endosome linker critical for cargo movement in vivo. *J Cell Biol.* 204:1009-1026.

APPENDIX I: INVOLVEMENT OF THE MYO4P TAIL IN MEMBRANE ATTACHMENT AND TETHERING

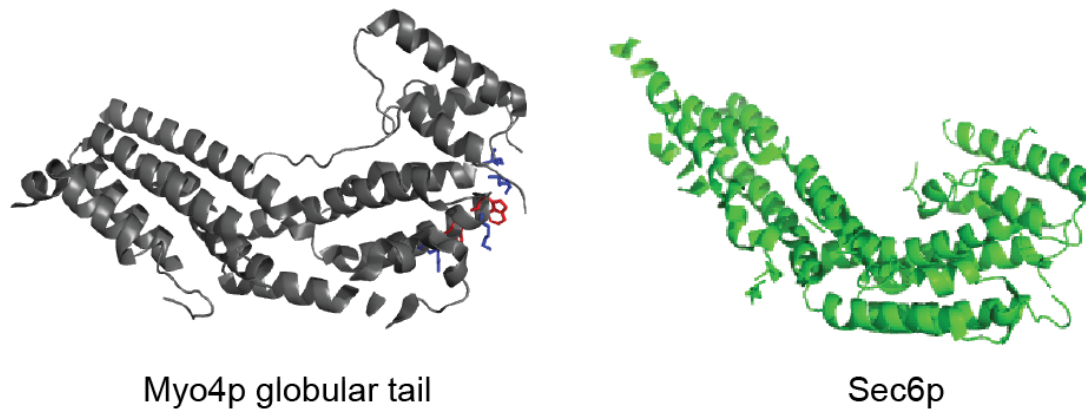
mRNA anchoring

In the presence of a localizing mRNA transcript, She2p activates Myo4p-She3p processivity by inducing the formation of a double-headed complex that takes coordinated steps on actin (Hodges et al., 2008; Krementsova et al., 2011; Sladewski et al., 2013). Thus, the dual function of She2p in binding mRNA and activation of Myo4p processivity is an elegant regulatory strategy that couples Myo4p activity with mRNA binding.

Myo4p has cellular functions outside of mRNA transport that do not require She2p. Curiously, one of these is mRNA anchoring. She2p associates with a relatively small fraction of Myo4p-She3p complexes *in vivo* indicating that She2p may only associate with motor complexes during active transport. Unlike Myo4p, She2p localization is diffuse in the bud. This indicates that once the mRNA reaches the bud tip, She2p dissociates (Gonsalvez et al., 2004). Furthermore, tethering *ASH1* mRNA to She2p supports its transport but these complexes are defective for anchoring (Gonsalvez et al., 2004). This has led to the general hypothesis that the Myo4p-She2p-She3p-mRNA complex rearranges to form an anchoring complex once it reaches the bud tip.

How does the Myo4p-mRNA complex dock into the membrane? The Myo4p globular tail shows structural similarity to Sec6p, Sec15p and Exo70p, subunits of multi-protein exocyst complex that localizes to the bud tip and is a major site of exocytosis (Heuck et al., 2010; TerBush et al., 1996) (**Appendix I - Fig. 1**). These subunits were

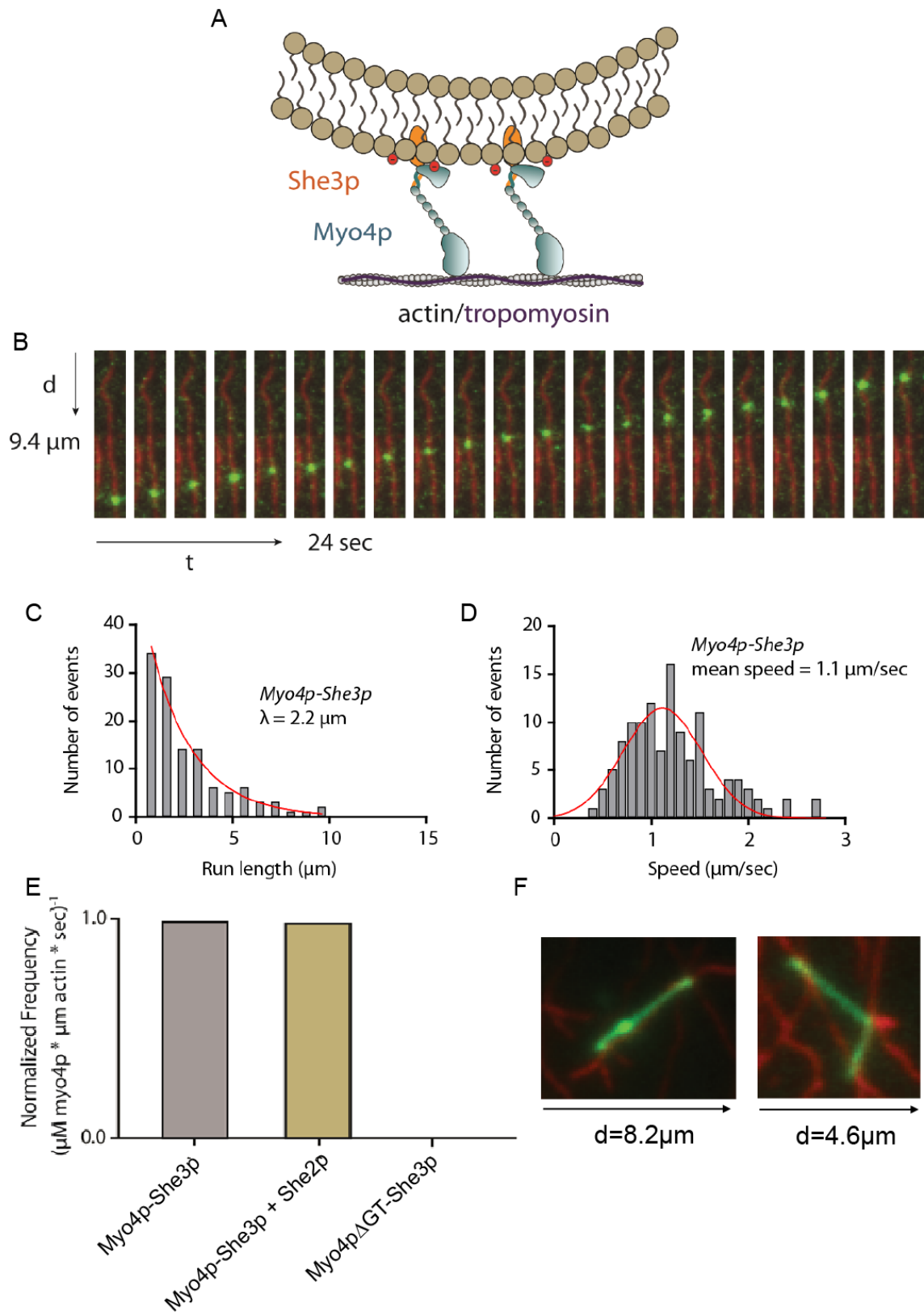
shown to play a role in directly tethering the complex to PI(4,5)P₂ in the plasma membrane through positively charged residues (He and Guo, 2009). This observation raises the intriguing possibility that Myo4p may anchor mRNA to the bud tip by directly binding to the plasma membrane.



Appendix I - Figure 1. Structural comparison between the Myo4p globular tail and exocyst subunit Sec6p. Atomic resolution structure of the Myo4p globular tail (grey) (Heuck et al., 2010) and Sec6 (green) (Sivaram et al., 2006) shows a similar protein fold.

Cortical ER transport

Myo4p and She3p are required for the inheritance of cortical ER from the mother to the daughter cell in budding yeast (Estrada et al., 2003). Cortical ER is a dynamic network of tubules that line the cell periphery. They are inherited soon after bud emergence in an actin dependent fashion (Du et al., 2001; Estrada et al., 2003). Similar to mRNA anchoring, She2p is not required for this process (Estrada et al., 2003).



Appendix I - Figure 2. Myo4p–She3p directly binds lipid vesicles through the Myo4p globular tail domain. (A) Cartoon showing that multiple Myo4p-She3p heterodimers (blue and orange) bind to vesicles (tan) containing PI(4,5)P₂ (red circles) and supports motility on actin/tropomyosin filaments. (B) Montage of a DiO labeled vesicle extruded to 200 nm in diameter (green) transported on actin (red) by Myo4p-She3p over time in a TIRF *in vitro* motility assay. Histograms showing (C) characteristic run length and (D) average speed of vesicle motility. (E) Vesicle run frequencies on actin filaments comparing Myo4p-She3p, Myo4p-She3p + She2p and a Myo4p-She3p construct lacking the Myo4p globular tail (Myo4pΔGT-She3p). (F) Image of a lipid tubule (green) formed by Myo4p-She3p stretching a lipid vesicle extruded at 650 nm over actin filaments in an *in vitro* motility assay.

We developed a single molecule assay to determine if the Myo4p-She3p complex interacts directly with lipid vesicles (collaboration with Shane Nelson and David Warshaw). DiO labeled vesicles containing 85% DOPC, 5% cholesterol and 5% PI(4,5)P₂ were prepared using extrusion. The Myo4p-She3p was premixed with vesicles and added to flow chambers containing labeled actin, and motile vesicles were visualized by TIRF microscopy. Surprisingly, the Myo4p-She3p complex associates with vesicles extruded to 200 nm in diameter and supports robust motility on actin filaments *in vitro* with a characteristic run length of 2 μm and an average speed of 1.1 μm/sec (**Appendix I - Fig. 2, A-D**). Myo4p-She3p constructs lacking the Myo4p globular tail did not support vesicle motility. Thus, the interaction between Myo4p-She3p and lipid vesicles is mediated through the globular tail domain. This is consistent with structural data showing the Myo4p tail adopts a similar fold to membrane tethering proteins. This is the first report to my knowledge that Myo4p interacts directly with membranes and supports a role for Myo4p

in directly tethering mRNA to the plasma membrane. Vesicle interactions may also be important for cortical ER inheritance.

Addition of She2p has no effect on the number of observed events (**Appendix I - Fig. 2, E**). This indicates that She2p is not required for membrane binding and motility which is consistent with *in vivo* studies showing that She2p is not involved in either mRNA anchoring or cortical ER transport (Estrada et al., 2003; Gonsalvez et al., 2004). She2p is required for Myo4p-She3p dimerization so vesicle motility is likely supported by the association of multiple Myo4p-She3p monomers which function as ensembles to support vesicle movement. However, Myo4p contains a short coiled-coil sequence at the base of the rod so it cannot be ruled out that Myo4p dimerizes when clustered on a vesicle.

Vesicles extruded to 650 nm deformed into membrane tubes that appeared to stretch out along actin filaments (**Appendix I - Fig. 2, F**). It is unlikely that Myo4p is required for the formation of cortical ER membrane tubes *in vivo* since cortical ER morphology in the cell is unaffected in Myo4p knockouts (Estrada et al., 2003). It is interesting to note that *in vitro* vesicle motility does not require PI(4,5)P₂. This is surprising since PI(4,5)P₂ is needed for membrane anchoring proteins in exocyst complexes that show structural similarity to the Myo4p globular tail (Sivaram et al., 2006).

The Myo4p globular tail domain is not required for either cortical ER inheritance or correct mRNA localization to the bud tip. However, budding yeast strains lacking the globular tail show clear defects in both processes (Bookwalter et al., 2009). Thus, the direct vesicle interaction may be one of many interactions that stabilize tethering or cortical ER transport complexes. We showed that multiple interactions between components of the

ASH1 mRNA transport complex are required for stability at physiological ionic strength (140 mM KCl). Vesicle-motor complexes are non-motile *in vitro* at 140 mM KCl suggesting other cellular components are needed to stabilize this interaction in the cell. One candidate is She2p. While She2p is not necessary for cortical ER inheritance, it has been shown to associate with ER derived vesicles in yeast cell extracts (Genz et al., 2013). Interestingly, these associations are impaired by mutations that disrupt She2p tetramerization (Genz et al., 2013). Determining the requirements for She3p and She2p in membrane transport are interesting questions to pursue to understand at a mechanistic level how Myo4p transports cortical ER in budding yeast.

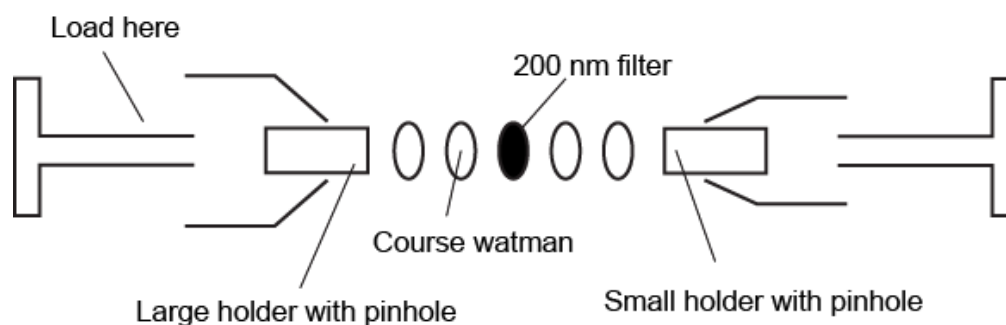
Mice that fail to express myosin Va have light colored coats due to defects in melanosome transport (Wu et al., 1997). These mice also have neurological disorders that may result from defects in cortical ER transport into dendritic spines (Wagner et al., 2011). Myosin transports ER in other systems including plants (Foissner et al., 1996) and *Xenopus* egg extracts (Wollert et al., 2002). Thus, this process is conserved in a number of organisms. Understanding the molecular mechanisms of cortical ER inheritance in budding yeast will shed light on ER migration in higher eukaryotes.

METHODS

Vesicle preparation

Lipid stocks were warmed to room temperature before opening. In a small glass tube mix 30uL 25mg/mL DOPC (85%), 2.3uL 10mg/mL cholesterol (5%), 50uL 1mg/mL PI(4,5)P₂ (5%) (AVANTI 840046X), and 1uL DiO. Being carefull not to blow the solution

out of the tube, evaporate off the chloroform using an N₂ stream. Place glass tube in eppendorph tube and speed vac 2-3 hours to form lipid sheets. Add 200uL of buffer B with no DTT (25mM Imidazole, pH 7.4, 1mM EGTA, 4mM MgCl₂, 25mM KCl). Cover with parafilm and sit overnight at 4°C. Soak extruder in liquinox overnight and rinse several times with water. Assemble extruder as shown (**Appendix I - Fig. 3**). Always wash from one side of the devise and add sample to the other. Twist syringes on slowly to avoid leakage. Load lipid mixture. Passage the sample 15-20 times through a 200nm filter. Vesicle preparations can be stored 30min-60min before use in assays. For assays used to form lipid tubes, the same preparation was used except PI(4,5)P₂ was omitted from the mixture and vesicles were extruded using a 650nm filter.



Appendix I - Figure 3. Extruder setup. From left to right: syringe containing sample, large tephlon holder with pinhole, two pieces of Watman paper soaked in water, 200nm filter, two pieces of Watman paper soaked in water, small holder with pinhole, syringe. See Avanti website for further operation details.

Vesicle motility

Clarify all proteins diluted 10/50 in B300 (25mM Imidazole, pH 7.4, 1mM EGTA, 4mM MgCl₂, 300mM KCl, 10mM DTT) 95K, 20 min. In buffer B, mix 2.8μM Myo4p-She3p, 5.6μM She2p and 5uL vesicle preparation described above. Dilute motor to 9nM in buffer B containing 0.1 mg/mL yCaM and Mlc1p, 2 μM Tpm1p, 1 mM Mg-ATP and ATP-regeneration and oxygen-scavenging systems and image vesicles moving on actin with TIRF microscopy as described previously (Krementsova et al., 2011).

REFERENCES

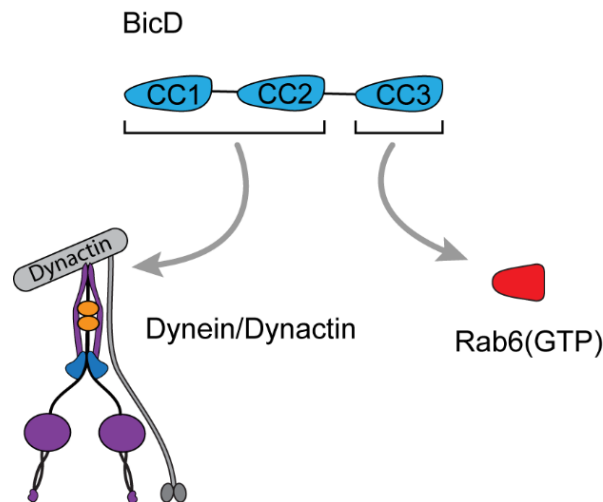
- Bookwalter, C.S., M. Lord, and K.M. Trybus. 2009. Essential features of the class V myosin from budding yeast for ASH1 mRNA transport. *Mol Biol Cell*. 20:3414-3421.
- Du, Y., M. Pypaert, P. Novick, and S. Ferro-Novick. 2001. Aux1p/Swa2p is required for cortical endoplasmic reticulum inheritance in *Saccharomyces cerevisiae*. *Mol Biol Cell*. 12:2614-2628.
- Estrada, P., J. Kim, J. Coleman, L. Walker, B. Dunn, P. Takizawa, P. Novick, and S. Ferro-Novick. 2003. Myo4p and She3p are required for cortical ER inheritance in *Saccharomyces cerevisiae*. *J Cell Biol*. 163:1255-1266.
- Foissner, I., I.K. Lichtscheidl, and G.O. Wasteneys. 1996. Actin-based vesicle dynamics and exocytosis during wound wall formation in characean internodal cells. *Cell Motil Cytoskeleton*. 35:35-48.
- Genz, C., J. Fundakowski, O. Hermesh, M. Schmid, and R.P. Jansen. 2013. Association of the yeast RNA-binding protein She2p with the tubular endoplasmic reticulum depends on membrane curvature. *J Biol Chem*. 288:32384-32393.
- Gonsalvez, G.B., J.L. Little, and R.M. Long. 2004. ASH1 mRNA anchoring requires reorganization of the Myo4p-She3p-She2p transport complex. *J Biol Chem*. 279:46286-46294.

- He, B., and W. Guo. 2009. The exocyst complex in polarized exocytosis. *Curr Opin Cell Biol.* 21:537-542.
- Heuck, A., I. Fetka, D.N. Brewer, D. Huls, M. Munson, R.P. Jansen, and D. Niessing. 2010. The structure of the Myo4p globular tail and its function in ASH1 mRNA localization. *J Cell Biol.* 189:497-510.
- Hodges, A.R., E.B. Krementsova, and K.M. Trybus. 2008. She3p binds to the rod of yeast myosin V and prevents it from dimerizing, forming a single-headed motor complex. *J Biol Chem.* 283:6906-6914.
- Krementsova, E.B., A.R. Hodges, C.S. Bookwalter, T.E. Sladewski, M. Travaglia, H.L. Sweeney, and K.M. Trybus. 2011. Two single-headed myosin V motors bound to a tetrameric adapter protein form a processive complex. *J Cell Biol.* 195:631-641.
- Sivaram, M.V., M.L. Furgason, D.N. Brewer, and M. Munson. 2006. The structure of the exocyst subunit Sec6p defines a conserved architecture with diverse roles. *Nat Struct Mol Biol.* 13:555-556.
- Sladewski, T.E., C.S. Bookwalter, M.S. Hong, and K.M. Trybus. 2013. Single-molecule reconstitution of mRNA transport by a class V myosin. *Nat Struct Mol Biol.* 20:952-957.
- TerBush, D.R., T. Maurice, D. Roth, and P. Novick. 1996. The Exocyst is a multiprotein complex required for exocytosis in *Saccharomyces cerevisiae*. *EMBO J.* 15:6483-6494.
- Wagner, W., S.D. Brenowitz, and J.A. Hammer, 3rd. 2011. Myosin-Va transports the endoplasmic reticulum into the dendritic spines of Purkinje neurons. *Nat Cell Biol.* 13:40-48.
- Wollert, T., D.G. Weiss, H.H. Gerdes, and S.A. Kuznetsov. 2002. Activation of myosin V-based motility and F-actin-dependent network formation of endoplasmic reticulum during mitosis. *J Cell Biol.* 159:571-577.
- Wu, X., B. Bowers, Q. Wei, B. Kocher, and J.A. Hammer, 3rd. 1997. Myosin V associates with melanosomes in mouse melanocytes: evidence that myosin V is an organelle motor. *J Cell Sci.* 110 (Pt 7):847-859.

APPENDIX II: ALTERNATIVE DYNEIN CARGOES AND RECRUITMENT OF KINESIN-1 FOR BIDIRECTIONAL TRANSPORT

Rab6 is a vesicular cargo adapter protein

Rab6 is a GTPase that when bound to GTP links dynein to Golgi-derived vesicles by binding CC3, the C-terminal coiled-coil of BicD (Grigoriev et al., 2007; Liu et al., 2013; Martinez et al., 1997) (**Appendix II - Fig. 1**). Isothermal calorimetry and gel filtration show that Rab6 binds BicD with a subunit stoichiometry of 2:2 (1 BicD dimer: 2 Rab6 monomers) (Liu et al., 2013), indicating that Rab6 is able to bind to both chains of the BicD dimer (Liu et al., 2013).



Appendix II - Figure 1. Diagram showing interactions between BicD, dynein/dynactin and Rab6. The N-terminus of BicD (blue) binds dynein through its coiled-coil CC1 and CC2 domains. The GTP-bound form of Rab6 (Rab6^{GTP}) binds the C-terminal cargo binding domain of BicD, CC3.

BicD has a well-established role in linking dynein to cargo. Thus, it was surprising when studies in HeLa cells showed that the majority of Rab6-associated vesicles exit the

Golgi and move toward the microtubule plus-ends to the cell periphery, consistent with a kinesin-driven process (Grigoriev et al., 2007). Yeast-2-hybrid and mass spectrometry analysis showed that kinesin-1 associates with the second coiled-coil domain (CC2) in BicD (Grigoriev et al., 2007). Knockdown of kinesin-1 resulted in a significant decrease in the run length of vesicles (Grigoriev et al., 2007). Dynein was also shown to be important for plus-end movements in this system. This result indicates that dynein is an important component in this process, but kinesin activity ultimately determines the direction of transport.

These studies led to the hypothesis that Rab6-BicD is capable of recruiting both dynein and kinesin motors for transport, and that kinesin “wins” to promote plus-end movement of Rab6 associated cargoes. In support of this idea, Rab6 vesicle motion is bidirectional. The molecular mechanisms underlying bidirectional transport are currently a subject of intense debate. Simplified tug-of-war models are sufficient to explain some bidirectional behavior. These models describe a mechanical competition between dynein and kinesin where the strongest force “wins” and determines the directional bias of the cargo (Hendricks et al., 2010; Soppina et al., 2009). A simple prediction from this model is that if you eliminate one of these motors from the cell, the other motor will dominate the motility. Intriguingly, for many cargoes (e.g. localizing mRNAs and Rab6-associated vesicles), the opposite is observed. Knocking down either dynein or the kinesin-1 heavy chain inhibits the motility of cargoes in both the retrograde and anterograde directions (Bullock et al., 2006; Grigoriev et al., 2007; Ling et al., 2004). This property has also been observed for fast axonal transport in squid axoplasm, melanosome transport in *Xenopus*

laevis, axonal neurofilament transport in cultured sympathetic neurons, and the transport of multiple cargoes in *Drosophila* (Ally et al., 2009; Gross et al., 2002; Martin et al., 1999; Pilling et al., 2006; Uchida et al., 2009; Waterman-Storer et al., 1997). Results from these studies indicate that the activities of kinesin and dynein are tightly coupled (Ling et al., 2004), but the molecular mechanisms are unknown. Here we present work toward understanding how dynein and kinesin are coordinated on Rab6 cargoes to produce plus-end movement in the cell.

Rab6^{GTP} alone is not sufficient to activate BicD

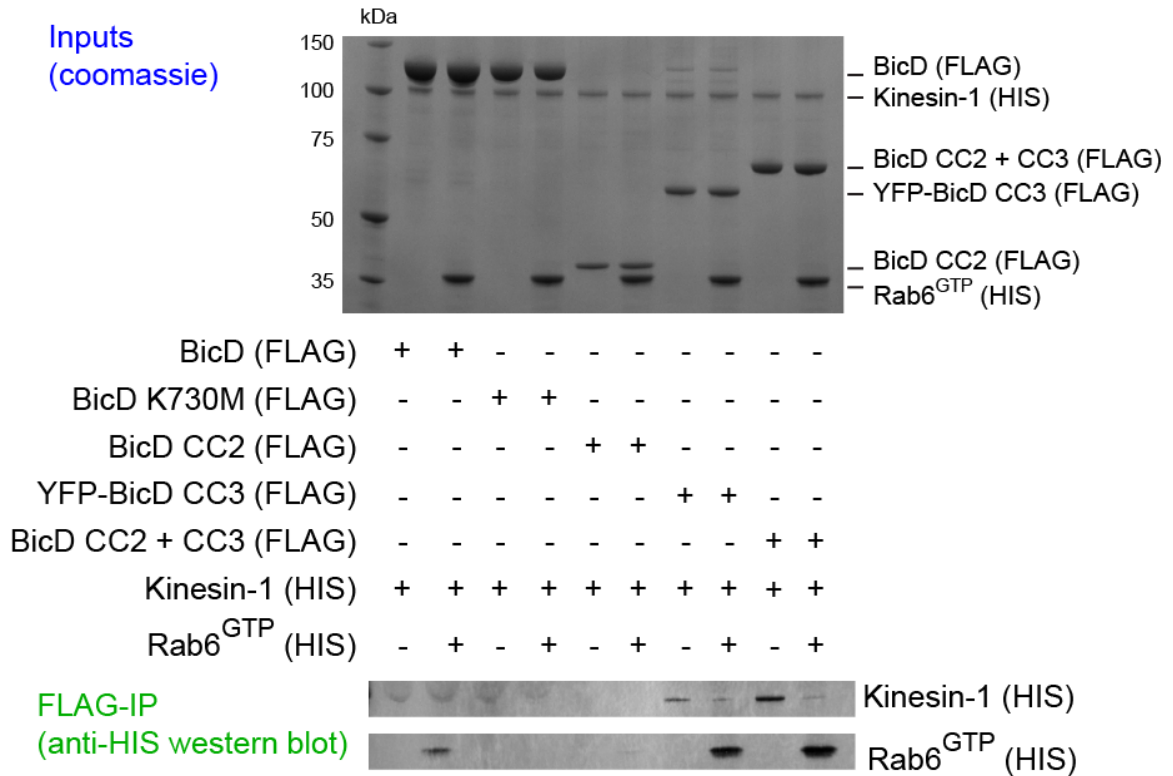
The simplest model of activation of BicD by Rab6 cargoes is that the nucleotide state of Rab6 determines binding and activation of BicD. The GTP-bound form of Rab6 is the active, membrane-bound state, while the GDP-bound form is predominantly cytosolic (Grosshans et al., 2006). We tested if Rab6 binding to BicD relieves its auto-inhibition and activates dynein for transport.

We reconstituted a complex containing Rab6^{GTP} with a C-terminal biotin tag bound to a quantum dot (Qdot), full-length BicD, dynein and dynactin, and visualized the complex in a flow cell on labeled microtubules using a single molecule TIRF assay. A mutant version of Rab6 (Rab6Q71L) was used to ensure that it exists in the GTP bound state (Bergbrede et al., 2005). In buffers containing 25 mM KOAc, complexes visualized with a Qdot on Rab6^{GTP} bound to microtubules but did not move. Controls showed that omitting any component of the reconstitution resulted in no quantum dot decoration of microtubules. These results show that dynein/dynactin is recruited to BicD-Rab6 complexes at low ionic strength but other components may be required to activate the dynein-dynactin-BicD-

Rab6^{GTP} complex for transport. We explored the possibility that kinesin-1 binding to BicD activates dynein-dynactin-BicD-Rab6 complexes for motility as suggested from cell biological studies.

To confirm that *Drosophila* kinesin-1 lacking its light chains interacts with the second coiled-coil domain (CC2) of *Drosophila* BicD (Grigoriev et al., 2007) and that Rab6^{GTP} interacts with the third coiled-coil (CC3) of BicD, pull-downs were performed with purified proteins. We show that Rab6^{GTP} but not kinesin binds full-length BicD (**Appendix II - Fig. 2**). As a control, a single point mutation in BicD (K730M) is sufficient to disrupt this binding. Pull-downs with BicD truncation constructs show that Rab6^{GTP} binds specifically with the CC3 of BicD consistent with previous studies (Matanis et al., 2002). Surprisingly, we find that *Drosophila* kinesin interacts with the a BicD construct containing CC2 + CC3 domains of BicD and not with construct containing only the CC2 domain, implying that kinesin interacts with the CC3 domain of BicD. The interaction between *Drosophila* kinesin and *Drosophila* BicD CC3 domain is surprising because previous studies, using immunoprecipitation and yeast-2-hybrid assays, show that human kinesin interacts with the CC2 domain of human BicD2 (Grigoriev et al., 2007).

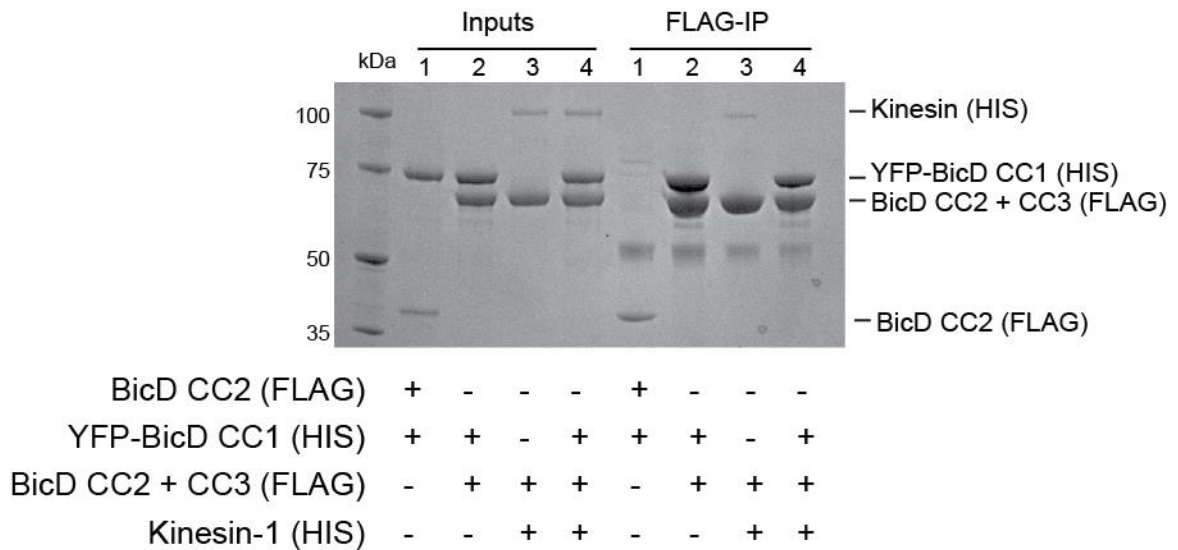
Because both Rab6^{GTP} and kinesin interact with the CC3 domain we tested if excess amounts of Rab6^{GTP} outcompetes kinesin for BicD binding. We show that the presence of Rab6^{GTP} prevents kinesin from binding BicD, indicating that kinesin and Rab6^{GTP} interact with similar regions within the CC3 domain (**Appendix II - Fig. 2**).



Appendix II - Figure 2. FLAG BicD pull-downs with *Drosophila* kinesin-1 (no light chains) and Rab6^{GTP}. (Top) Coomassie stained gel showing inputs of purified proteins. All BicD constructs contain a C-terminal FLAG tag for purification. *Drosophila* BicD is full-length and BicD K730M contains a point mutation that prevents Rab6^{GTP} binding. Other *Drosophila* BicD truncation constructs are BicD CC2, BicD CC2 + CC3, and YFP-BicD CC3. *Drosophila* kinesin-1 is full length without light chains, and has a C-terminal HIS tag. Rab6 (Q71L) is a mutant version of Rab6 that is locked in the GTP-binding state (Rab6^{GTP}). HIS western blot of FLAG immunoprecipitations shows that Rab6^{GTP} binds full-length BicD but not BicD K730M. Rab6^{GTP} binds to BicD CC3 and BicD CC2 + CC3 constructs but not the BicD CC2 construct. Kinesin-1 does not bind to full-length BicD or BicD CC2, but does bind to BicD constructs containing only the CC3 domain. Rab6^{GTP} binding outcompetes kinesin-1 for these interactions.

We show that kinesin interacts with truncation constructs of BicD but not with full-length BicD (**Appendix II - Fig. 2**). Previous studies also show that the interaction between human kinesin and human BicD2 is suppressed with full-length BicD, indicating that BicD is auto-inhibited for kinesin-1 binding (Grigoriev et al., 2007).

Because our data indicate that *Drosophila* kinesin binds to the CC3 of BicD, we tested if a BicD construct containing only the CC1 domain outcompetes kinesin for the CC3 domain. We repeated previous results showing that kinesin-1 interacts with the third coiled-coil domain of BicD (CC3), but not with CC2 (**Appendix II - Fig. 3**). Interestingly, we find that the interaction between kinesin and BicD can be outcompeted by a BicD construct containing CC1, which binds the CC3 domain of BicD (**Appendix II - Fig. 3**). Identification of kinesin-1 was further confirmed using an anti-HIS western blot (data not shown). These data imply that kinesin cannot bind to full-length BicD because the intramolecular interaction between CC1 and CC3 prevents kinesin from binding the CC3 domain of BicD.



Appendix II - Figure 3. FLAG BicD pull-downs with *Drosophila* kinesin-1. Input (left lanes). BicD constructs used are: *Drosophila* BicD CC2 domain with FLAG tag; and *Drosophila* BicD CC2 + CC3 with a FLAG tag; human HIS-YFP-BicD CC1 that contains the dynein interacting domain fused to YFP and a HIS tag. *Drosophila* kinesin is full length kinesin-1 with a HIS tag. FLAG immunoprecipitations (FLAG-IP) (right lanes) show that BicD CC1 interacts with BicD CC2 + CC3 but not with BicD CC2 (lanes 1 and 4). BicD

CC2 + CC3 interacts with kinesin and this interaction is outcompeted by BicD CC1 (lanes 3 and 4).

Taken together, these data show that BicD is auto-inhibited for kinesin binding and that Rab6^{GTP} and kinesin binding to BicD are mutually exclusive. In the cell, Rab6 associated vesicles require kinesin-1 for transport (Grigoriev et al., 2007), implying that kinesin and Rab6 cooperate to move cargo. There may be several reasons for the apparent inconsistency between *in vivo* and *in vitro* data. First, an excess of Rab6 was used in our pull-downs. Experiments should be repeated with an equimolar amount of Rab6 and kinesin-1 to determine if both can bind simultaneously to BicD. Additionally, differences may exist between *Drosophila* and mammalian systems. Pull-downs should be repeated using mammalian sequences of kinesin and BicD2. Another more interesting possibility is that dynein-dynactin are required for simultaneous kinesin-1 and Rab6^{GTP} associations with BicD, consistent with cell biological data showing impaired plus-end directed motility of Rab6 vesicles in cells depleted for dynein (Grigoriev et al., 2007).

To determine if kinesin-1 binding to BicD requires dynein/dynactin association, single molecule pull-downs on microtubules can be performed (described in **Chapter 3**). Reconstitutions would include dynein, dynactin, YFP-BicD, and kinesin-1 with a C-terminal biotin tag for Qdot attachment. If kinesin-1 bound quantum dots co-localize with YFP-BicD then this is good evidence to support the hypothesis that kinesin-1 will only bind dynein/dynactin associated BicD. Various BicD truncation constructs can be used to verify the BicD domain that binds kinesin-1. Single molecule pull-downs can also be used to test the requirements for Rab6^{GTP} to bind to dynein, dynactin, and YFP-BicD.

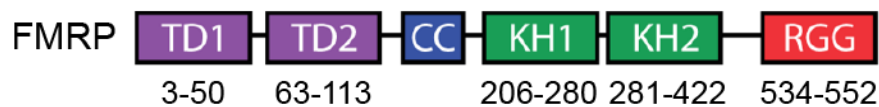
Activation of dynein/dynactin by the BicD-Egalitarian complex requires mRNA (**Chapter 3**). The requirement of an mRNA cargo for BicD activation raises the question of whether a vesicular cargo is required for the activation of a dynein-dynactin-BicD-Rab6^{GTP} complex. Our results using reconstituted mRNA-dynein complexes show that recruitment of multiple copies of Egalitarian to mRNA is needed for efficient activation of mRNA motility. Similarly, it is possible that vesicles containing multiple copies of Rab6^{GTP} are needed to activate BicD for recruitment and activation of dynein (for details see thesis discussion in **Chapter 4**). This hypothesis can be tested by binding Rab6^{GTP} containing a C-terminal biotin tag to streptavidin bound liposomes (Nelson et al., 2014). Then, a fully reconstituted dynein-vesicular transport complex can be assembled by adding dynein, dynactin and BicD. Labeling the vesicles allows activated complexes to be visualized moving on microtubules in a TIRF-based single molecule motility assay. Based on our results from mRNA reconstitutions, the recruitment of multiple Rab6-BicD complexes will be required to recruit and activate BicD-dynein-dynactin for long range transport on microtubules *in vitro*.

Another possibility is that Rab6^{GTP} can activate dynein for transport in the absence of cargo, but under single molecule conditions that were not tested here. Experiments showing that Rab6^{GTP} did not activate dynein for transport were performed under low salt conditions and at limiting Rab6 stoichiometry. These assays should be repeated under more physiological salt conditions to test whether the lack of movement was an artifact of sub-optimal ionic strength conditions. The stoichiometry of Rab6^{GTP} binding to BicD was shown to be one BicD dimer to two Rab6 monomers. It is possible that having Rab6

limiting may have prevented two Rab6 molecules from binding BicD. To test this possibility, experiments should be repeated with an excess of Rab6 over BicD. Optimization of both ionic strength and stoichiometry will be needed to fully understand the requirements for BicD activation by Rab6 cargoes for dynein motility.

FMRP is an mRNA cargo adapter protein

Fragile X mental retardation protein (FMRP) is another adapter that links dynein to mRNA cargoes by binding to the C-terminal region of BicD (Bianco et al., 2010). The N-terminal region of FMRP contains two Tudor domains (TD1 and TD2) important for mediating protein-protein interactions, followed by a coiled-coil sequence (CC) that may promote protein dimerization (Ramos et al., 2006; Siomi et al., 1996). FMRP binds mRNA through two central K Homology domains (KH1 and KH2) and a C-terminal RGG box (Darnell et al., 2005; Schaeffer et al., 2001) (**Appendix II - Figure 4**).



Appendix II - Figure 4. FMRP domain structure. FMRP contains N-terminal tudor domains (TD1 and TD2), a coiled-coil domain (CC), and three predicted mRNA binding domains (KH1, KH2, and RGG). Amino acid numbers are shown below each domain.

FMRP plays a role in transporting mRNA to dendritic spines of neurons (Rackham and Brown, 2004). Immunoprecipitation studies in *Drosophila* show that FMRP binds specifically to the CC3 domain of BicD and this interaction requires a localizing mRNA transcript (Bianco et al., 2010). FMRP also binds kinesin-1 in cell extracts (Ling et al.,

2004). In *Drosophila* S2 cells this interaction is through the kinesin-1 heavy chain (Ling et al., 2004), while in mammalian neurons, the interaction is through the kinesin-1 light chain (Dictenberg et al., 2008). The association of FMRP directly with kinesin and indirectly with dynein, through BicD, indicates that these motors likely cooperate to transport FMRP mRNA granules (Gagnon and Mowry, 2011; Ling et al., 2004).

FMRP forms protein droplets

Using pull-downs and single molecule techniques, we have not been able to replicate results suggesting a direct interaction between FMRP and *Drosophila* kinesin-1 (Ohashi et al., 2002). One possibility is that kinesin-1 interacts indirectly with FMRP via its association with BicD. Another possibility is that only mRNA bound FMRP will interact with kinesin. To test this latter idea, we reconstituted complexes *in vitro* containing a labeled *FMR1* mRNA transcript, FMRP and a constitutively active construct of kinesin-1 lacking hinge 2 in the stalk (Friedman and Vale, 1999), and visualized complexes on microtubules. FMRP and kinesin were expressed using the baculovirus/*Sf9* system. We first confirmed that kinesin-1 lacking hinge 2, when labeled directly with a quantum dot, moves processively on microtubules. However, we did not observe *FMR1* mRNA motility on microtubules. Because motility with the constitutively active kinesin construct is an indicator of mRNA binding, we concluded that mRNA-bound FMRP does not interact with kinesin. Addition of full-length BicD, or a truncated BicD construct containing only the CC3 domain, did not promote FMRP binding to kinesin. We also ruled out that the kinesin light chain was important for this interaction, and directly imaged FMRP with a YFP-

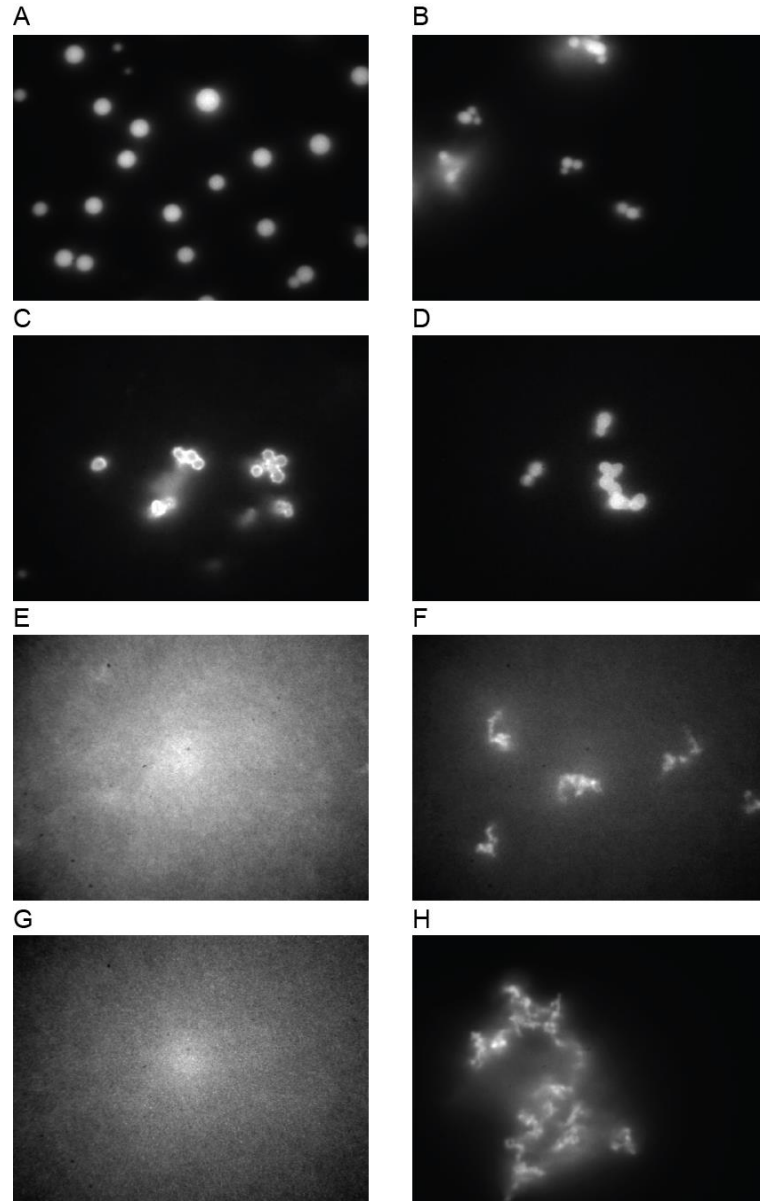
FMRP fusion to rule out defects in mRNA binding. Thus, additional factors are likely required to link FMRP to kinesin-1.

FMRP contains stretches of poly-glutamine sequences and disordered regions that are similar to the those found in the mRNA binding protein Whi3 (Zhang et al., 2015). These sequences allow the mRNA binding protein Whi3 to undergo a phase transition to form protein droplets (Jiang et al., 2015; Zhang et al., 2015). Interestingly, mRNA is needed to drive the phase transition at higher salt concentrations (Zhang et al., 2015). These protein droplets create a microenvironment in the cell with distinct properties from the cytoplasm.

We find that FMRP also undergoes a phase transition. At 25 mM KCl, an FRMP YFP fusion forms regular ~3.5 μ m diameter protein droplets (**Appendix II - Fig. 5, A**). Mixing ratios of 1:8 YFP-FMRP to FMRP, the protein droplets are smaller (~2 μ m) and tend to aggregate (**Appendix II - Fig. 5, B**). Droplets formed with only FMRP are able to bind labeled *FMR1* mRNA (**Appendix II - Fig. 5, C**) and a BicD construct containing YFP fused to the CC3 of BicD (YFP-BicD-CC3) (**Appendix II - Fig. 5, D**). Binding of FMRP to BicD was independent of mRNA binding and vice versa. At physiological ionic strength, FMRP droplets do not form (**Appendix II - Fig. 5, E**). Interestingly, addition of *FMR1* mRNA to FMRP at physiological ionic strength induces the formation of aggregate-like structures. These particles are likely composed of multiple *FMR1* mRNA transcripts given their large ~6 μ m size (**Appendix II - Fig. 5, F**).

Particles do not form in the absence of FMRP (**Appendix II - Fig. 5, G**) so they are not the result of an interaction between *FMR1* mRNA and YFP-BicD-CC3 that is used

to visualize the structures. When left overnight, the FMRP-mRNA structures continue to oligomerize into large aggregates (**Appendix II - Fig. 5, H**).



Appendix II - Figure 5. Formation of FMRP protein droplets and mRNA-dependent FMRP micro-domains. Protein droplets visualized with YFP-FMRP were formed from (A) YFP-FMRP and (B) 1:8 ratio of WT FMRP: YFP-FMRP. (C) Alexa488 *FMRI* mRNA bound to unlabeled FMRP protein droplets. (D) YFP-BicD-CC3 bound to unlabeled FMRP

protein droplets. **(E)** FMRP does not form protein droplets at physiological ionic strength (140 mM KCl). **(F)** Addition of mRNA induces the formation of FMRP aggregates at 140 mM KCl. **(G)** Formation of mRNA-dependent structures requires FMRP. **(H)** Structures aggregate to form large structures with extended incubation times. YFP-BicD-CC3 was used for visualization in panels D-H.

Our finding that FMRP forms mRNA-dependent micro-domains may explain why single molecules of FMRP do not bind kinesin and support *FMRI* mRNA motility. Single molecule motility may have not been observed because FMRP is likely an integral component of the mRNA cargo that is required for motility. *In vivo* studies show that FMRP oligomerizes *in vivo* (Siomi et al., 1996) supporting the idea that it may form micro-domains in the cell. In addition, FMRP associates with heavy sedimenting structures (Siomi et al., 1996), and cargoes visualized in the cell appear as large granules (Rackham and Brown, 2004).

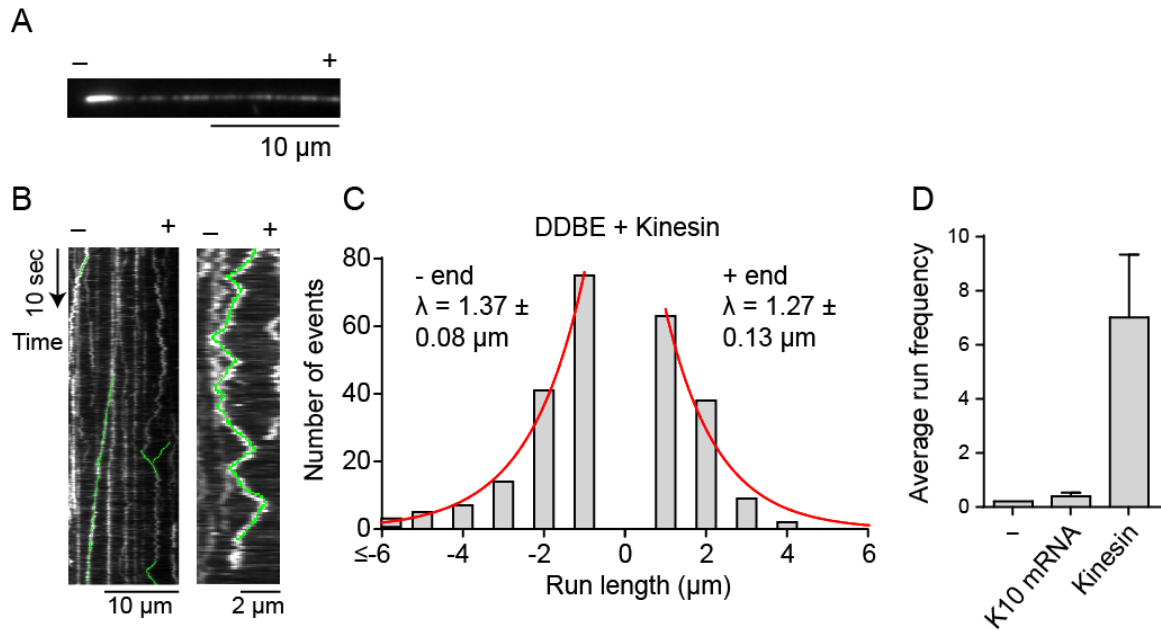
The requirement for mRNA to form FMRP droplets may explain why the association of FMRP with BicD requires mRNA in *Drosophila* S2 cells (Bianco et al., 2010). One possibility is that FMRP only interacts with BicD in mRNA-dependent micro-domains.

One exciting result from these studies is that FMRP-mRNA droplets appear to promote the recruitment of BicD. Our data suggest that Egalitarian oligomerizes on an mRNA cargo and this allows Egalitarian to interact functionally with BicD (**Chapter 3**). Thus, one possibility is that FMRP only interacts functionally with BicD when oligomerized into micro-domains which requires mRNA. This would ensure that only FMRP/mRNA micro-domains activate BicD for dynein transport on microtubules.

Cell biological data suggest that kinesin and dynein cooperate to move FMRP cargoes. Thus, *in vitro* reconstitution of FMRP complexes coupling dynein and kinesin would offer a useful system to understand how motors coordinate their activities for net directional motion. These studies are ambitious given the number of purified components involved, but would certainly yield mechanistic insight into how the activities of opposing motors are coupled on native cargoes.

Dynein and kinesin motor coupling through a shared cargo

We have worked towards coupling dynein and *Drosophila* kinesin-1 through BicD and the adapter Egalitarian. We previously showed (**Chapter 3**) that mRNA is required for motility of complexes containing dynein, dynactin, BicD and Egalitarian. Interestingly, when we add quantum dot labeled full-length *Drosophila* kinesin-1 (without a light chain) to reconstitutions containing dynein, dynactin, BicD and Egalitarian, and add them to a flow cell containing polarity marked microtubules (**Appendix II - Fig. 6, A**), we observe bidirectional motility in the absence of mRNA (**Appendix II - Fig. 6, B**). Long directed runs were observed in both directions on microtubules (**Appendix II - Fig. 6, C**). In the absence of cargo, full-length kinesin-1 is auto-inhibited. Thus, we show that kinesin is active when incorporated into complexes containing dynein, dynactin, BicD, and Egalitarian. Importantly, controls showed that this motility required both BicD and Egalitarian. This result indicates that kinesin-1 will only associate with Egalitarian-bound BicD and/or dynein-dynactin.



Appendix II - Figure 6. Bidirectional motility of reconstituted complexes containing dynein and *Drosophila* kinesin-1. (A) Polarity marked microtubule (Howard and Hyman, 1993) to determine direction of transport. (B) Kymographs (time vs displacement) showing bidirectional motility of complexes containing dynein, dynactin, BicD, Egalitarian, and kinesin labeled with a Qdot in the absence of mRNA. Green segments indicate directed runs defined by moving continuously for $>1 \mu\text{m}$. (C) Histogram quantifying run lengths (λ) in the minus or plus-end directions. (D) Run frequency (normalized per μM dynein per μm microtubule per sec) of complexes containing dynein, dynactin, BicD, Egalitarian in the absence or presence of *K10* mRNA and in the presence of kinesin. Kinesin enhances run frequency 17-fold in the absence of mRNA.

The most striking result is that kinesin-1 enhances run frequency of the dynein-dynactin-BicD-Egalitarian complex much more effectively compared to a localizing mRNA transcript. The reason for this is not yet clear, but suggests that kinesin-1 is likely part of the dynein-*K10* complex and functions to promote transport by either acting as a tether or shifting BicD to a more fully activated state (**Appendix II - Fig. 6, D**). This behavior is consistent with the observed co-dependence of motors in cargo transport. It is also consistent with the observation that mRNA transport in the cell is bidirectional

(Bullock et al., 2006). Our data showing unidirectional *K10* mRNA motility by dynein, dynactin, BicD and Egalitarian (**Chapter 3**) contrasts with the bidirectional motility observed *in vivo*. There is currently no evidence that any kinesin is associated with localizing mRNAs in *Drosophila*, so these data are the first evidence suggesting that a kinesin may be involved.

A number of questions need to be addressed regarding how kinesin-1 is involved in *K10* mRNA transport. We demonstrate that mRNA is required to activate the BicD-Egalitarian complex for dynein recruitment and minus-end directed transport. Here we show that kinesin-1 activates motility in the absence of a localizing mRNA transcript. However, this motility has no net bias in direction (**Appendix II - Fig. 6, C**). One possibility is that rather than simply being an activator, *K10* mRNA may serve to also bias the direction of mRNA transport by selectively activating dynein. This idea would be consistent with cell biological data showing that *K10* mRNA moves bidirectionally with a net minus-end bias (Bullock et al., 2006). Interestingly, even non-localizing mRNAs move bidirectionally in the cell, but with no net bias (Bullock et al., 2006). These movements require dynein, consistent with a role for mRNA in biasing direction rather than initiating transport (Bullock et al., 2006).

To determine how a localizing mRNA affects the net movement of bidirectional motility, these experiments should be repeated in the presence of *K10* mRNA. Dual labeling both the mRNA and kinesin is needed to ensure that complexes contain both components. I predict that a *K10* mRNA would bias the direction of dynein and kinesin-containing complexes to the minus end of the microtubule by selective activation of dynein.

Another question is whether the auto-inhibition of kinesin-1 is fully relieved when incorporated into BicD-containing complexes. To address this idea, a constitutively activated kinesin-1 lacking a hinge region in the stalk (Friedman and Vale, 1999) should be used in place of full-length kinesin in reconstitutions without mRNA. If directionality is biased to the plus-end, then we can infer that wild-type kinesin exists in a partially activated form when bound to BicD.

Our results indicate that kinesin-1 interacts with BicD via the CC3 coiled-coil domain (**Appendix II - Figure 2**). However previous studies show that the interaction is mediated through the CC2 domain (Grigoriev et al., 2007). Also, we show that Rab6^{GTP} out-competes kinesin-1 from CC3 (**Appendix II - Figure 3**). This observation is also inconsistent with our data implying that kinesin and Egalitarian bind simultaneously to motile complexes (**Appendix II - Figure 6, B**). One explanation is that kinesin has a different binding mode when BicD is bound to dynein and dynactin. In support of an alternative binding mode, the CC3 of BicD is shown to contain a heterotypic coiled-coil (Liu et al., 2013) (explained in detail in **Chapter 4**). The dynein coiled-coil stalk also changes its registry, which influence the binding affinity of dynein to microtubules (Carter, 2013). Thus, its conceivable that similar registry changes in BicD may alter kinesin binding affinity to the CC2 domain. Dynein-dynactin binding to BicD may induce a change in the heptad repeat in CC2 that provides an interface for kinesin-1 binding. Binding of kinesin-1 to dynein/dynactin-bound BicD can be tested using single molecule pull-downs on microtubules. Quantum dot labeled kinesin-1, dynein and dynactin can be added to a construct of BicD containing only the CC1 and CC2 domains labeled with YFP, and

monitored for binding on microtubules in the presence of AMP-PNP. If kinesin-1 co-localized with BicD then we can conclude that kinesin binds to the CC2 domain only when CC1 is complexed with dynein and dynactin.

METHODS

mRNA constructs

Constructs for the production of *Drosophila* FMRP mRNA (NP_611645.1 and NM_137801.4) includes the entire coding region of FMRP plus 233 bp of the 5'UTR. *K10* mRNA constructs are described in **Chapter 3**. All mRNA constructs were cloned behind the SP6 promoter in the pSP72 vector (Promega) followed by a polyA16 tail and an EcoRV site to allow the vector to be bluntly opened for use as a template for RNA transcription.

Protein constructs

Expression constructs for full-length *Drosophila* BicD (NP_724056.1 and NM_165220.3) and constitutively active human BicD2^{CC1} (NM_015250 or NP_056065.1) are described in **Chapter 3**. *Drosophila* BicD truncation constructs (NP_724056.1 & NM_165220.3) were cloned with an N-terminal FLAG and biotin tag or N-terminal FLAG and monomeric YFP tag where indicated and inserted into pACSG2 for *Sf9*/baculovirus expression. BicD CC2 contains the second coil-coiled region (amino acids L318-Q557). BicD CC2 + CC3 contains also the third coil-coiled region (amino acids L318-F782). YFP-BicD CC3 contains only the third coiled-coil region (amino acids A536-F782). YFP-BicD CC3 contains only the third coiled-coil region (amino acids A536-F782).

Full-length *Drosophila* Fragile Mental Retardation Protein (FMRP) (NP_611645.1 and NM_137801.4) was cloned from *Drosophila* S2 cDNA into pACSG2 for *Sf9*/baculovirus expression containing a C-terminal FLAG tag. *Drosophila* kinesin-1 heavy chain (AAD13353.1) was cloned into pACSG2 with either a C terminal FLAG or HIS tag for purification from *Sf9*/baculovirus. Both wild type and a constitutively active construct of kinesin-1 construct lacking hinge 2 (K521-D641) (Friedman and Vale, 1999) contains a C-terminal biotin tag for streptavidin conjugated-Qdot (Invitrogen) attachment. Constructs for expressing Rab6, Egalitarian, and rigor kinesin used for microtubule attachment to flow chambers are described in **Chapter 3**.

Protein expression and purification

Drosophila FMRP containing a N-terminal FLAG tag for affinity purification was expressed in the *Sf9*/baculovirus system and purified similar to Egalitarian described in Chapter 3 except that protein was dialyzed against storage buffer (25 mM Imidazole, pH 7.4, 300 mM NaCl, 1 mM EGTA, 50% glycerol, 1 mM DTT, 0.1 µg/mL leupeptin) for long term storage at -20°C. Purification of Rab6^{GTP} is described in **Chapter 3**.

Drosophila full-length kinesin-1 or a construct of kinesin-1 lacking the hinge 2 region containing a C-terminal FLAG tag was expressed without light chains and purified as described for full-length BicD (**Chapter 3**) except that lysis buffers contained 1 mM grade II MgATP and the purified protein was dialyzed into storage buffer (25 mM Imidazole, pH 7.4, 300 mM NaCl, 1 mM EGTA, 50% glycerol, 1 mM DTT, 0.1 µg/mL leupeptin) supplemented with 50 µM MgATP, snap frozen, and stored at -80°C.

For full-length kinesin constructs containing a C-terminal HIS tag, protein was purified similar to Egalitarian-HIS (**Chapter 3**), except that lysis and wash buffers contained 200 mM KCl and the purified protein was dialyzed into storage buffer (25 mM Imidazole, pH 7.4, 200 mM NaCl, 1 mM EGTA, 50% glycerol, 1 mM DTT, 0.1 μ g/mL leupeptin) supplemented with 100 μ M MgATP, snap frozen, and stored at -80°C.

Single molecule motility assays with Rab6^{GTP}

For Rab6 motility, 0.1 μ M nucleotide exchanged Rab6^{GTP} (see above) was mixed with 0.2 μ M BicD, 0.2 μ M dynein and dynactin and 0.2 μ M 655 quantum dots (Invitrogen) in buffer B (30 mM HEPES, pH 7.4, 25 mM KOAc, 2 mM MgOAc, 1 mM EGTA, 10% glycerol, 10 mM DTT) containing 2 mg/mL BSA and incubated 20 min at room temperature. The complex was then diluted 25-fold and added to a PEGylated flow cell containing adhered labeled microtubules for imaging of single molecules of quantum-dot bound Rab6 moving on microtubules in buffer Go25 (30 mM HEPES, pH 7.4, 25 mM KOAc, 2 mM MgOAc, 1 mM EGTA, 10% glycerol, 2 mM MgATP, 20 mM DTT, 8 mg/mL BSA, 0.5 mg/mL κ -casein, 0.5% pluronic F68, 10 μ M paxitaxol and an oxygen scavenger system (5.8 mg/mL glucose, 0.045 mg/mL catalase, and 0.067 mg/mL glucose oxidase; Sigma-Aldrich)). Procedures for PEGylating flow chambers are described in **Chapter 3**.

Motility assays for complexes containing kinesin-1 and dynein

Polarity marked microtubules were made by polymerizing NEM-treated labeled tubulin from highly labeled microtubule seeds produced in BRB80 (80 mM PIPES pH 6.9, 2 mM MgCl₂, 0.5 mM EGTA) supplemented with 1 mM GTP, 4 mM MgCl₂ and 40%

glycerol as described previously (Howard and Hyman, 1993). 0.1 μ M full-length kinesin-1 containing a C-terminal biotin tag, 0.125 μ M BicD, 0.05 μ M Egalitarian, 0.05 μ M dynein and dynactin and 0.2 μ M 655 quantum dots (Invitrogen) were mixed in buffer B (30 mM HEPES, pH 7.4, 25 mM KOAc, 2 mM MgOAc, 1 mM EGTA, 10% glycerol, 10 mM DTT) containing 2 mg/mL BSA and incubated 20 min at room temperature. Buffer B + BSA was mixed and incubated for 5 min at room temperature. Then adapters, kinesin and dynein were added and incubated for 2 minutes at room temperature followed by dynactin for 5 minutes, then transferred to ice. The mixture was diluted 50-fold in buffer Go100 (30 mM HEPES, pH 7.4, 100 mM KOAc, 2 mM MgOAc, 1 mM EGTA, 10% glycerol, 2 mM MgATP, 20 mM DTT, 8 mg/mL BSA, 0.5 mg/mL κ -casein, 0.5% pluronic F68, 10 μ M paclitaxol and an oxygen scavenger system (5.8 mg/mL glucose, 0.045 mg/mL catalase, and 0.067 mg/mL glucose oxidase; Sigma-Aldrich)) and applied to a PEGylated flow cell containing adhered labeled microtubules. Data were analyzed by kymograph analysis as previously described (Fu and Holzbaur, 2013).

FLAG immunoprecipitations

Rab6 was exchanged for GTP (see above). All other proteins were diluted in BB (30 mM HEPES, pH 7.4, 150 mM KOAc, 2 mM MgOAc, 1 mM EGTA, 1 mM DTT, 0.5% Tween-20 and 1 μ g/mL leupeptin), clarified 400,000 x g for 20 min and concentrations were determined by Bradford reagent. For incubations with FLAG affinity resin, 100 μ M GTP and 50 μ M MgATP was added to BB. In 250 μ l BB, BicD constructs were diluted to 1.5 μ M, Rab6^{GTP} was added to 3 μ M, and where indicated kinesin was added to 0.7 μ M. Samples were taken for running 'inputs' on a gel. BSA was then added to 1 mg/mL and 40

uL of a 1:1 slurry of FLAG affinity resin equilibrated in BB was added. Mixtures were rocked for 1 hour at room temperature, washed 4 times with 500 μ l of BB and eluted by boiling in 50 μ l of 2x SDS loading buffer. 10 μ l of input and 20 μ l of elution were loaded on a 4-12% SDS gel and run at 150 V until the dye front migrated to the bottom of the gel. The gel was stained with Coomassie or western blotted with an anti-HIS antibody for visualization.

Lipid droplet formation

YFP-FMRP and FMRP was purified using FLAG affinity chromatography as described previously except lysis and wash steps were performed at 1M KCl (Krementsova et al., 2011). BicD constructs were purified similarly by FLAG affinity chromatography as described (Krementsova et al., 2011). 120uL of 2mg/mL YFP-FMRP in glycerol storage was dialyzed against buffer A (25mM Imidazole, pH 7.4, 25mM KCl, 1mM DTT and 1x Leupeptin) for 2.5 hours to overnight. Solution became cloudy after 1 hour indicating that droplets appear within this short timeframe and form large homogeneous droplets. Droplets were visualized in glass flow chambers blocked with 30mg/mL BSA for 10min. To decorate unlabeled FMRP droplets with either YFP-BicD-CC3 or Alexa488 labeled *FMRI* mRNA, FMRP was dialyzed for 2.5 hours against buffer A. Then, 25uL of FMRP droplets were mixed with 7mg/mL BSA, 0.5% F127, 0.1mg/mL κ -casein and either 20nM YFP-BicD-CC3 or 1x RNase inhibitors and 30nM Alexa488 *FMRI* mRNA. Samples incubated for 30min on ice and added directly into blocked flow chambers. For the formation of mRNA-dependent FMRP microdomains, 2 μ M FMRP was mixed 50nM YFP-BicD-CC3, 1x RNase inhibitors and 25nM unlabeled *FMRI* mRNA in B150 (25mM Imidazole, pH

7.4, 150mM KCl, 1mM DTT and 1x Leupeptin). Mixtures were stored on ice for ~20 min and heated to 37°C for 1min before addition to a blocked flow cell for imaging using TIRF microscopy. Omission of either FMRP or mRNA results in the failure to form structures at 150mM KCl. FMRP structures can also be observed under these conditions with FMRP and Alexa488 *FMR1* mRNA for direct visualization of the mRNA. Reducing mRNA concentration causes fewer structures to form.

REFERENCES

- Ally, S., A.G. Larson, K. Barlan, S.E. Rice, and V.I. Gelfand. 2009. Opposite-polarity motors activate one another to trigger cargo transport in live cells. *J Cell Biol.* 187:1071-1082.
- Bergbrede, T., O. Pylypenko, A. Rak, and K. Alexandrov. 2005. Structure of the extremely slow GTPase Rab6A in the GTP bound form at 1.8Å resolution. *J Struct Biol.* 152:235-238.
- Bianco, A., M. Dienstbier, H.K. Salter, G. Gatto, and S.L. Bullock. 2010. Bicaudal-D regulates fragile X mental retardation protein levels, motility, and function during neuronal morphogenesis. *Curr Biol.* 20:1487-1492.
- Bullock, S.L., A. Nicol, S.P. Gross, and D. Zicha. 2006. Guidance of bidirectional motor complexes by mRNA cargoes through control of dynein number and activity. *Curr Biol.* 16:1447-1452.
- Carter, A.P. 2013. Crystal clear insights into how the dynein motor moves. *J Cell Sci.* 126:705-713.
- Darnell, J.C., C.E. Fraser, O. Mostovetsky, G. Stefani, T.A. Jones, S.R. Eddy, and R.B. Darnell. 2005. Kissing complex RNAs mediate interaction between the Fragile-X mental retardation protein KH2 domain and brain polyribosomes. *Genes Dev.* 19:903-918.
- Dictenberg, J.B., S.A. Swanger, L.N. Antar, R.H. Singer, and G.J. Bassell. 2008. A direct role for FMRP in activity-dependent dendritic mRNA transport links filopodial-spine morphogenesis to fragile X syndrome. *Dev Cell.* 14:926-939.

- Friedman, D.S., and R.D. Vale. 1999. Single-molecule analysis of kinesin motility reveals regulation by the cargo-binding tail domain. *Nat Cell Biol.* 1:293-297.
- Fu, M.M., and E.L. Holzbaur. 2013. JIP1 regulates the directionality of APP axonal transport by coordinating kinesin and dynein motors. *J Cell Biol.* 202:495-508.
- Gagnon, J.A., and K.L. Mowry. 2011. Molecular motors: directing traffic during RNA localization. *Crit Rev Biochem Mol Biol.* 46:229-239.
- Grigoriev, I., D. Splinter, N. Keijzer, P.S. Wulf, J. Demmers, T. Ohtsuka, M. Modesti, I.V. Maly, F. Grosveld, C.C. Hoogenraad, and A. Akhmanova. 2007. Rab6 regulates transport and targeting of exocytotic carriers. *Dev Cell.* 13:305-314.
- Gross, S.P., M.C. Tuma, S.W. Deacon, A.S. Serpinskaya, A.R. Reilein, and V.I. Gelfand. 2002. Interactions and regulation of molecular motors in *Xenopus melanophores*. *J Cell Biol.* 156:855-865.
- Grosshans, B.L., D. Ortiz, and P. Novick. 2006. Rabs and their effectors: achieving specificity in membrane traffic. *Proc Natl Acad Sci U S A.* 103:11821-11827.
- Hendricks, A.G., E. Perlson, J.L. Ross, H.W. Schroeder, 3rd, M. Tokito, and E.L. Holzbaur. 2010. Motor coordination via a tug-of-war mechanism drives bidirectional vesicle transport. *Curr Biol.* 20:697-702.
- Howard, J., and A.A. Hyman. 1993. Preparation of marked microtubules for the assay of the polarity of microtubule-based motors by fluorescence microscopy. *Methods Cell Biol.* 39:105-113.
- Jiang, H., S. Wang, Y. Huang, X. He, H. Cui, X. Zhu, and Y. Zheng. 2015. Phase transition of spindle-associated protein regulate spindle apparatus assembly. *Cell.* 163:108-122.
- Krementsova, E.B., A.R. Hodges, C.S. Bookwalter, T.E. Sladewski, M. Travaglia, H.L. Sweeney, and K.M. Trybus. 2011. Two single-headed myosin V motors bound to a tetrameric adapter protein form a processive complex. *J Cell Biol.* 195:631-641.
- Ling, S.C., P.S. Fahrner, W.T. Greenough, and V.I. Gelfand. 2004. Transport of *Drosophila* fragile X mental retardation protein-containing ribonucleoprotein granules by kinesin-1 and cytoplasmic dynein. *Proc Natl Acad Sci U S A.* 101:17428-17433.
- Liu, Y., H.K. Salter, A.N. Holding, C.M. Johnson, E. Stephens, P.J. Lukavsky, J. Walshaw, and S.L. Bullock. 2013. Bicaudal-D uses a parallel, homodimeric coiled coil with heterotypic registry to coordinate recruitment of cargos to dynein. *Genes Dev.* 27:1233-1246.

- Martin, M., S.J. Iyadurai, A. Gassman, J.G. Gindhart, Jr., T.S. Hays, and W.M. Saxton. 1999. Cytoplasmic dynein, the dynactin complex, and kinesin are interdependent and essential for fast axonal transport. *Mol Biol Cell*. 10:3717-3728.
- Martinez, O., C. Antony, G. Pehau-Arnaudet, E.G. Berger, J. Salamero, and B. Goud. 1997. GTP-bound forms of rab6 induce the redistribution of Golgi proteins into the endoplasmic reticulum. *Proc Natl Acad Sci U S A*. 94:1828-1833.
- Matanis, T., A. Akhmanova, P. Wulf, E. Del Nery, T. Weide, T. Stepanova, N. Galjart, F. Grosveld, B. Goud, C.I. De Zeeuw, A. Barnekow, and C.C. Hoogenraad. 2002. Bicaudal-D regulates COPI-independent Golgi-ER transport by recruiting the dynein-dynactin motor complex. *Nat Cell Biol*. 4:986-992.
- Nelson, S.R., K.M. Trybus, and D.M. Warshaw. 2014. Motor coupling through lipid membranes enhances transport velocities for ensembles of myosin Va. *Proc Natl Acad Sci U S A*. 111:E3986-3995.
- Ohashi, S., K. Koike, A. Omori, S. Ichinose, S. Ohara, S. Kobayashi, T.A. Sato, and K. Anzai. 2002. Identification of mRNA/protein (mRNP) complexes containing Puralpha, mStaufen, fragile X protein, and myosin Va and their association with rough endoplasmic reticulum equipped with a kinesin motor. *J Biol Chem*. 277:37804-37810.
- Pilling, A.D., D. Horiuchi, C.M. Lively, and W.M. Saxton. 2006. Kinesin-1 and Dynein are the primary motors for fast transport of mitochondria in Drosophila motor axons. *Mol Biol Cell*. 17:2057-2068.
- Rackham, O., and C.M. Brown. 2004. Visualization of RNA-protein interactions in living cells: FMRP and IMP1 interact on mRNAs. *EMBO J*. 23:3346-3355.
- Ramos, A., D. Hollingworth, S. Adinolfi, M. Castets, G. Kelly, T.A. Frenkiel, B. Bardoni, and A. Pastore. 2006. The structure of the N-terminal domain of the fragile X mental retardation protein: a platform for protein-protein interaction. *Structure*. 14:21-31.
- Schaeffer, C., B. Bardoni, J.L. Mandel, B. Ehresmann, C. Ehresmann, and H. Moine. 2001. The fragile X mental retardation protein binds specifically to its mRNA via a purine quartet motif. *EMBO J*. 20:4803-4813.
- Siomi, M.C., Y. Zhang, H. Siomi, and G. Dreyfuss. 1996. Specific sequences in the fragile X syndrome protein FMR1 and the FXR proteins mediate their binding to 60S ribosomal subunits and the interactions among them. *Mol Cell Biol*. 16:3825-3832.

- Soppina, V., A.K. Rai, A.J. Ramaiya, P. Barak, and R. Mallik. 2009. Tug-of-war between dissimilar teams of microtubule motors regulates transport and fission of endosomes. *Proc Natl Acad Sci U S A*. 106:19381-19386.
- Uchida, A., N.H. Alami, and A. Brown. 2009. Tight functional coupling of kinesin-1A and dynein motors in the bidirectional transport of neurofilaments. *Mol Biol Cell*. 20:4997-5006.
- Waterman-Storer, C.M., S.B. Karki, S.A. Kuznetsov, J.S. Tabb, D.G. Weiss, G.M. Langford, and E.L. Holzbaur. 1997. The interaction between cytoplasmic dynein and dynactin is required for fast axonal transport. *Proc Natl Acad Sci U S A*. 94:12180-12185.
- Zhang, H., S. Elbaum-Garfinkle, E.M. Langdon, N. Taylor, P. Occhipinti, A.A. Bridges, C.P. Brangwynne, and A.S. Gladfelter. 2015. RNA Controls Poly-glutamine Protein Phase Transitions. *Mol Cell*. 60:220-230.